



BROL
AEROSPACE



BROL
Aircraft Family
Conceptual Design



MTOW: 1800 lb

ZFW: 1600 lb



Max: 155 kts

Cruise: 138 kts

Stall: 56 kts



1175 nmi
(reserve: 45')

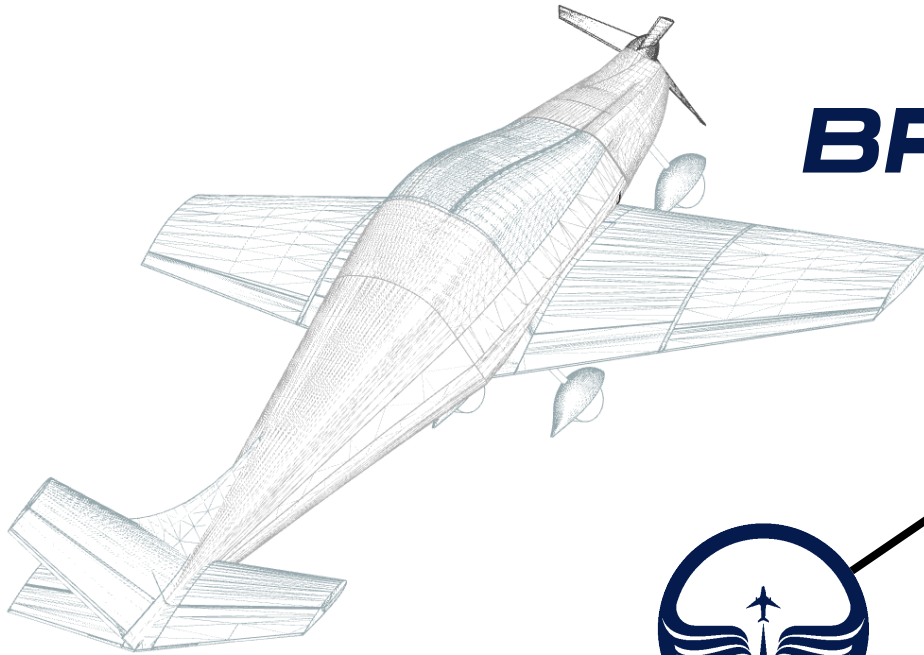


Cruise: 8 000 ft

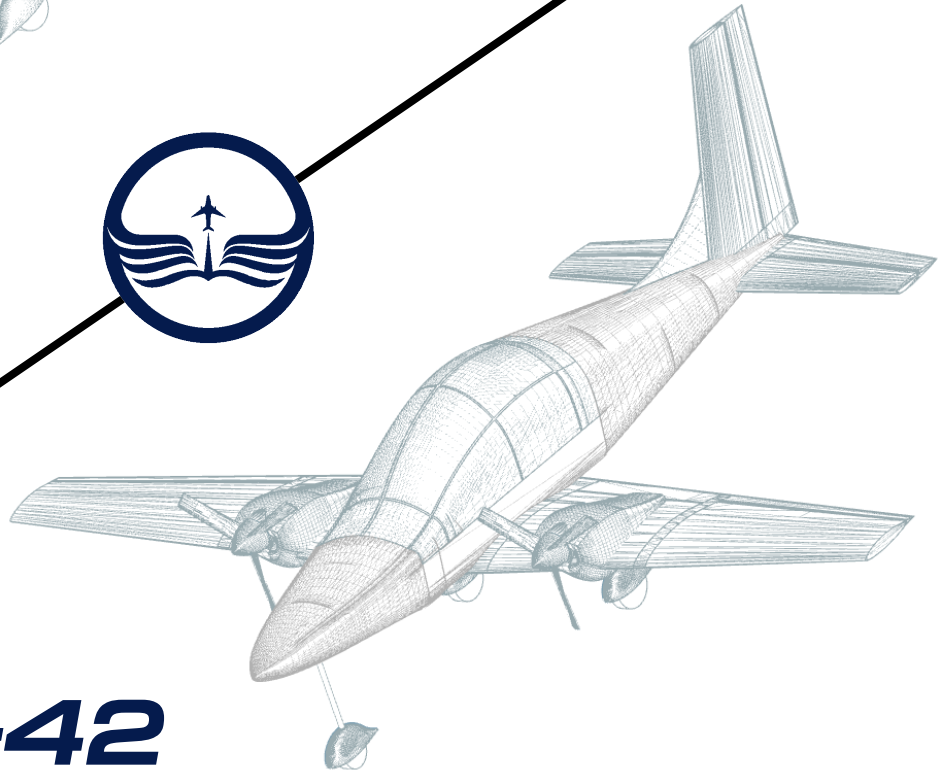
Ceiling: 30 600 ft



231 000 US\$



BROL-21



BROL-42



MTOW: 3500 lb

ZFW: 3100 lb



Max: 201 kts

Cruise: 181 kts

Stall: 71 kts



1550 nmi
(reserve: 45')



Cruise: 12 000 ft

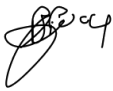







Ceiling: 23 000 ft



399 000 US\$



TEAM MEMBERS

Name	AIAA N°	Mail	Signature
Amaury BILOCCQ	1082017	amaury.bilocq@student.uliege.be	
François CUSTINNE	1082185	francois.custinne@student.uliege.be	
Hadrien DELATTE	1081551	hadrien.delatte@student.uliege.be	
Armand DUBUC	1081692	armand.dubuc@student.uliege.be	
Casimir FAYT	1081596	fayt.casimir@gmail.com	
Mickaël LAUBACHER	1081796	micka.laubacher@gmail.com	
Bérénice MICHAUX	1876994	berenice.michaux@student.uliege.be	
Elliott THIRY	1081923	elliott.thiry@student.uliege.be	

FACULTY MEMBERS

Professors	Assistants
Ludovic NOELS	Adrien CROVATO
Grigorios DIMITRIADIS	Thomas LAMBERT

CONTENT

Introduction	1		
Target market	1		
1 Mission requirements	4		
2 Configuration	5		
2.1 Existing configurations	5		
2.2 Design Methodology	6		
2.3 Design altitudes and velocities . .	7		
2.4 BROL aircraft family CAD	8		
3 Component Design	10		
3.1 Wing	10		
3.1.1 Wing overall planform . .	10		
3.1.2 Airfoil selection	11		
3.1.3 Aileron and high lift devices	13		
3.2 Empennage	15		
3.2.1 Horizontal tail and elevator	15		
3.2.2 Fin and rudder	16		
3.3 Propulsion system	17		
3.3.1 Piston engine selection . .	18		
3.3.2 Propeller design	20		
3.3.3 Fuel/oil selection	21		
3.3.4 Frame integration	22		
3.4 Fuselage	24		
3.4.1 Material selection	25		
3.4.2 Shape	25		
3.4.3 Internal layout	27		
3.5 Landing gear	29		
3.5.1 Material selection	29		
3.5.2 Configuration	29		
3.5.3 Geometrical layout	30		
3.5.4 Wheels and shock absorber	31		
3.6 Systems	32		
3.6.1 Systems and avionics . . .	32		
3.6.2 Control	34		
3.7 Weight Calculation	35		
4 Aircraft analysis	38		
4.1 Aerodynamics	38		
4.1.1 Lift curve analysis	38		
4.1.2 Drag determination	39		
4.1.3 Drag polar and Lift-to-drag ratio	43		
4.2 Static stability	44		
4.2.1 Longitudinal Stability . .	44		
4.2.2 Directional stability	46		
4.2.3 Lateral stability	47		
4.3 Dynamic stability	48		
4.3.1 Stability derivatives	48		
4.3.2 Longitudinal modes	50		
4.3.3 Lateral modes	51		
4.4 Structure	51		
4.4.1 Flight envelopes	52		
4.4.2 Aircraft loading	54		
4.4.3 Fuselage loading	56		
4.4.4 Wing loading	56		
4.4.5 Analytical analysis	57		
4.4.6 Finite element analysis . .	60		
4.5 Performance	67		
4.5.1 Payload-range diagram . .	67		
4.5.2 Placard diagram	69		
4.5.3 Takeoff	69		
4.5.4 Climb	71		
4.5.5 Cruise	74		
4.5.6 Turning rate and banking agnle	75		
4.5.7 Landing	78		
5 Trade-off study	79		
6 Costs analysis	81		
6.1 Non-recurring costs	81		
6.2 Production method	82		
6.3 Recurring costs	83		
6.4 Selling price	84		
6.5 Cost-volume-profit analysis	85		
6.6 Operational costs and features . .	86		
7 Conclusion	88		
Appendices			
A Acronyms	I		

INTRODUCTION

Recent studies show that air service for small cities experience troubles to find pilots and are constrained to limit their activities. This trend can be explained by the transfer of pilots to larger national and global airlines. For monetary stability reasons, the current pilots in training have a tendency to join those larger airlines. On top of that, the average age of airline pilots is increasing and there is a decline in the number of military pilots.

Driven by the need of training a large number of pilots with an economical way of flying, the American Institute of Aeronautics and Astronautics has issued a request for proposal for general aviation trainer aircraft family. As the development of light sport and transport aircraft became more important for the last twenty years, the trainer aircraft market has been neglected. In order to answer to the request for proposal, two aircraft (with single and twin-engine configuration) have to be designed to best serve the pilot training market for both career and leisure pilots. The designed aircraft family should be focused on a “utility” value proposition.

This report presents the characteristics and performance of the BROL aircraft family in the scope of the AIAA Graduate Team Competition. During the whole design process, the focus is placed on producing simple, efficient and versatile aircraft. BROL Aerospace has for main objective to make flight accessible for everyone. Furthermore, the design choices developed throughout this report are motivated by reducing purchase price and flying costs. Training aircraft should stay relatively inexpensive to fly as well as to buy.

Target market

Training and business aircraft are already well established in the general aviation market. This section will help to position the new aircraft family. In a saturated market, the aircraft should make the difference based on price and new features as a differentiator. Fig.1 shows the split of general



aviation forecast by region from 2019-2024. North America market has a low potential in growth, while Europe is average and Asia shows a high potential [1].

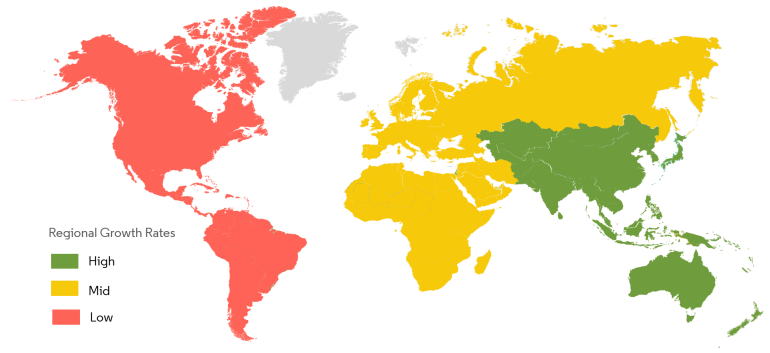


Figure 1: Growth rate of civil aviation flight training and simulation market, by region (2019-2024)

From a pilot stand point, the forecast follows the market demand. 41% of the new pilots will be in Asia Pacific. North America and Europe have the second-best rate with 17% of new pilots [2]. The light aircraft market is estimated at USD 7.1 billion in 2018 with up to USD 13.9 billion in 2030. Pacific Asia shows a higher compound annual growth rate (CAGR) from that period, which averages around 5.8% [3]. The highest potential of the market is clearly in Asia. However according to the request for proposal describing the certification, the new aircraft family will be developed in the USA. Then, based on the market analysis, the family will be sold in Asia. Later on, to offer a less expensive product and a quick delivery, aircraft could be directly produced in Asia if technology transfer constraints are fixed. Once the break-even point reached, a second market will be targeted such Europe or North America, upon market review.

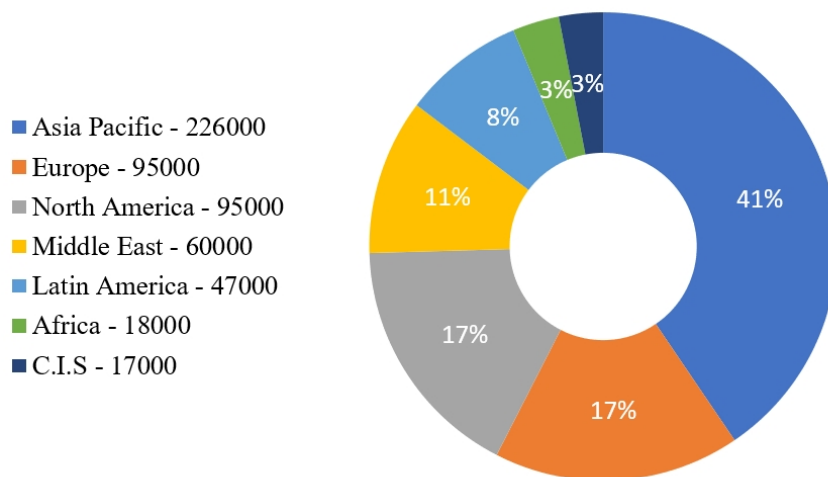


Figure 2: New pilots demand forecast 2015-2035. Adapted from [2]

It should be noted that the COVID-19 virus will certainly have an impact on the general aviation market. A decrease of pilot demand is expected as human priorities changed. That may force training companies around the world to financial trouble or to chapter 11. Some of them may decide to postpone planned investments which will make the market more competitive. Those assumptions should be reviewed in the coming months based on new market data.



1 MISSION REQUIREMENTS

The mission requirements from the AIAA request for proposals are given in Tab. 1.1.

	BROL-21	BROL-42
Crew	1 Pilot Required, 2-Pilot (Dual Instruction) Capable	
Passengers	1+	3+
Takeoff Distance	< 1500 ft	< 2500 ft
Landing Distance	< 1500 ft	< 2500 ft
Endurance	> 3 hr	> 4 hr
Ferry Range	> 800 nmi	> 1000 nmi
Service Ceiling	> 12,000 ft	> 18,000 ft
Certification Category	Utility	Normal

Table 1.1: Request for proposal mission requirements

When a student learns to fly, the idea is to train for takeoffs and landings with short flights. The flight plan for a typical mission is shown in Fig. 1.1 for the single-engine, called BROL-21, and the twin-engine, BROL-42. For private pilots, the cruise time is generally longer, with only one takeoff and landing. To be able to tackle lessons of takeoff and landing as well as maneuvers and long flight, the typical design parameters of a flight are chosen accordingly to the Fig. 1.1.

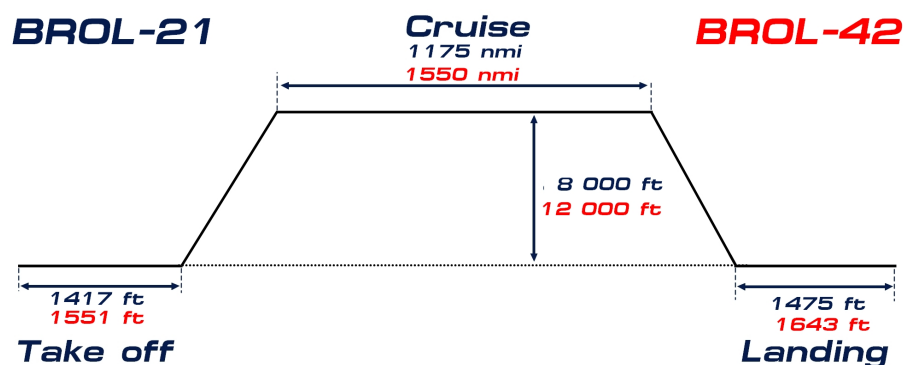


Figure 1.1: Typical mission for the BROL aircraft family

2 CONFIGURATION

2.1 Existing configurations

The proposed design is the result of a review of existing solutions. As a matter of fact, several comparisons have been made to find the optimal configuration. Choices are based on the objectives and constraints described on the request for proposal.

In order to determine a new aircraft design for training, a survey of existing models was made. On the basis of this survey, it was possible to make a first selection of usable designs. Some configurations are shown in Fig. 2.1.



(a) Pecnam P2206



(b) Diamond DA20



(c) Piaggio P.180 Avanti



(d) Sonaca 200

Figure 2.1: Different aircraft configurations

A starting design can be defined after comparing the different models on the basis of defined criteria. The latter are based on the advantages and drawbacks of several choices such as the position and the shape of the wings, the position of engines or the shape of the tail.

For this training aircraft, a conventional tail has been selected because it offers good stability, easy access for maintenance and it is light, which is a great advantage since weight is an important design criterion. The wings are placed in the low position to provide an easy access to the cabin and for maintenance. This position also allows good maneuverability compared to the high position. Despite the fact that the canard configuration avoids the stall of the main wing, it will not be selected. Indeed, it is a reassuring element but the student must be able to recover his plane in any situation, especially when stalling. Finally, a tractor (puller) configuration is chosen because it shows lower manufacturing cost, and is safer for pilots and especially for students¹. Finally, the landing gear show a tricycle configuration damped by a solid spring gear leg for both aircraft. The final concept will be similar to the one proposed by *Sonaca Aircraft (Sonaca 200)*.

2.2 Design Methodology

The methodology used to determine the aircraft family's general design is presented in Fig. 2.2. Matlab software is employed to implement the flowchart and to carry out the design. The methodology inputs are mission and mandatory requirements, objectives and chosen aircraft configuration. Using this information and the characteristics of similar aircraft, the power and wing loading can be approximated. First guesses of aircraft weights can then be determined. This allows to select general aircraft dimensions.

¹A pusher configuration decreases the landing error margin as the propeller could hit the ground before the tail.



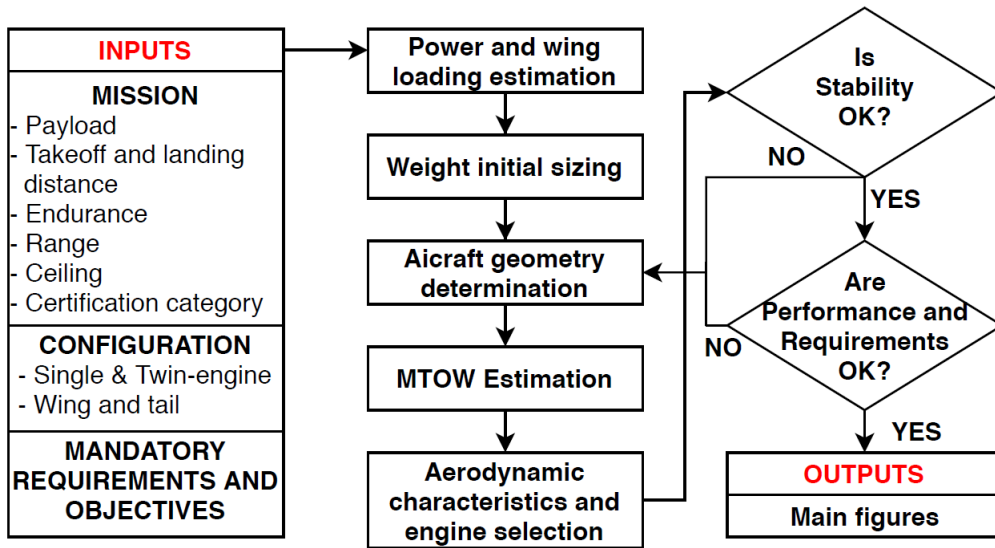


Figure 2.2: Flowchart of the design methodology

While the weight initial sizing does not consider all the aircraft components, the MTOW estimation takes every main aircraft components into account. This more accurate weight value allows to compute the aerodynamics characteristics as well as to select the engine(s). In order to validate the design, the aircraft stability, performances and satisfaction of the requirements have to be investigated. If one of the aircraft parameters does not fit with the desired values, the aircraft geometry must be modified. This iterative process is completed in relation to regulation 14 CFR Part 23.

2.3 Design altitudes and velocities

The various design altitudes and velocities selected to evaluate BROL aircraft family characteristics and performance are shown in Tab. 2.1.

	BROL-21	BROL-42
Cruising altitude	8 000 ft	12 000 ft
Cruising speed	122 KEAS	151 KEAS
Maximum speed	137 KEAS	168 KEAS

Table 2.1: Design altitudes and velocities



2.4 BROL aircraft family CAD



Figure 2.3: BROL-21 CAD model

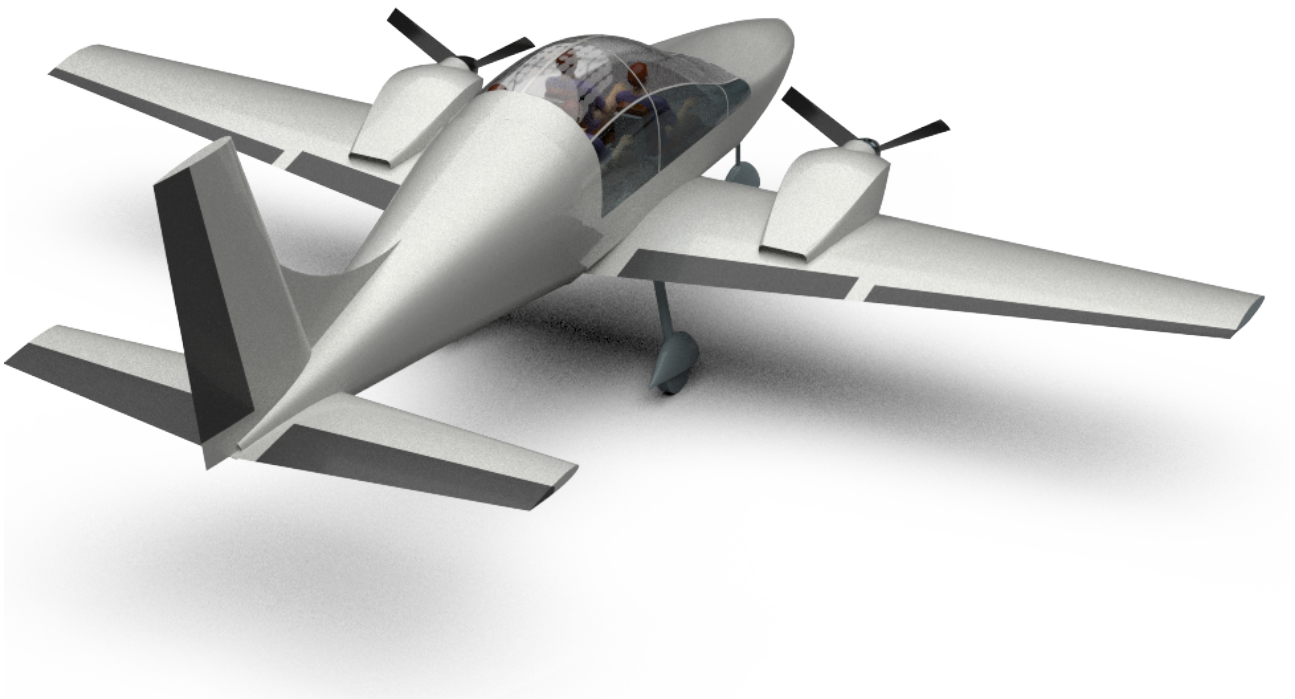


Figure 2.4: BROL-42 CAD model

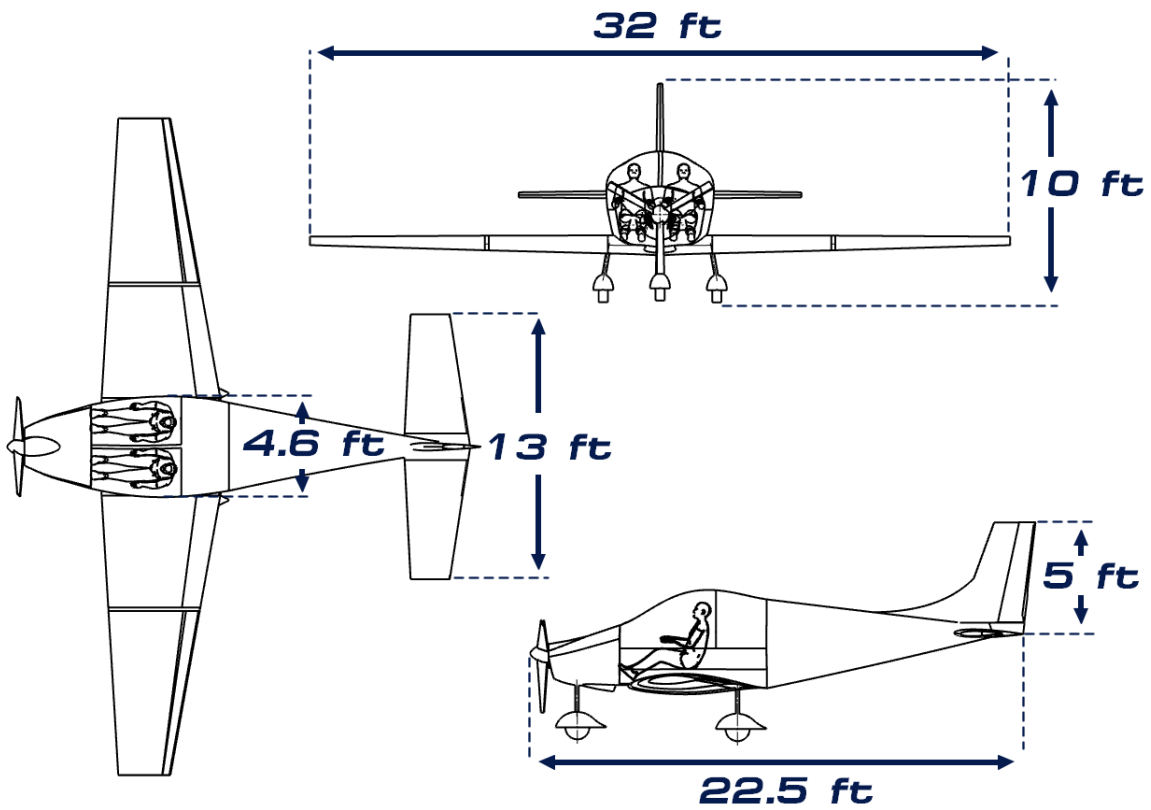


Figure 2.5: Three-view draft of the BROL-21 aircraft

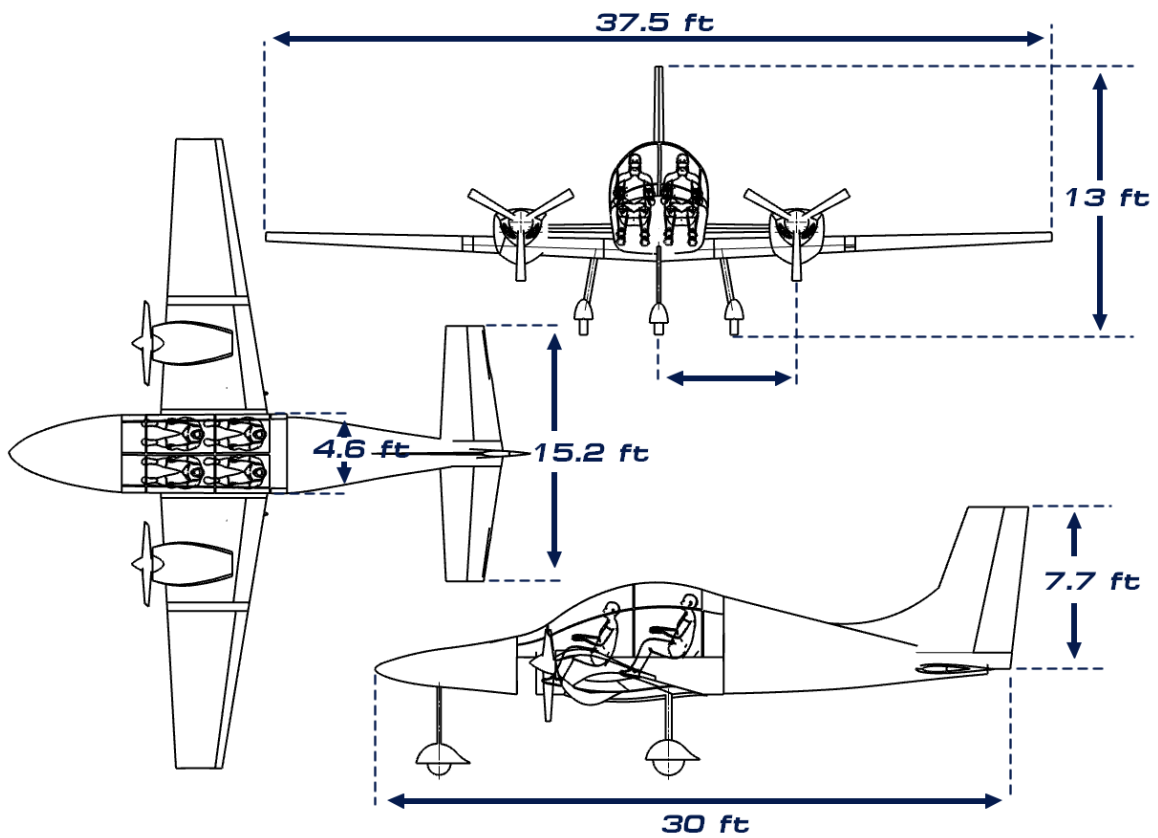


Figure 2.6: Three-view draft of the BROL-42 aircraft



3 COMPONENT DESIGN

3.1 Wing

3.1.1 Wing overall planform

The wing planform is designed to provide an easy flight for beginner pilots and to reduce the manufacturing cost. As stated in section 2.1, a low-wing configuration has been picked. Fig. 3.1 & Fig. 3.2 illustrate the wing planform for both aircraft while Tab. 3.1 & Tab. 3.2 summarize the geometric parameters.

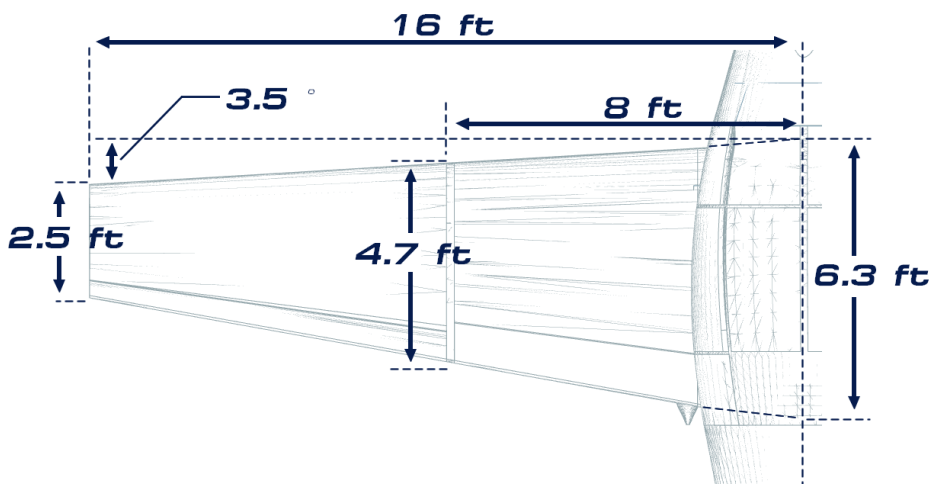


Figure 3.1: BROL-21 wing planform

BROL-21	
Area [ft ²]	142
i_w [°]	1
γ [°]	1.5
AR [—]	7.2
λ [—]	0.4
$\Lambda_{c/4}$ [°]	0

Table 3.1: BROL-21 wing parameters

The planform exhibits the following geometric parameters:

- The Aspect Ratio (AR) impacts the induced drag of the wing. Values of $AR = 7.2$ for the BROL-21 and $AR = 7.8$ for the BROL-42 offer a good balance between low induced drag and good roll response, allowing a good glide possibility for a quite light structure [4];
- The taper ratio (λ) allows a reduction of the drag and increases the aerodynamic performance of the wing. A value of $\lambda = 0.4$ allows a good compromise between low induced drag and good stall properties. However, it requires a moderate washout [4];
- The washout (γ) prevents the wing tip to stall before the wing root. Indeed, for ease of manufacturing, the same airfoil is chosen along the span. Hence, a washout of $\gamma = 1.5^\circ$ is chosen

[5];

- The dihedral (Γ) ensures the stability of the aircraft as a low wing configuration has been imposed. Resolving the lateral stability problem in Sec.4.2.3 gives a dihedral of 3° for both aircraft;
- The sweep angle ($\Lambda_{c/4}$) is chosen to be 0° as both aircraft fly at Mach numbers lower than 0.3;
- The wing incidence (i_w) is fixed at 1° for both aircraft. It provides enough lift at cruise condition and allows the wing planform to produce minimum drag, as shown in Sec. 3.1.2. Finally, it ensures that the angle of attack of the fuselage is 0° for cruise condition.

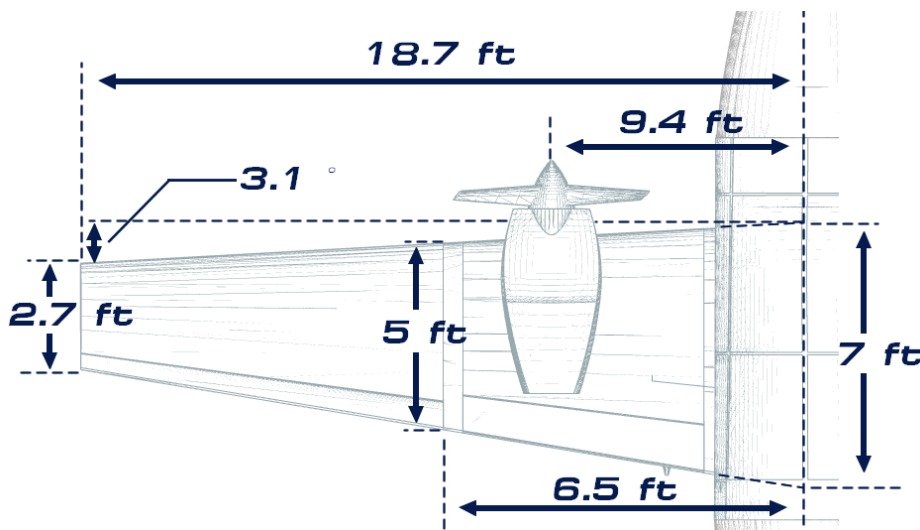


Figure 3.2: BROL-42 wing planform

BROL-42	
Area [ft ²]	180
i_w [°]	1
γ [°]	1.5
AR [—]	7.8
λ [—]	0.4
$\Lambda_{c/4}$ [°]	0

Table 3.2: BROL-42 wing parameters

The next step of the design aims to define the aerodynamic properties of the two planforms presented above. Therefore, an airfoil selection must be performed.

3.1.2 Airfoil selection

The selected airfoil must meet four criteria: provide an airfoil ideal cruise lift coefficient $c_{l_i} \sim 0.3$, computed using the design cruise weight of the aircraft, a maximum lift coefficient $c_{l_{\max}} \sim 1.55$, computed using the maximum takeoff weight, present minimal drag to reduce the cost of a training session and a docile stall for the safety of beginner pilots. Moreover, as the fuel is carried inside the wing, a relatively thick airfoil must be chosen. NACA 65₂415 is selected as it fulfils all the mentioned requirements. Fig. 3.3 shows the lift curve and the drag polar of the airfoil for the Reynolds

number of $5.5e6$ (BROL-21) and $7e6$ (BROL-42). The design point is at an altitude of 8 000 ft and a velocity of 138 kt for BROL-21 and at an altitude of 12 000 ft and a velocity of 181 kt for BROL-42.

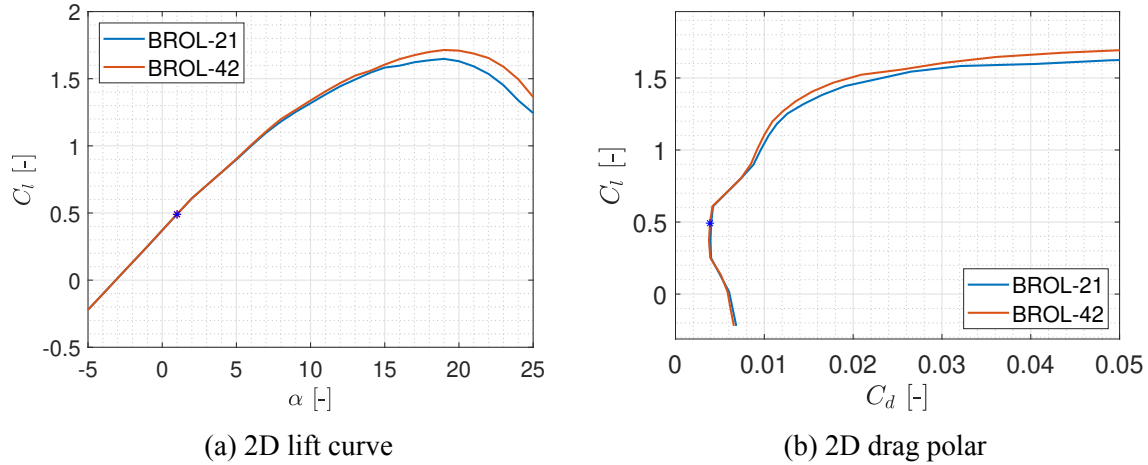


Figure 3.3: Aerodynamic properties of the airfoil for the Reynolds number of the aircraft computed with Xfoil. The star on both plots represents the value at cruise condition.

An interesting feature of the NACA 6-digits is the low drag bucket. Hence, the airfoil sustains an extensive laminar flow region and a low minimum drag for $c_l \in [0.2; 0.6]$. Tab. 3.3, based on Fig. 3.3 summarizes the values of the various airfoil characteristics.

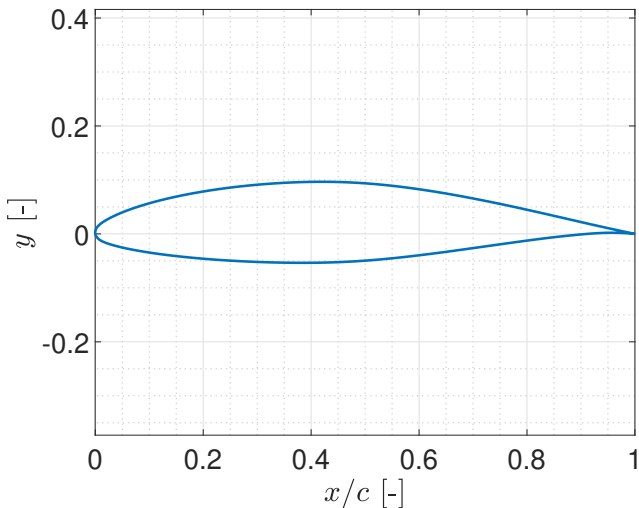


Figure 3.4: Airfoil geometry

The airfoil is the same for both aircraft to reduce the development and production costs.

Finally, Tab. 3.4 illustrates the aerodynamic properties of the wing planform at cruise condition without high lift devices deployed. The lift coefficient of the wing at cruise (C_L^W) and the maximum lift coefficient of the wing (C_L^{\max}) are higher than the one required by the entire aircraft (respectively

	BROL-21	BROL-42
$c_{l_{\text{cruise}}}$ [—]	0.47	0.47
$c_{l_{\text{max}}}$ [—]	1.6479	1.7142
α_{max} [°]	19	19
$c_{d_{\text{min}}}$ [—]	0.0039	0.0037

Table 3.3: Airfoil characteristics

$C_L^{aircraft}$ and $C_L^{maxWing}$). However, even if both aircraft could takeoff and land without flaps, the wings are equipped with high lift devices to allow easier landing to pilots by reducing the approach velocity. These devices are investigated in Sec. 3.1.3.

	BROL-21	BROL-42
α_{0L} [°]	-2.175	-2.175
α_{stall} [°]	13.5	13.5
$C_{L\alpha}$ [-]	5.15	5.15
C_L^W [-]	0.2760	0.2898
$C_L^{aircraft}$ [-]	0.2649	0.2452
$C_L^{maxWing}$ [-]	1.4532	1.5508
$C_L^{maxAircraft}$ [-]	1.3232	1.4512

Table 3.4: Aerodynamic properties of the wing planform for both aircraft.

3.1.3 Aileron and high lift devices

Ailerons and high lift devices are added to the planform, as seen in Fig. 3.5.

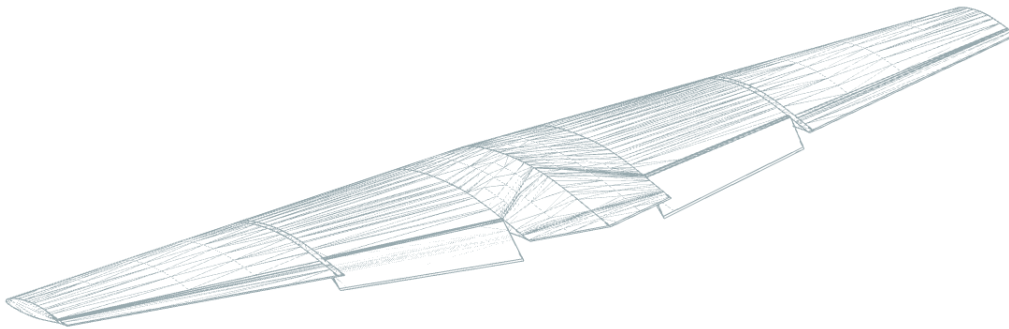


Figure 3.5: Configuration of the wing planform of BROL-21 with ailerons and flaps deployed at 35° .

Slotted flaps were chosen for both aircraft. This kind of flaps allows a high increase of lift without modifying the stall angle, as seen in Fig. 3.6, in contrast to plain flaps. Furthermore, they are safer for a beginner pilot learning how to use flaps.

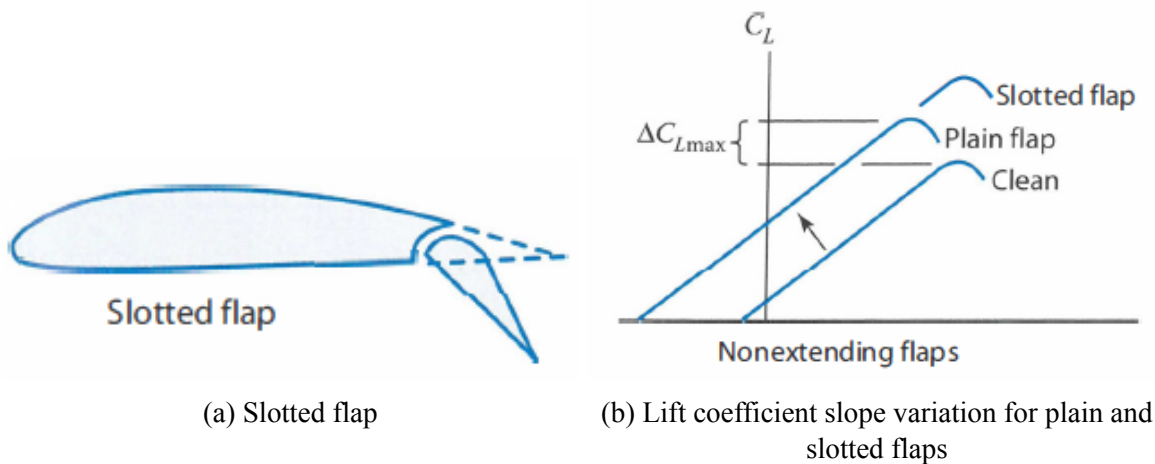
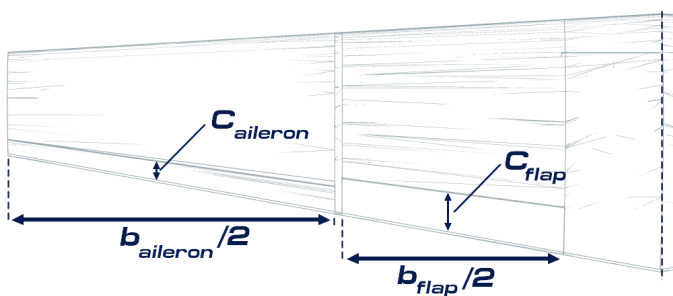


Figure 3.6: High lift devices parameters [5]

During landing, the approach velocity is reduced by deploying the flaps at an angle of 35° . Their deployment increases the lift coefficient and thus reduces the stall velocity. Moreover, it allows to reduce the landing distance by increasing the drag. The variation of the stall velocity can be seen in Tab. 4.30 and Tab. 4.31.

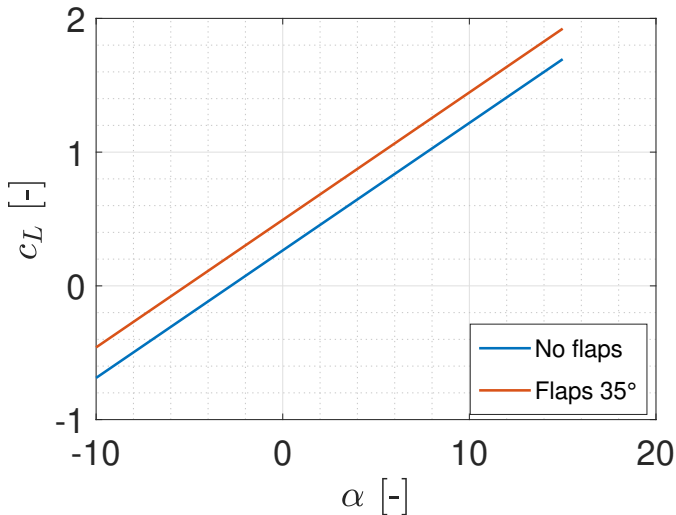
The aerodynamic characteristics of the flaps are computed using the Wing Partition Method described in Gudmundsson[4]. Fig. 3.5 shows the dimensions of the high lift devices used to compute the properties of the wing planform with flaps out. This figure also gives the geometrical aspect of the ailerons computed using statistical data from Raymer [5]. The span of the aileron is equal to 50% of the span of the wing and the mean aerodynamic chord (MAC) is equal to 15% of the wing MAC . The values were then validated during the dynamical stability analysis in Sec. 4.3.



	BROL-21	BROL-42
Flaps		
Flapped area [%]	30	30
MAC [ft]	0.942	1.02
Span [ft]	5.44	6.22
Aileron		
Area [ft²]	11.35	7.11
MAC [ft]	0.71	0.76
Span [ft]	15.98	18.73

Table 3.5: Geometrical properties of the ailerons and high lift devices for both aircraft.

Fig. 3.7 shows the impact of the slotted flaps on the lift curve slope of the aircraft. In addition, the variation of the lift coefficient and the zero-lift angle of attack are noted.



	BROL-21	BROL-42
ΔC_L [-]	0.2331	0.2111
C_L^{\max} [-]	1.6863	1.7611
$\Delta\alpha_{0L}$ [°]	-2.625	-2.625
α_{0L} [°]	-5	-5

Figure 3.7: Variation of the lift curve slope due to flaps deployment for BROL-21 on the left; values of interest on the right. The aerodynamic analysis is explained in Sec. 4.1.

3.2 Empennage

3.2.1 Horizontal tail and elevator

The horizontal tails of the BROL-21 and BROL-42 present similar geometric parameters such as an aspect ratio of 5, a taper of 0.6 and no sweep angle. Even the same NACA 0012 airfoil is used. This profile has several advantages: the symmetry allows to easily calibrate the lift needed, it produces low drag during cruise, the low thickness reduces the weight of the horizontal tail and finally, it is easy to produce at low cost. Moreover, the elevators are added to the horizontal tail.

Tail volume coefficient method and statistical data are applied as an approach to size the horizontal tail. The tail volume coefficient data used are 0.7 for the BROL-21 and 0.8 for the BROL-42 and the statistical data, found in [5], are given above. The angles of incidence of 0° for the BROL-21 and -1° for the BROL-42 were computed to ensure the right amount of lift given by the tails at cruise conditions. Finally, a moment arm of 64% of the fuselage for BROL-21 and 55% for BROL-42 were fixed to enhance the static margin of the aircraft as seen in Sec. 4.2.

The elevator is sized with statistical data found in [5], yielding a span of 90% and a mean aerodynamic chord of 45% of the horizontal tail.

Fig. 3.6 shows the geometric properties for both the horizontal tail and elevators and the aerodynamic properties of the tail.

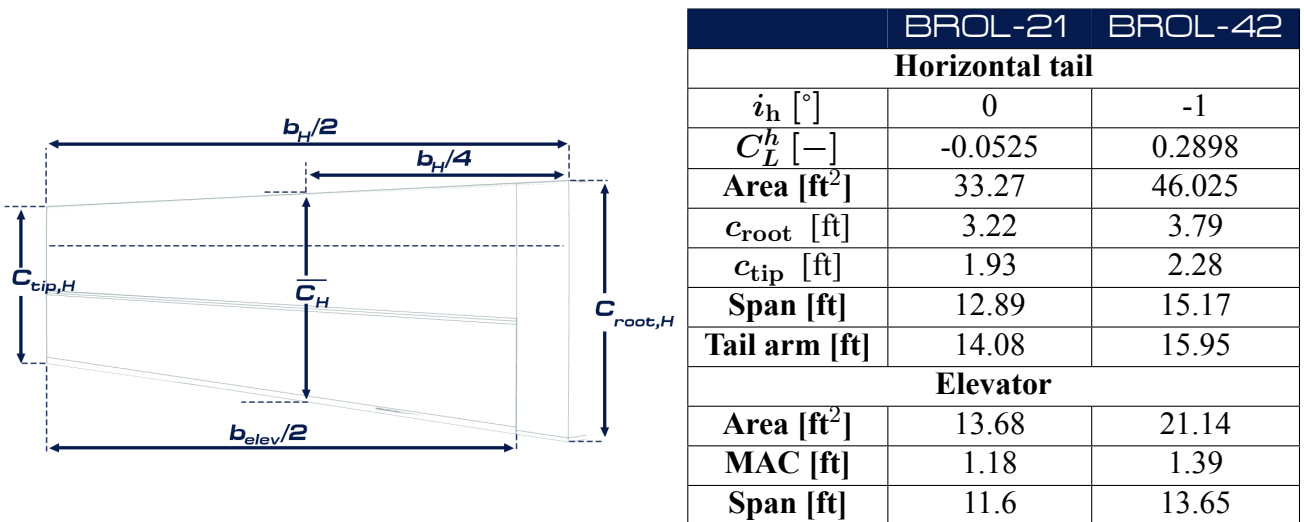


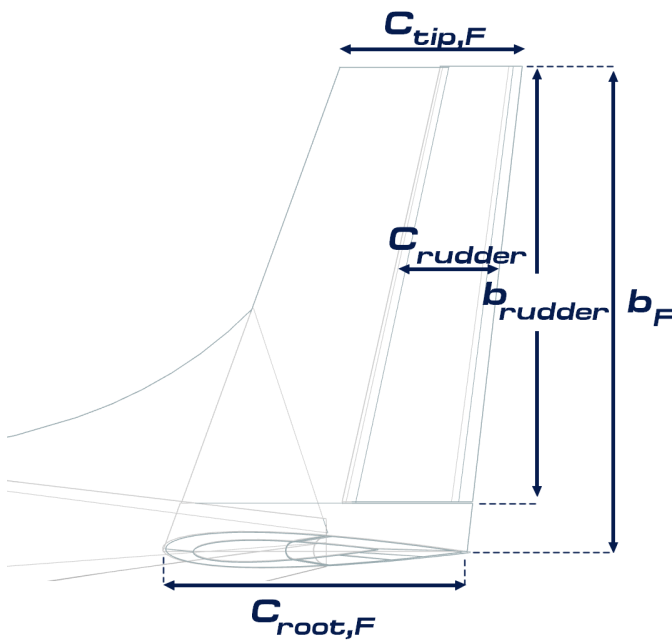
Table 3.6: Geometrical design and aerodynamic properties of the horizontal tail and the elevator for both aircraft.

The features of the horizontal tails were validated during the aerodynamic analysis in Sec. 4.1 and the longitudinal static stability analysis in Sec. 4.2. The elevators were validated during the dynamical stability analysis in Sec. 4.3.

3.2.2 Fin and rudder

The purpose of the vertical empennage is to stabilize the aircraft in the lateral direction. Rudders are added to make the aircraft yaw. The chosen airfoil is again the NACA 0012 for the same reasons mentioned above. As with the horizontal tail, some geometric parameters of the fin are the same for both aircraft. Namely, an aspect ratio of 2, a taper of 0.6 and a sweep angle of 20° at the leading edge. The other parameters are illustrated in Fig. 3.7.

Tail volume coefficient data used to size the fins are 0.04 for BROL-21 and 0.07 for BROL-42. The rudder is designed by taking a span of 90% and a mean aerodynamic chord of 40% of the fin.



	BROL-21	BROL-42
Fin		
Area [ft ²]	12.89	29.6
c_{root} [ft]	3.17	4.81
c_{tip} [ft]	1.9	2.88
Span [ft]	5.08	7.69
Rudder		
Area [ft ²]	4.71	10.51
MAC [ft]	1.03	1.57
Span [ft]	4.57	6.92

Table 3.7: Geometrical design of the fin and the rudder for both aircraft.

The features of the fins were validated during the lateral static stability analysis in Sec. 4.2. Moreover, the area of the fin of the BROL-42 provides a maximum rudder deflection of 21° , lower than the maximum allowable deflection of 25° [6] for the minimum control speed with one engine inoperative.

3.3 Propulsion system

The propulsion system of the BROL family has been designed in order to meet the RFP requirements. As in our case and in general aviation aircraft in general, the cruising speeds are moderately high, piston powered engines with propellers are chosen thanks to their simplicity. Besides, they allow to meet the strict FAA regulation involved for basic pilot training.

As already mentioned in Sec. 2.1, both aircraft show a propulsion system in puller configuration. The engines are thereby mounted in the nose for the BROL-21 and in nacelles on the wing for the BROL-42. Particular attention is brought to the propeller tip ground clearance as specified in 14 CFR §25.925.

The propulsion design takes care of reducing all operating and maintenance costs since they represent

a large part of the total cost of a trainer aircraft.

3.3.1 Piston engine selection

The computation of power requirements for both aircraft is based on the methodology developed by Daniel P. Raymer [5]. This method derives the thrust-to-weight ratio given by

$$\left(\frac{T}{W}\right)_{\text{cruise}} = \frac{1}{(L/D)_{\text{cruise}}} = \left(\frac{C_D}{C_L}\right)_{\text{cruise}} \quad (3.1)$$

where $C_{L,\text{cruise}}$ is the cruise lift coefficient and $C_{D,\text{cruise}}$ is the total drag coefficient of the aircraft during cruise. The latter's computation is explained in Sec. 4.1.2. This ratio is then converted to power-to-weight ratio which allows, with the weight of the aircraft, to compute the required power for a steady flight cruise condition. This value is then adjusted to sea-level condition in order to take into account the power loss due to altitude, following the Gagg and Ferrar model:

$$\text{Power} = \text{Power}_{\text{sea-level}} \left(\frac{\rho}{\rho_{SL}} - \frac{1 - \frac{\rho}{\rho_{SL}}}{7.55} \right). \quad (3.2)$$

ρ_{SL} and ρ are the air density at sea-level and cruise altitude respectively [5]. The cruising altitude effect for the BROL-21/42 engines decrease their power ability to only 75.8% and 65.3% of their sea-level power. This is where turbocharged engines are advantageous since they do not lose power under a critical altitude, which allows to use smaller and lighter engine. Finally, by assuming that a piston-engine aircraft typically cruise at 75% of its takeoff power, the required power can be assessed for both BROL aircraft. Those requirements are presented in Tab. 3.8 in the case of both turbocharged and non-turbocharged engines.

	Units	BROL-21		BROL-42	
Turbocharged		Yes	No	Yes	No
Required power	[hp]	93.3	123.1	233	356.8

Table 3.8: Power requirements of the BROL aircraft family

In addition to these rough values, other parameters such as the fuel consumption, the dry-weight, the



Time Between Overhaul (TBO) and the power-density must be considered. The possibility of using unleaded and/or lower-cost fuel (e.g. MoGas) is also taken into account in the selection. Engines that use UL fuel require indeed less periodic inspection than low-leaded ones. A trade between available engines is given in Tab. 3.9. One may note that the fuel consumption is presented in term of manufacturer nominal Brake Specific Fuel Consumption (BSFC) expressed in liters per hour per unit of power.

	Power [hp]	BSFC [l/hr/hp]	Dry weight [lb]	Turbocharger	Power density [hp/lb]
Continental IO-240	125	0.36	277.6	none	0.45
Lycoming O-360	180	0.37	258	none	0.70
Rotax 914 iS	115	0.30	140.8	up to 15000 ft	0.82
Rotax 915 iSc	141	0.32	186.4	up to 15000 ft	0.76
UL350 iS	130	0.31	173	none	0.75
UL520 iS	180	0.32	238	none	0.76

Table 3.9: Characteristic of different piston-powered engines

From the comparison of the engines characteristics given in Tab. 3.9, the Rotax[®] engines come up on top. The Rotax 914 is selected for the BROL-21, and two Rotax 915 are selected for the BROL-42. A more complete review of their specifications is given in Tab. 3.10. Both are turbocharged up to 15 000 ft, and the Rotax 915 presents a service ceiling of 23 000 ft. Moreover, thanks to manufacturer’s performance curves, the available power as well as the maximal torque and the fuel consumption were determined for the different flight regimes. It allows to assess cruise specific fuel consumption of 0.2576 l/hr/hp and 0.2252 l/hr/hp for BROL-21 and 42 engines respectively [7, 8].

	Units	Rotax 914	Rotax 915
Dry weight	[lb]	140.8	186.4
Max. takeoff power	[hp]	115 at 5 800 rpm	141 at 5 800 rpm
Max. continuous power	[hp]	100 at 5 500 rpm	135 at 5 500 rpm
Max. torque	[lbf.ft]	106	130
Gearbox ratio	[-]	2.43	2.54
Turbocharged		up to 15 000 ft	up to 15 000 ft
TBO	[hr]	2 000	1 200
Service ceiling	[ft]	/	23 000
Cruise BSFC	[l/hr/hp]	0.2576	0.2252

Table 3.10: Rotax[®] engines specifications [7, 8].



3.3.2 Propeller design

As already mentioned, a propeller has been chosen to generate thrust for both BROL-21/42. Constant speed propellers are chosen since they show several advantages. They can deliver peak performance for each phase thanks to an adjustment of the blade pitch in order to maintain a constant rotational speed. This process is automated to facilitate piloting [4]. A study is then made with the performance analysis part in order to characterise the thrust requirements for steady cruise flight and takeoff.

Finally, a deeper analysis based on the Blade Element Momentum Theory (BEMT) is conducted in order to characterise the effect of different parameters such as the blades number, diameter, airfoil, twist angle, taper and rotational velocity on the thrust and torque generated [9]. Through an iterative process, the propeller diameter as well as the rotor speed have been computed to avoid all sonic flows. Since largest velocities occur at tip, the tip speed must thereby not exceed Mach number of 0.7. In addition, the rotational velocity has been chosen such that the aircraft cruise at about 80% of the total power available for the same rotor speed. This additional constraint will allow to have enough power backup and hence flexibility in the case of maneuvers (e.g. climb or turn).

For a preliminary design, only linear twist and taper have been considered in this study. The airfoil chosen is a CLARK-Y for both aircraft. On the one hand, it reduces the manufacturing cost, and on the other hand, this airfoil has a good lift-to-drag ratio for wide range of AoA. Moreover, its well known performance allow to facilitate efficiently the whole analysis [10, 11, 12]. The use of a constant speed propeller associated with the geometric "optimisation" done with the BEMT Matlab implementation achieves cruise propeller efficiencies of $\eta_{\text{prop}} = 0.93$ for the BROL-21 and $\eta_{\text{prop}} = 0.95$ for the BROL-42 [9, 13].

A summary of the different parameters and performances for both BROL aircraft propellers is presented in Tab. 3.11. A solid CAD view is also available in Fig. 3.8.

	Units	BROL-21		BROL-42	
		Cruise	Takeoff	Cruise	Takeoff
Number of blades	[-]	3		3	
Diameter	[in]	65		67	
Root / Tip chord	[in]	6.7 / 4.33		7.28 / 5	
Ogive diameter	[in]	8.7		14.6	
RPM	[min ⁻¹]	2160	2387	2120	2283
Thrust	[lbf]	181.64	704.1	189.2	805.56
Power	[hp]	80.6	113.6	107.3	134
Torque	[lbf.ft]	80.5	102.4	102	121
Collective pitch	[°]	16	5	21	6.5
Twist	[°]	-41.4		-42	

Table 3.11: Propeller characteristics and performances (Values per engine).

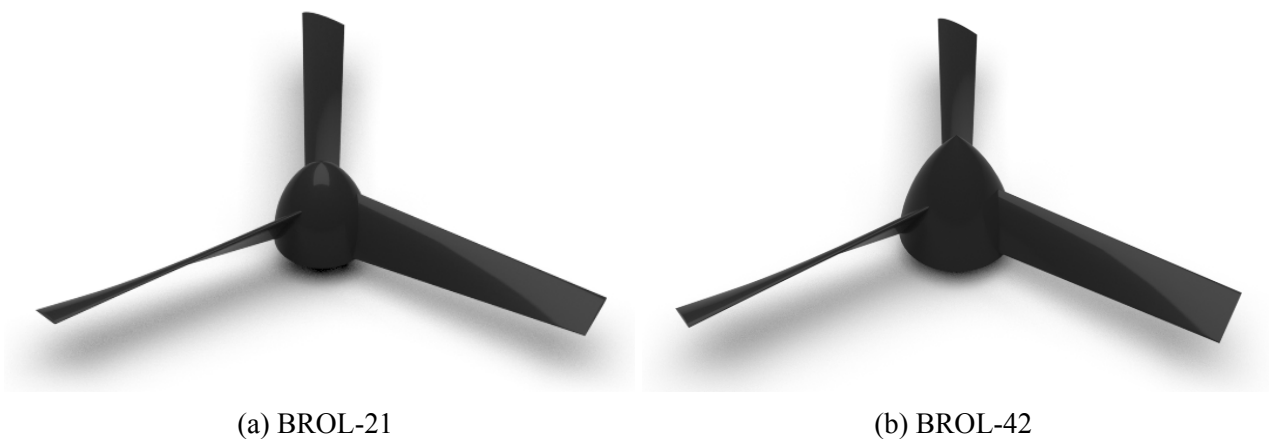


Figure 3.8: Solid CAD model of the propellers (not to scale).

3.3.3 Fuel/oil selection

According to the manufacturer Rotax, the minimum Moteur Octane Number (MON) recommended for both engines is MON 85. Hence, the unleaded fuel UL 91 in EU and UL 94 in the US are chosen. The use of unleaded fuel follows the environmental FAA recommendations which stands for a transition from Low-leaded fuel (LL) with the most commonly used 100 LL to unleaded ones [15, 14, 16]. Moreover, the Rotax 914 and Rotax 915 are also compatible with Automotive Gasoline (MoGas), which are cheaper. However, MoGas are not available everywhere although both AvGas and

MoGas require the same maintenance. Regarding the motor oil, Rotax[®] recommends to use *AeroShell Oil Sport Plus* for both Rotax 914/915. This oil is thereby chosen for both aircraft.

3.3.4 Frame integration

Fuel tank integration

The fuel tanks are integrated inside the wing as depicted in Fig. 3.9 for the BROL-42. Both aircraft show similar integration. Stainless steel is used for fuel tanks and their volume are respectively 33.73 and 67.45 US gallons for the BROL-21 and 42. Moreover, their accesses and structural integration have been thought in accordance with 14 CFR §23.963.

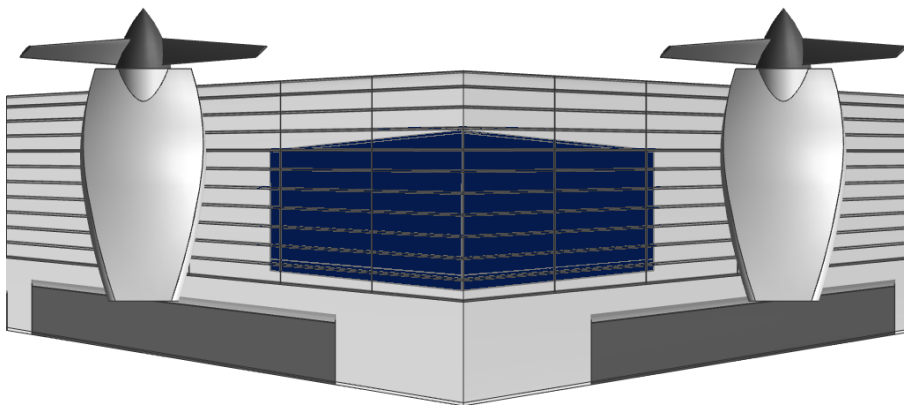


Figure 3.9: BROL-42 fuel tank integration in wing.

Engines cooling

According to the manufacturer datasheet, the engines are liquid cooled but also air cooled, which needs a design process. Downdraft cooling is chosen because of several advantages over updraft cooling, especially for single-engine in tractor configuration [4, 5]. As a matter of fact, updraft cooling dumps hot air in front of the cabin. It may lead to a heating blurring of the windshield in case of oil leaking which is unwanted in our case.

An additional study is then made to size efficiently the inlet and outlet airframes of the engine compartment, based on the cooling requirements. This design ensures a steady and continuous flow of

cold air through the compartment without over-increasing the cooling drag. The method used is the *Inlet-radiator-exit method* presented by McCormick [10]. This method considers idealised engines as a three steps system of inlet, radiator and exit. Adiabatic compression and expansion are assumed at the inlet and exit, idealised as a diffuser and a nozzle, as depicted in Fig. 3.10.

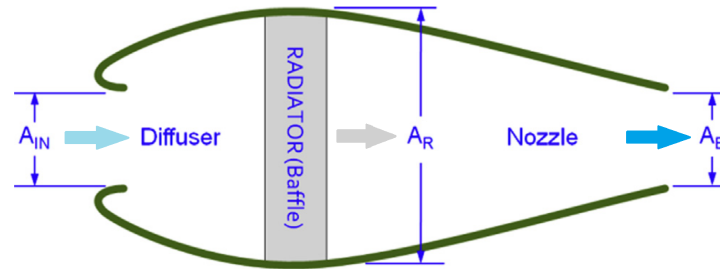


Figure 3.10: Schematics of engine idealisation used in the *Inlet-radiator-exit method* [4].

Knowledge of the heat dissipation requirement of both engine baffles and their maximum Cylinder-Head-Temperature (CHT), proper air mass flow rate through the engine compartment are determined, as well as the inlet and exit air velocities. The inlet and exhaust areas are computed based on the fluid continuity principle. The corresponding results are presented in Tab. 3.12 for the cruise condition. Solid CAD views of both engine compartments are available in Fig. 3.11 and Fig. 3.12.

	Units	BROL-21	BROL-42
Air mass flow rate	[lb/s]	3.42	3.75
Inlet area	[ft ²]	0.27	0.26
Exhaust area	[ft ²]	0.36	0.35

Table 3.12: Air-cooling properties found from the inlet-radiator-exit method during cruise condition.

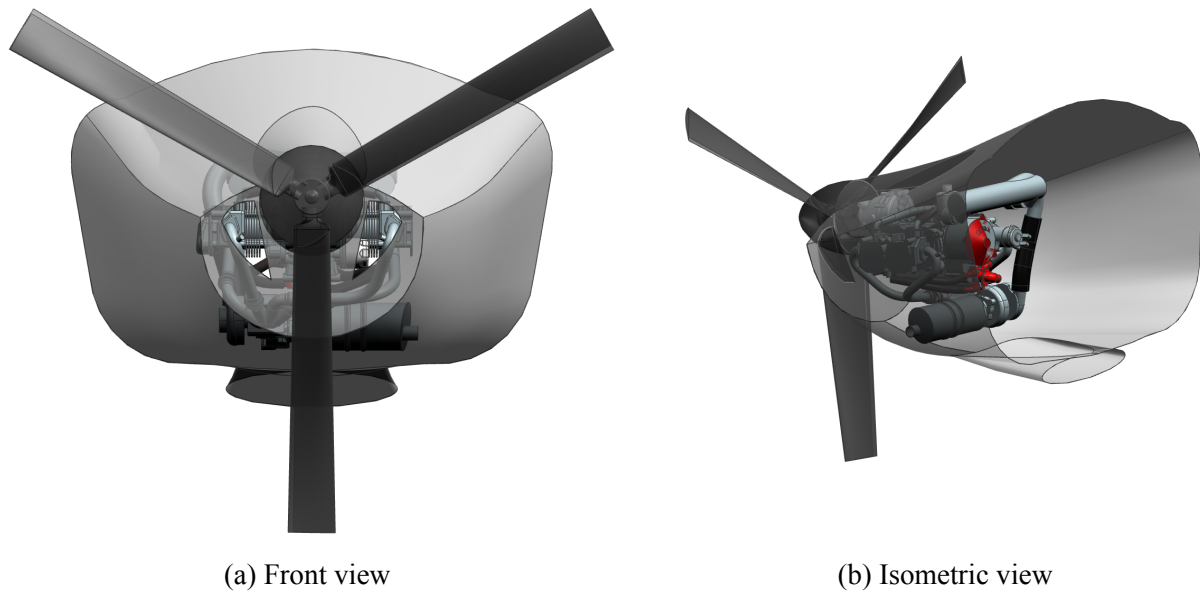


Figure 3.11: Solid CAD view of the engine compartment (in the nose) of the BROL-21 which integrates proper air intake and exhaust areas.

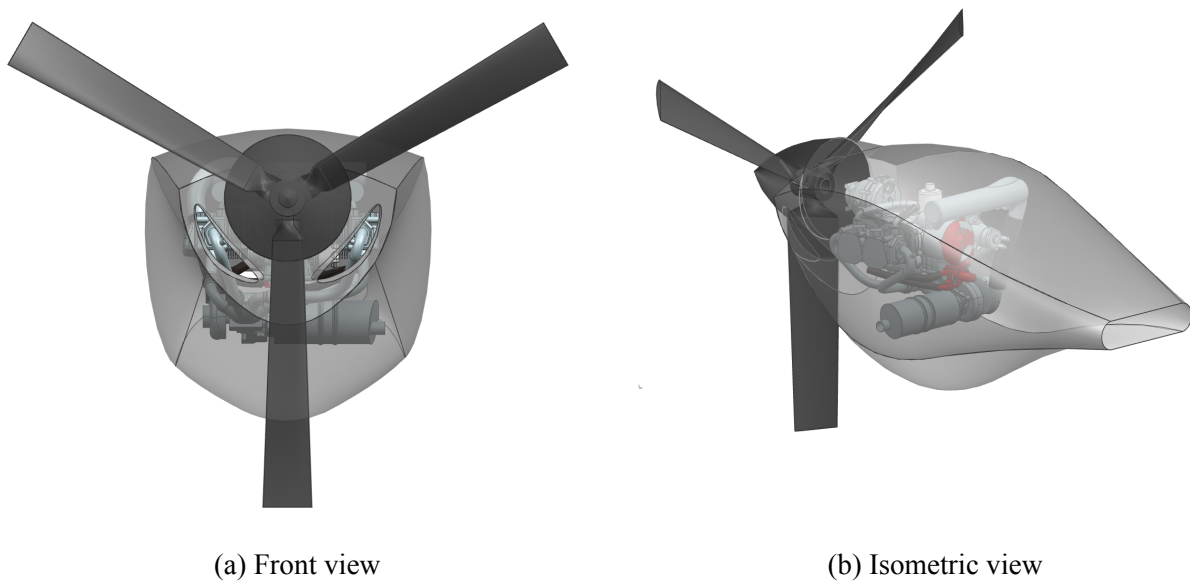


Figure 3.12: Solid CAD view of the engine compartment (in nacelles) of the BROL-42 which integrates proper air intake and exhaust areas.

3.4 Fuselage

The fuselage is the body part of the airplane, linking the lifting surfaces, the engines and providing room for the payload. In this case the payload includes the cabin, the crew, the people on board

and the potential luggage.

3.4.1 Material selection

In order to define the best-in-class material for aircraft skin and structural elements, the following material specifications are taken into account:

- Low **Price**
- Low **Crack Growth**
- Low **Density**
- High **Buckling Resistance**
- High **Fracture Toughness**
- High **Yield strength**
- Good **Corrosion Resistance**
- Good **UV Radiation Resistance**
- Good **Flammability Behaviour**

Those requirements are implemented into the CES EduPack 2018 software [17]. The analysis considers 2024 T3 aluminum alloy as optimal material. It is therefore used for wing and fuselage skin. The wing spars, stringers and ribs as well as the fuselage frames and stringers are also built using this particular aluminum alloy. Using the same material for such a large amount of components allows high reductions of production costs. The properties of interest of 2024 T3 aluminum alloy are shown in Tab. 3.13.

Property	Units	2024 T3 Aluminum
Price	\$/lb	0.86
Density	lb/in ³	0.1
0.1% Proof Stress	psi	33 600
Shear Strength	psi	21 030

Table 3.13: 2024 T3 Aluminum alloys properties

3.4.2 Shape

The shape of the fuselage is driven by the drag that it will induce. As a consequence most fuselages have an extended shape with a small cross-section to length ratio.



As in this case, the only restriction on the fuselage is to provide room for a cabin, a tadpole shape has been chosen. This shape provides small wetted and projected areas, with few material, allowing to decrease the mass of the fuselage. In the case of the BROL-21, the engine is mounted in the nose of the fuselage such that air intakes and exhausts must be taken into account while designing the outside skin. All considerations lead to the design shown in Fig. 3.13 and Fig. 3.14.

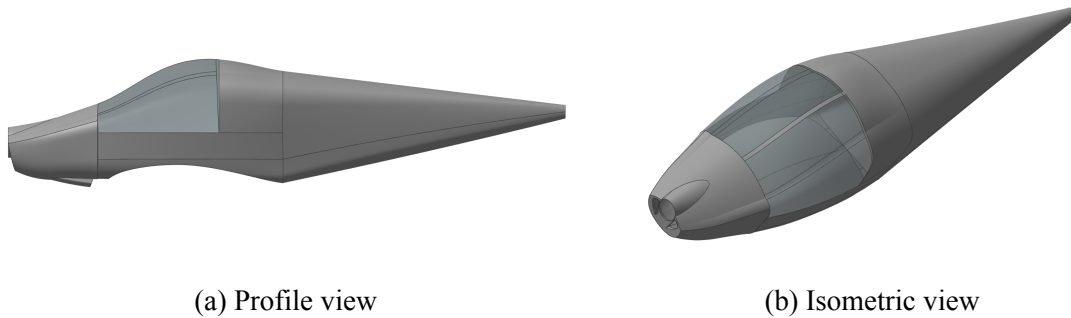


Figure 3.13: BROL-21 fuselage overview

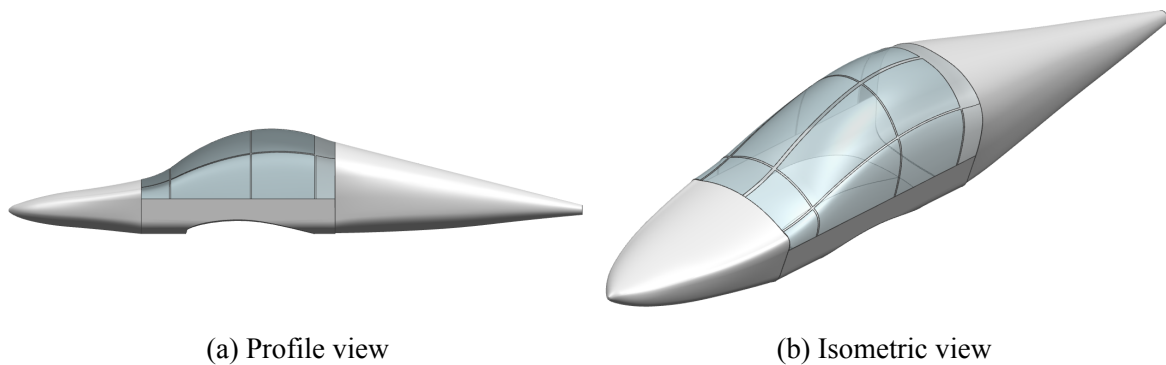


Figure 3.14: BROL-42 fuselage overview

The mass of the fuselage can be computed by taking a thickness of 0.04 in, as determined in Sec. 4.4. In order to do so, the material used for the windows has been defined on acrylic transparent plastic. The plastic windows are hold by an aluminum structure. The total mass and Center of Gravity of the whole fuselage are given in Tab. 3.14. Subdivision of mass and gravity centers between elements can be found in Tab. 3.19.

	BROL-21	BROL-42
Mass	135.77 lb	221.198 lb
CG	9.79 ft	13.48 ft

Table 3.14: Mass and CG of the BROL aircraft total fuselage



Figure 3.15: Access to the cabin

The access of the cabin is made by rotating the roof, as shown in Fig. 3.15.

3.4.3 Internal layout

The internal layout of both aircraft has to provide the best learning experience, safety and low weight. To this end, the seats have been added by rows of two, allowing to put an instructor next to the student. A console is placed in front of the seats, placing the flight instruments always in the low field of view. Controllers are placed directly between the legs, or on the central console between the seats. All controls and instruments are directly reachable by people in the front seats (usually student and instructor), to achieve the best learning atmosphere as well as to ensure safety from beginners errors. As flights may be short or long, and as the aircraft may be used by veteran pilots as well as beginners, seats with movable armrests have been chosen.

The whole cockpit is mainly surrounded by transparent plastic, decreasing the blind spots for pilot and instructor, as well as offering a great flight experience for passengers.

The passengers of BROL-42 sit in the second row of seats behind the pilot-instructor row. All seats are the same for both aircraft. This characteristic allows to easily fix, repair or replace a seat if one is broken, and reduces the manufacturing costs. The second row of the BROL-42 is vertically elevated, giving a better point of view on the controls and actions of the student (in case of an instructor taking

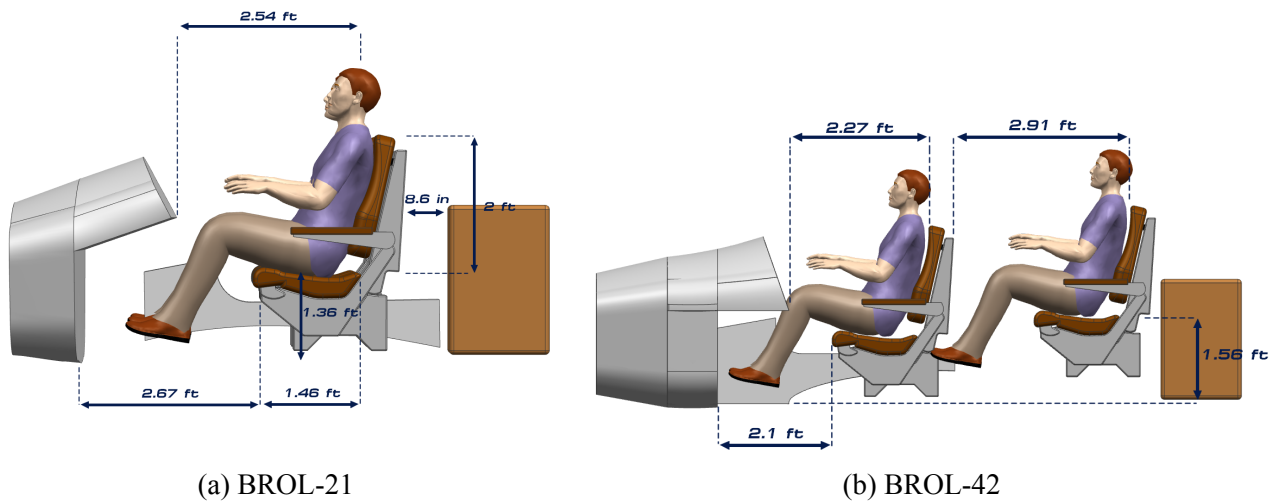


Figure 3.17: Profile view of the internal layout of the BROL aircraft family

place at the rear) and on the surroundings (for leisure passengers). The internal layouts are illustrated in Fig. 3.16 and Fig. 3.17.

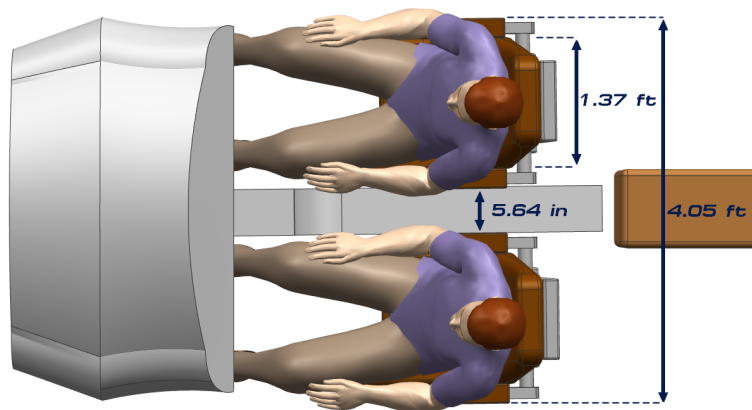


Figure 3.16: Top view of BROL-21. The BROL-42 shows similar measurements

The similarities between the two internal layouts are not a coincidence. The similar design of consoles, seats, configuration and arrangement reduces the development cost and allows to easily switch components between the two aircraft and increase the interchangeability. This versatility allows to tackle problems such as a broken seat in one aircraft. With no inter-changeable seats, the plane would be stuck on the ground for a given amount of time. However, the versatility of the BROL family allows to use a seat from one aircraft to make the other fly again. Moreover, it allows to reduce spare parts stored by the owner of the BROL family and to reduce the development cost of the aircraft.

3.5 Landing gear

The landing gear design is of paramount importance, especially for cases where the aircraft will be used for learning, including repeated phases of approach, landing and takeoff, resulting in accelerated ageing. For this reason, the landing gear needs to be stable, able to withstand "hard" landings, as well as strong and robust.

3.5.1 Material selection

The choice of landing gear material is driven by the following material characteristics:

- Low **Price**
- Low **Density**
- High **Young's Modulus**
- High **Fracture Toughness**
- High **Compressive Strength**
- Good **Corrosion Resistance**

By performing a CES [17] study that meets the listed requirements, the selected material for landing gear is AISI 4340 low alloy steel, quenched and tempered. The properties of interest of AISI 4340 low alloy steel are shown in Tab. 3.15.

Property	Units	AISI 4340 Steel
Price	\$/lb	0.32
Density	lb/in ³	0.28
Young's Modulus	kpsi	145
Compressive Strength	kpsi	145 000

Table 3.15: AISI 4340 low alloy steel properties

3.5.2 Configuration

For learning goals, a tricycle arrangement with two wheels aft of the CG and one in front is mostly used. One of the main advantage of this configuration is the stability it provides, by allowing a quite large crab angle at landing. It also increases the forward visibility which is important for learning.



The landing gear design takes into account the clearance of the wing tip in case of a 5° roll, as well as tail strike during landing or takeoff. The possibility of retract the landing gear would decrease the drag, but induces additional weight due to the mechanism. It also increases the complexity and the cost of the aircraft. On the other hand, the fixed landing gear provides more robustness and lower cost. The drag induced by the landing gear is reduced by adding streamlined fairings to the wheels. The final configuration of the BROL family is a tricycle arrangement with fixed landing gears, chosen for its robustness and adaptability to different pilot skill levels.

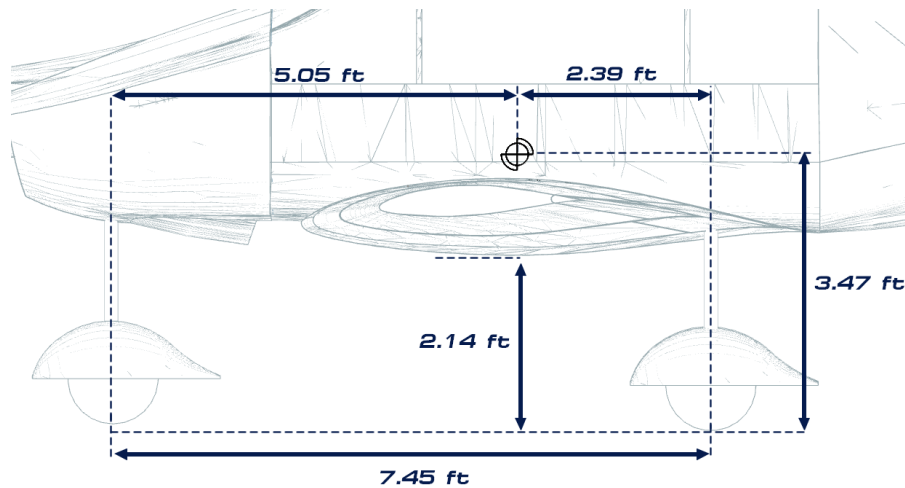
3.5.3 Geometrical layout

The wheelbase, the distance between the main and nose landing gears, is chosen such that the aircraft are stable upon different phases involving the landing gears. The geometrical layout has to ensure that the overturn angle is below 63° , that the smallest angle between the CG and the main landing gear is larger than the tailstrike angle, and that the wingtip ground clearance under a 5° roll is above 6 inches [5]. The details of the geometrical layout designed are given in Tab. 3.16

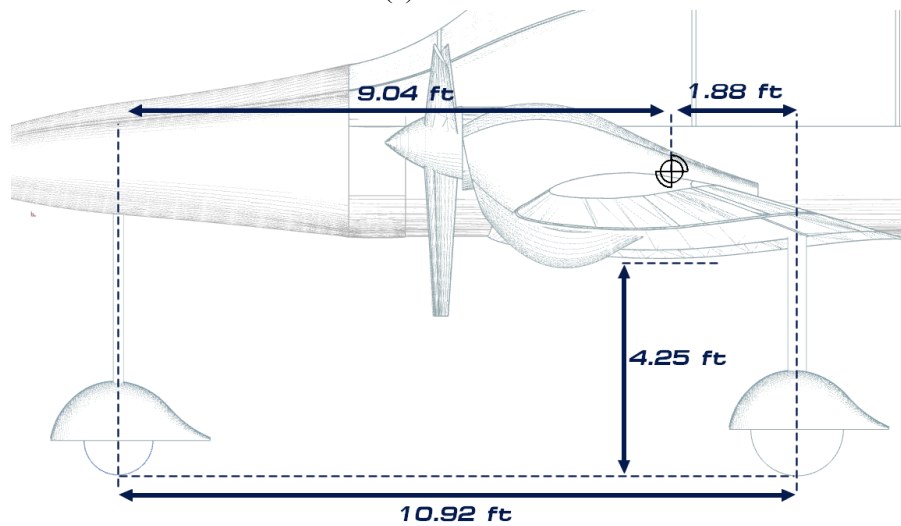
	BROL-21	BROL-42
Overturn angle ($< 63^\circ$)	61°	60°
Tailstrike angle	17°	18°
Angle between CG and main landing gear	31°	21°
Wheel track	5.2 ft	7.2 ft

Table 3.16: Geometrical parameters of the landing gear

As the wings show a positive dihedral angle and an initial height above 2 ft, the wing tip clearance is automatically fulfilled for a roll of 5° . The resulting geometrical layout is shown in Fig. 3.18.



(a) BROL-21



(b) BROL-42

Figure 3.18: Geometrical layout of the landing gear of the BROL aircraft family

3.5.4 Wheels and shock absorber

The wheels and tires are designed to withstand the loads and friction needed to land and slow down to a complete stop. To define the wheel and tire needed, the loads during takeoff and landing must be defined. The methodology from [5] has been followed to compute these loads.

Once the loads are computed, the values are compared to the data given in [5]. The smallest tire able to carry the maximum load is selected, as a smaller tire induces smaller landing gears, less drags, less wear, less weight. With this methodology, a safety margin of more than 35% is used, to ensure the suitability of the tire to almost all situations.

	BROL-21		BROL-42	
	Main	Nose	Main	Nose
Name	'5.00-4'		'18 x 4.4'	'5.00-4'
Max load	1200 lb		4350 lb	1200 lb
Inflation pressure at max load	55 psi		100 psi	55 psi
Tire width	5.05 in		4.45 in	5.05 in
Tire diameter	13.25 in		17.90 in	13.25 in
Wheel diameter	4.0 in		10.0 in	4.05 in

Table 3.17: Wheels and tires sizing for BROL aircraft

As shown in Tab. 3.17, the same tire is selected for three of the four wheels needed. Once again, this design choice increases the possibility to easily fix and replace a damaged landing gear by having only one type of tires in spare parts, and to exchange parts between both aircraft of the same family.

The role of the shock absorbers is to smooth and damp the oscillations and shocks due to landing and takeoff. The easiest and strongest design has been chosen: the solid spring gear. On the one hand, it shows a bouncy behaviour upon bad landing, may increase the wearing rate of the tires because of the lateral motion coming from the deflection of the landing gear strut, and is generally heavier than other systems. On the other hand, it presents the best robustness, manufacturing ease and cheapest cost. The system is simpler to implement and to fix, and will last longer than other systems. As the BROL aircraft are designed to carry out more takeoffs and landings than common aircraft, the robustness has been defined as the driving requirement.

3.6 Systems

3.6.1 Systems and avionics

Instruments indicate the status of the aircraft to the pilot at all times. To reduce the overall production costs, the same dashboard is used for all family members. Sections 23.1303 (Flight and navigation instruments) and 23.1305 (Powerplant instruments) of the Federal Aviation Regulation [6] list the minimum required instruments. To complete the basic instrument set and to allow day and



night flights, several components must be added. They must meet the Visual and Instrument flight rules (VFR and IFR) [6]. Those are listed in Tab. 3.18.

Required instruments	VFR/IFR instruments
Airspeed indicator	Variometer
Altimeter	Artificial horizon
Heading indicator	Position and anticollision light system (Beacon and strobe)
Fuel quantity gauge for each fuel tank	Turn indicator
Oil pressure and temperature indicator for each engine	Slip/skid indicator
Tachometer	Two-way radio communication and navigation
Oil quantity measuring device for each oil tank	Clock displaying hours, minutes, and seconds with a sweep-second pointer

Table 3.18: Instruments

Other navigational aids that use ground stations or satellites to provide reliable indications of the aircraft's position in space are inserted. The Global Navigation Satellite System (GNSS) will allow the pilot to know his position on the globe. So, a Global Positioning System (GPS) is selected. The Very-High Frequency Omnidirectional Range (VOR) is a positioning system, at short and medium distances, using very high frequencies. The onboard receiver provides a continuous indication of the magnetic bearing of the aircraft relative to a ground station and allows the aircraft to follow a magnetic track toward the beacon. The onboard equipment includes an antenna, a receiver and an indicator instrument.

An Instrument Landing System (ILS) is also installed to land in instrument flight regime. The system consists of a localizer and a glideslope providing, respectively, horizontal and vertical guidance and of marker beacons which provide distance from-the-runway information. The all-in-one GPS/Nav/Comm solution, GNS 430, of Garmin is selected.

In order to have a semi-autonomous flight, an autopilot is used. A two-axis autopilot is set and allows to control the aircraft in pitch and roll axis. The autopilot control system is shown in Fig.3.19. The Inertial Measurement Unit (IMU) sends data to the control unit. Next, the data is converted, filtered, processed and sent to the computing part, which also intercepts data from the flight controller (human interface), and sends signals to the output elements (interfaces and servo actuators). Values and



messages are displayed on the LCD screen. Actuators move the control surfaces to adjust or maintain the position of the aircraft. Finally, the pitch and roll momentum are change to keep the desired direction. An autothrottle must be integrated with the autopilot. S-TEC 3100 Digital Flight Control System (DFCS) is selected. It is suitable for both aircraft and is compatible with digital sources and displays from Garmin, Aspen and others.

To increase the fly flexibility and allow flying in known icing conditions, an ice protection system is necessary. It is designed to prevent the formation of ice, particularly on the leading edges of the wings, tailplane and propellers. This accumulation can change the shape of the wings and paralyse the control surfaces, leading to a possible decrease in lift. The selected in-flight de-icing system is based on thermoelectric strips arranged on wing, horizontal and vertical stabilizer leading edges, propellers and air data probes. It is light and does not alter the wing or empennage profile.

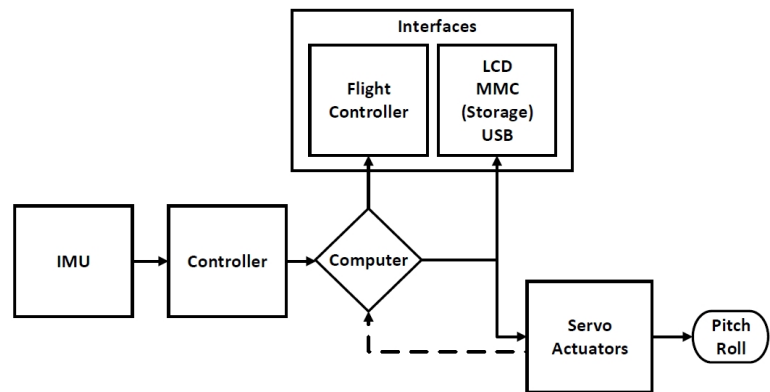


Figure 3.19: Autopilot block diagram

Hydraulic systems are only used to provide pressure to activate the wheel brakes. They provide several advantages. They are easy to install, light, compact and required little maintenance. These systems are more flexible and more robust than electrical one thanks to small pipe diameter. Electrical systems are present for starting engines and generate power.

Hydraulic systems are only used to provide pressure to activate the wheel brakes. They provide several advantages. They are easy to install, light, compact and required little maintenance. These systems are more flexible and more robust than electrical one thanks to small pipe diameter. Electrical systems are present for starting engines and generate power.

3.6.2 Control

The control of the aircraft is done with pilot controls. The main ones are the control column, the rudder pedals and the throttle. The control column acts on ailerons and regulates the aircraft's roll and pitch. Pedals are used to control yaw and the throttle impacts on the engine's power. Secondary controls are the compensators. In order to control elevator trim, a wheel is used.

Mechanical flight control systems are chosen for both aircraft because it is light, easy to maintain and cheap. Mechanical system means that the controls are connected to the control surfaces by cables and

pulleys. This is the most basic method used for light aircraft.

3.7 Weight Calculation

The initial estimation of the empty and total weight is calculated using weight fractions between the different flight configurations (takeoff, climb, cruise, descent, etc...). Those are based on historical values and are given in [5]. The obtained results are $W_{total} = 1944$ lbs and $W_{total} = 3934$ lbs for the BROL-21 and BROL-42 respectively. Using this first design gross weight estimation, a more detailed weight estimation is performed using empirical formulas also given in [5]. The final masses of the main components computed using Siemens NX software for both aircraft are displayed in Tab.3.19. The masses of the passengers are given by the FAR part 23: 170 pounds for each occupant for normal category airplanes, and 190 pounds for utility category airplanes [6]. The mass of the wing, horizontal empennage and fin include the control surfaces. This gives a Maximum Take-Off Weight (MTOW) of 3487 lbs for BROL-42 and 1816 lbs for BROL-21.



Component(s)		BROL-21		BROL-42	
		CG [ft]	Mass [lb]	CG [ft]	Mass [lb]
Fuselage	Nose	2.57	21.44	4.17	29.19
	Cockpit	7.44	28.1	11.67	37.59
	Tail	14.71	61.29	21.72	62.25
	Windshield	8.02	33.1	11.78	81.7
Lifting surfaces	Wing	7.26	333.8	12.05	552.4
	Horizontal empennage	20.85	46.6	27.47	69.66
	Fin	21.03	14.65	27.85	30.04
Landing gear	Main	9.48	96.24 (×2)	13.97	118 (×2)
	Nose	2.16	47.9	3.04	62.9
Cabin	Central console	6.3	110.2	9.1	220.5
	Frontal console	4.00	165.3	7.1	220.5
	Front seats	7.91	33.1 (×2)	11.14	33.1 (×2)
	Rear seats	/	/	14.83	33.1 (×2)
Payload	Pilot (+ front passenger)	7.48	190 (×2)	9.57	170 (×2)
	Rear passenger(s)	/	/	13.27	170 (×2)
	Furnishing	7.26	48.5	16.51	165.3
Propulsion	Engine(s)	2.26	140.8	11.14	187.4 (×2)
	Propeller(s)	0.56	10.65	9.05	9.03 (×2)
	Fuel + tank	5.89	237.2	12.31	424.4
	Nacelle			11.58	54.36 (×2)

Table 3.19: Mass and gravity centers of the main components measured from nose for both aircraft

The gravity centers of the main components calculated using the Siemens NX CAD software are shown in Fig. 3.20 and 3.21 for both aircraft. The longitudinal positions of the general gravity centers measured from nose at MTOW are at 6.98 and 12.07 feet for the BROL-21 and BROL-42 respectively.



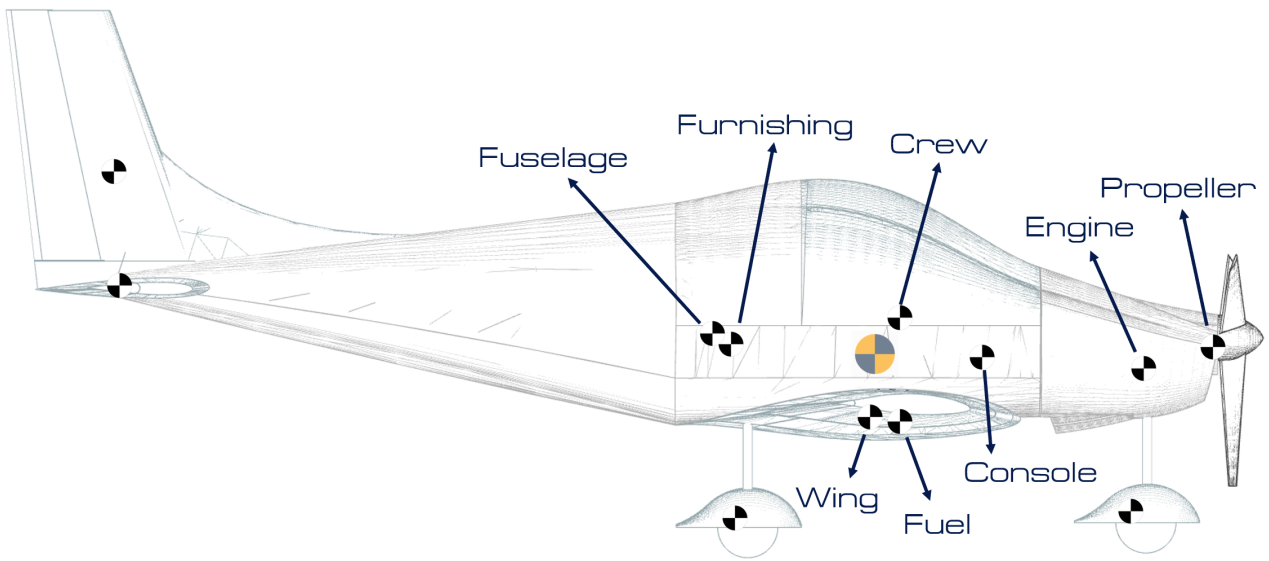


Figure 3.20: Center of gravity positions for BROL-21 at MTOW
General CG is indicated in yellow & grey

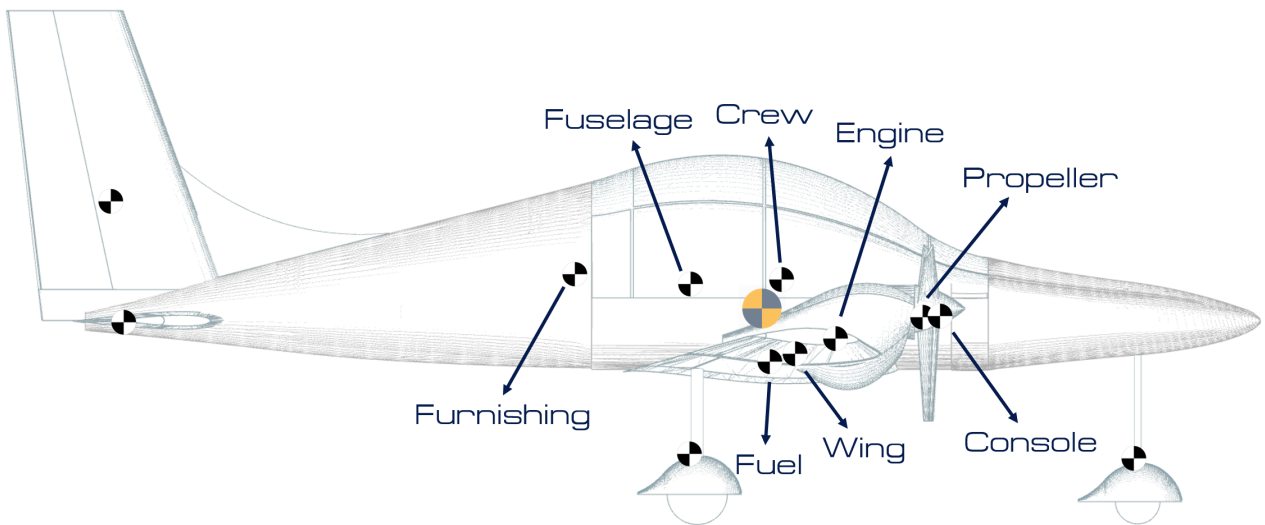


Figure 3.21: Center of gravity positions for BROL-42 at MTOW
General CG is indicated in yellow & grey

4 AIRCRAFT ANALYSIS

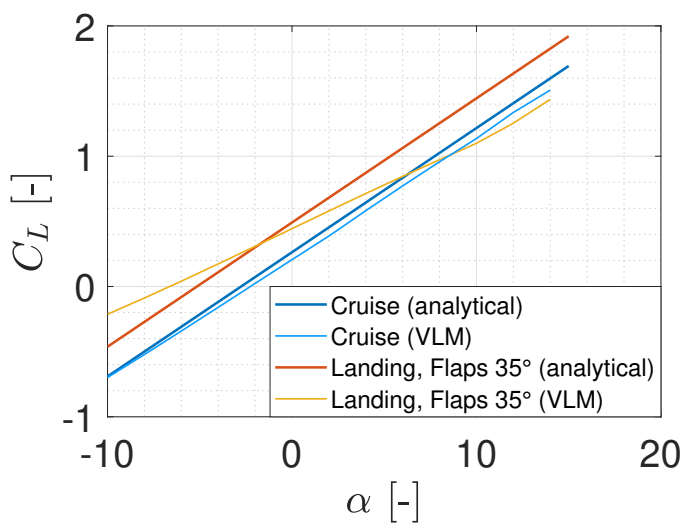
4.1 Aerodynamics

The aerodynamic analysis of the BROL aircraft family is based on two approaches:

- An analytical study of the lift and drag coefficients is performed thanks to the Raymer and Gudmundsson methodologies [4, 5].
- A numerical study using a Vortex Lattice Method (VLM) developed in [18] with a code from [19]. The results are used to validate the drag and the lift defined by the analytical study at different flight conditions. As this numerical tool is based on potential flow theory, the flow considered is inviscid.

4.1.1 Lift curve analysis

In the following section, the lift curve slope is analysed for both cruise and landing flight conditions and for both aircraft. As all the methodologies proposed by Raymer [5] and Gudmundsson [4] as well as the VLM take into account inviscid flow, the part near the stall angle (13.5°) can not be trusted. The takeoff lift curve coincides with the cruise curve as no flaps are deployed.



BROL-21		
Cruise	VLM	Analytical
$\alpha = 0 [^\circ]$	0.27	0.24
$\alpha = 13.5 [^\circ]$	1.42	1.51
$C_{L\alpha} [-]$	5.07	5.15
Landing	VLM	Analytical
$\alpha = 0 [^\circ]$	0.44	0.49
$\alpha = 13.5 [^\circ]$	1.40	1.78
$C_{L\alpha} [-]$	3.89	5.15

Figure 4.1: Value of the lift coefficient at given angles of attack computed with VLM and the analytical method. The comparison is done only with BROL-21 as BROL-42 shows the same behaviour.

Fig. 4.1 shows a good match between the lift coefficient slopes at cruise conditions computed analytically and numerically. In the other hand, the lift coefficient slope at landing conditions calculated with VLM shows spurious behaviours such as a different slope and lower lift coefficients at higher angles of attack. Hence, the results of VLM for landing considerations (with flaps) will not be taken into consideration for the next analysis.

4.1.2 Drag determination

To perform the analysis, the drag is separated in two parts, the parasite drag and the induced drag: $C_D = C_{D_0} + C_{D_i}$. Fig. 4.2 illustrates the total drag breakdown and the subdivision between the different drag sources. The parasite drag is splitted into the profil drag, the miscellaneous drag and the leakage and protuberance drag. Due to the inviscid hypothesis of VLM, the parasite drag, which is due to viscous effects, is only developed analytically while the induced drag, which is created by the lift, is compared with the numerical tool.

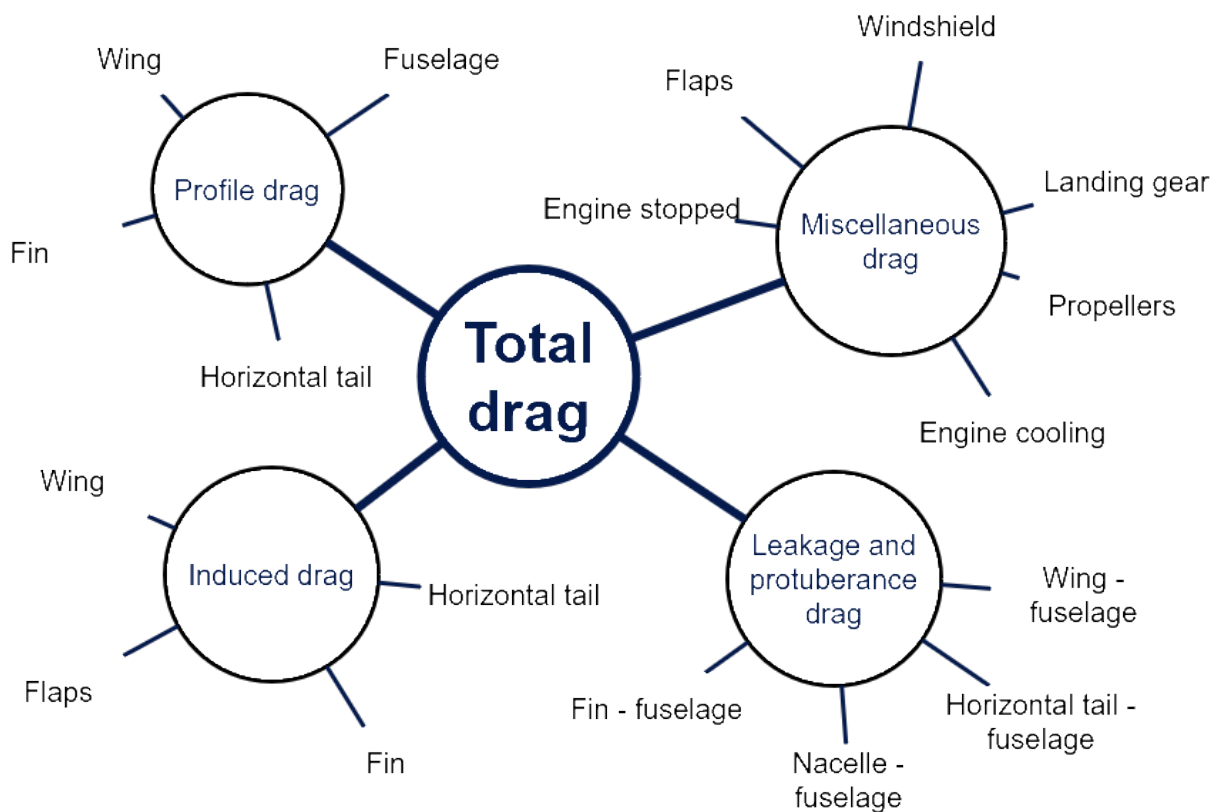


Figure 4.2: Diagram of the drag calculation.

A. Parasite drag

A component buildup method [5] is applied to estimate the subsonic¹ parasite drag of the aircraft:

$$(C_{D_0})_{\text{subsonic}} = \frac{\Sigma (C_{f_\epsilon} FF_c Q_c S_{\text{wet}_c})}{S_{\text{ref}}} + C_{D_{\text{misc}}} + C_{D_{L\&P}} \quad (4.1)$$

First, the profile drag of each component is computed. It is composed by the flat-plate skin-friction coefficient (C_{f_ϵ}), the form factor (FF) (estimating the pressure drag due to viscous separation) and the interference effects on the component drag (Q), multiplied by the ratio between the wetted surface, given in Tab. 4.1, and the reference surface of the wing, given in Sec. 3.1.1. The skin friction coefficient can be derived analytically:

$$C_f^{\text{lam}} = \frac{1.628}{\sqrt{\text{Re}}} \quad \text{and} \quad C_f^{\text{turb}} = \frac{0.455}{(\log_{10} \text{Re})^{2.56} [1 + 0.144M^2]^{0.65}} \quad (4.2)$$

where the Reynolds number depends on the component. For the fuselage where the skin surface is relatively rough, a fictitious cutoff Reynolds number [5] that increases the turbulent friction coefficient C_f^{turb} is determined:

$$R_{\text{cutoff}} = 38.21(\ell/k)^{1.053} \quad (4.3)$$

where ℓ is the characteristics length and k is a skin roughness value equals to $2.08e - 5$ for smooth paint surface. Finally, the wing skin friction drag is computed as a weight sum of the laminar and turbulent coefficients while the other components are computed only with the turbulent coefficient. Hence, the transition needs to be taken into account for the wing. After computation with the software Xfoil, it can be found that $x^{\text{tr}} = 0.55$ (normalized by the chord) for both aircraft. Since this value seems optimistic and can hardly be obtained in a real flight, a value of $x^{\text{tr}} = 0.25$ is used for both aircraft. The form factor and the interference effects are simply computed using the formulas given in [5].

The next term, the miscellaneous drags ($C_{D_{\text{misc}}}$), represents the special features of the aircraft such as the windshield and the landing gears. This drag is mostly based on the drag area of the compo-

¹As the aircraft operate in low subsonic regime, no wave-drag and compressibility effects are taken into account.



ment, found in [4] and [5], and the projected area computed from the drawing and given in Tab. 4.1. Finally, the last term estimates the contributions to the parasite drag from the leakage and protuberances ($C_{D_{L\&P}}$). Their contribution is estimated to be 5% of the entire drag for a propeller aircraft [5]. Tab. 4.3 gives the different drag contributions.

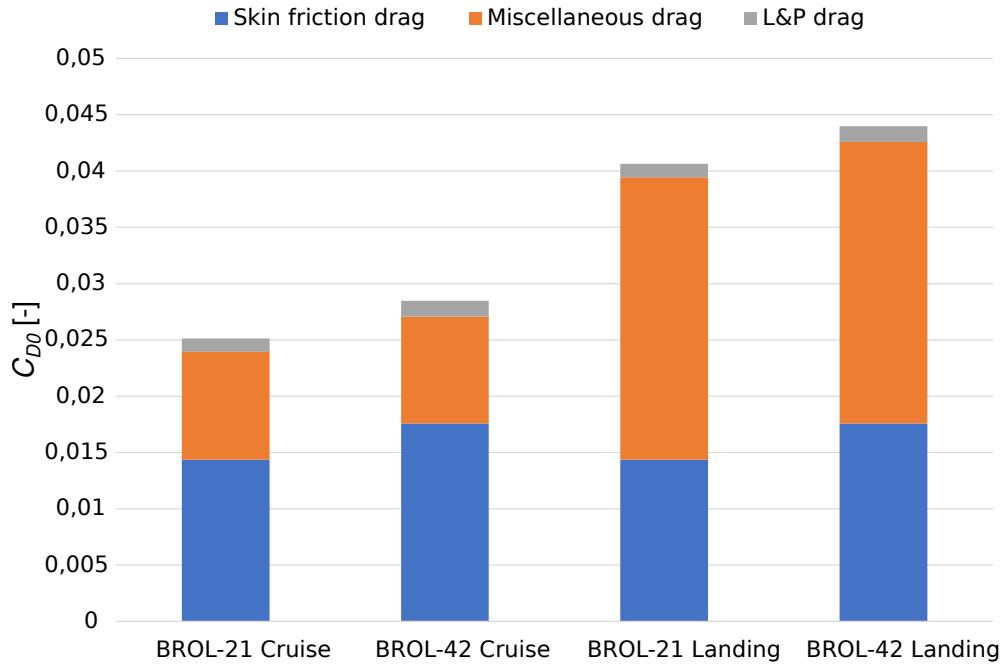


Figure 4.3: Component buildup method applied to the BROL family. Two cases are taken into consideration, flight at cruise without flaps and with flaps for BROL-21 and BROL-42.

At cruise conditions, the highest contributor to the parasite drag is the skin friction drag and especially the one due to the wing. Without flaps, the landing gears are the major contributors to the miscellaneous drag. Their contribution could be reduced by using retractable landing gears but the goal of the BROL family is to propose the simplest aircraft possible. However, the flaps become the highest contributor when they are deployed. Hence, the major part of the drag is the miscellaneous one. Finally, Tab. 4.3 gives the value of $C_{D_0} = 0.0248$ at cruise for BROL-21 and $C_{D_0} = 0.0284$ for BROL-42. Tab. 4.1 gives the main wetted and projected area used to compute the profile and miscellaneous drag for both aircraft.

	Wetted Area [ft ²]			Projected Area [ft ²]	
	BROL-21	BROL-42		BROL-21	BROL-42
Wing	232	422	Windshield	7.68	10.85
Fuselage	189	297	Main landing gear	2.53	3.6
Horizontal tail	63	88	Nose landing gear	1.27	1.37
Vertical tail	28	60			

Table 4.1: Distribution of wetted and projected area for the main components of BROL-21 and BROL-42.

B. Induced drag

The induced drag is computed using a modified quadratic model based on the Oswald's efficiency factor (e) which takes into account the lift coefficient at the minimum drag ($C_{L_{\text{mind}}}$) in order to enhance the physics of the model [4]:

$$C_D = C_{D_0} + \frac{1}{\pi AR e} \cdot (C_{L_{\text{mind}}} - C_L)^2 \quad \text{where} \quad e = 1.78 \cdot (1 - 0.45 \cdot AR^{0.68}) - 0.64 \quad (4.4)$$

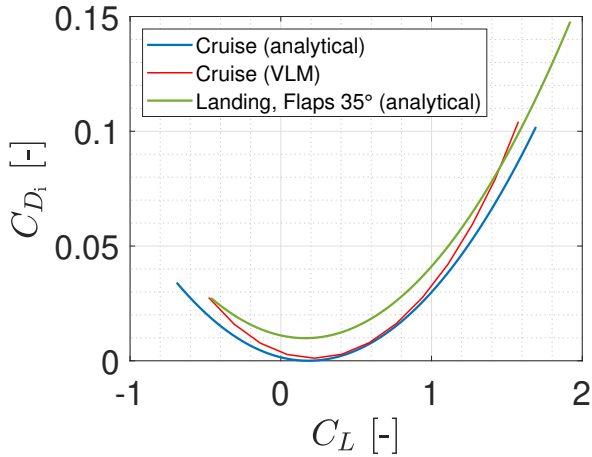
The idea is to validate this model with the Vortex Lattice Method. Since the latter does not use viscous properties, the numerical results are shifted to consider the lift coefficient at minimum drag avoiding a minimum induced drag at zero lift coefficient. Two main parts of the aircraft generate induced drag: the wing and the horizontal tail. The induced drag produced by the fuselage is negligible. Moreover, there is no induced drag produced by the vertical tail for the considered flight conditions as it provides no lift. Tab. 4.2 summarizes the different values to compute the induced drag of the main components:

	BROL-21			BROL-42		
	$C_{L_{\text{mind}}}$	AR	e	$C_{L_{\text{mind}}}$	AR	e
Wing	0.276	7.2	0.833	0.289	7.8	0.8162
Horizontal tail	0	5	0.9	0	5	0.9

Table 4.2: Value of the aspect ratio (AR) and the Oswald's efficiency factor for the wing and the horizontal tail for BROL-21/42.

In the case of the horizontal empennage, the lift coefficient is normalised with respect to the ratio between the tail and the wing area. Fig. 4.3 shows the drag polar of BROL-21. BROL-42 behaves

similarly, thus it is not shown here. Moreover, the comparison between VLM and the analytical model shows a good match between the results. The induced drag computed with VLM at cruise conditions equals 0.0015 (at $C_L = 0.268$) for BROL-21 and 0.0013 (at $C_L = 0.24$) for BROL-42.



BROL-21			
	C_L [-]	C_D [-]	
		VLM	Analytical
Takeoff	1.18	0.051	0.044
Climb	1.057	0.036	0.034
Cruise	0.268	0.0015	0.0004
Approach	1.4	/	0.08

Table 4.3: Comparison between the induced drag computed by VLM and the analytical model. The stars are flight conditions computed with VLM.

4.1.3 Drag polar and Lift-to-drag ratio

Fig. 4.4 shows the drag polars, computed numerically for cruise conditions and analytically for landing conditions as explained in Sec. 4.1.1, of the BROL family. From these polars, the various drag coefficients for different flight conditions can be deduced.

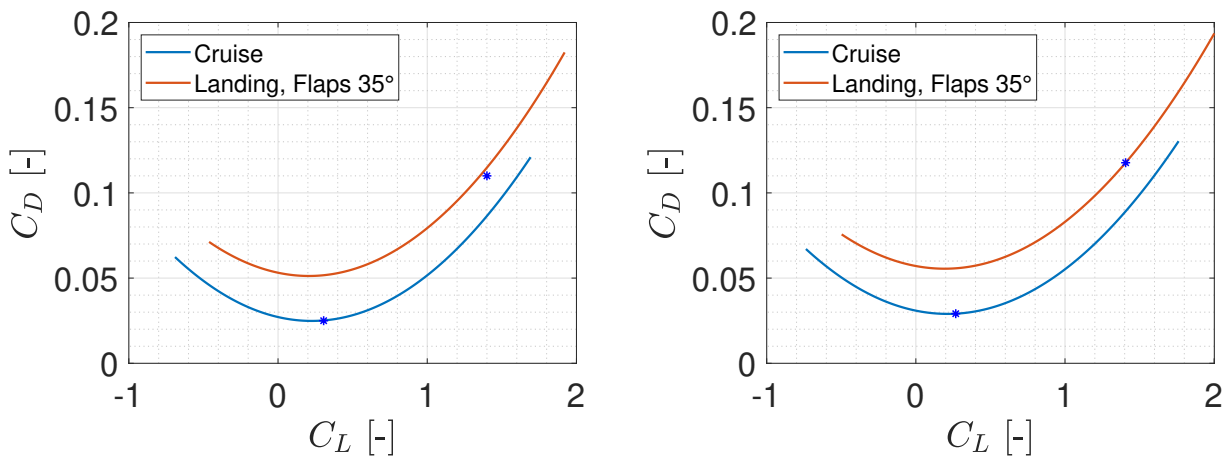


Figure 4.4: Drag polar for BROL-21 (left) and BROL-42 (right) at cruise and landing conditions. The stars represents the cruise flight and the approach.



Finally, the total drag coefficient varies from 0.02615 at cruise to 0.115 during the approach due to the deployment of the flaps for BROL-21. Similarly, it varies from 0.029 to 0.117 for BROL-42.

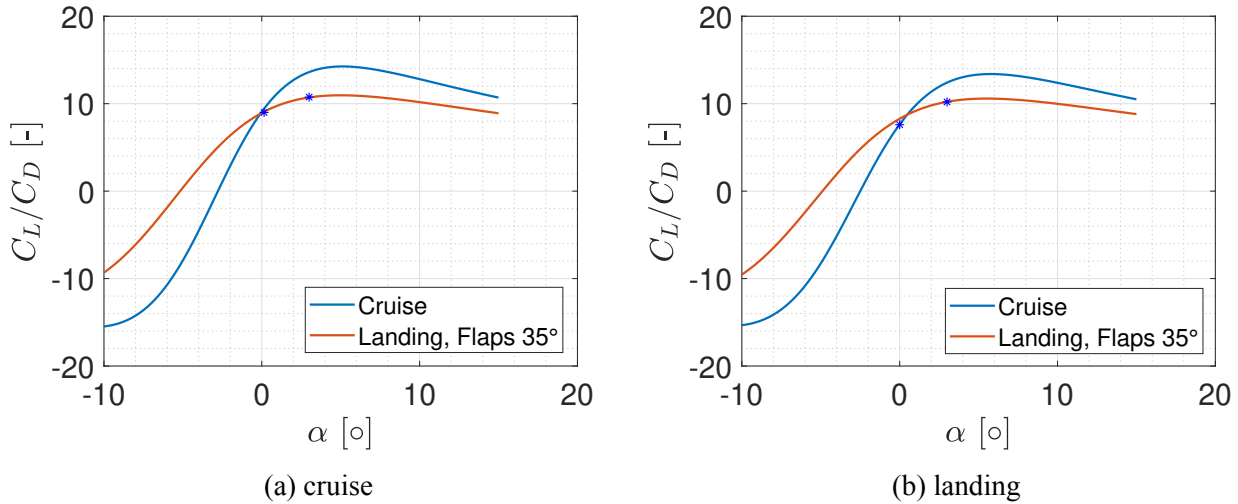


Figure 4.5: Lift-to-drag ratio for BROL-21 (left) and BROL-42 (right) at cruise and landing conditions.

Fig. 4.5 shows the variation of the lift-to-drag ratio computed similarly to the drag polars. The maximum lift-to-drag ratio is equal to 14 for BROL-21 and 13.2 for BROL-42. Finally, a deeper drag analysis should be performed in the next step of the design. As the computation is done with a quadratic model, the drag bucket of the airfoil is not taken into account during this analysis. The consequence of the drag bucket could be to reduce the drag coefficient and thus, increase the lift-to-drag ratio.

4.2 Static stability

4.2.1 Longitudinal Stability

The static stability is computed using the wind axis system following Daniel P. Raymer's methodology [5]. The longitudinal stability is characterised by the Static margin K_n defined as the distance between the neutral point and the aircraft center of gravity normalised by the MAC:

$$K_n = \bar{X}_{np} - \bar{X}_{cg} = -\frac{C_{m\alpha}}{C_{L\alpha}}$$

where \bar{X} denotes a distance measured from nose normalised by the MAC. The aircraft are designed to obtain results in the range $K_n \in [5 - 15]\%$ for enough maneuverability and stability according to the FAR Part 23[6].

Neutral point

The neutral point is estimated by considering the contribution of the wings, fuselage and horizontal empennage using:

$$\bar{X}_{np} = \frac{C_{L\alpha} \bar{X}_{acw} - C_{m_{\alpha, fus}} + \eta_h \frac{S_h}{S_w} C_{L\alpha_h} \left(1 - \frac{d\epsilon}{d\alpha}\right) \bar{X}_{ach}}{C_{L\alpha} + \eta_h \frac{S_h}{S_w} C_{L\alpha_h} \left(1 - \frac{d\epsilon}{d\alpha}\right)} \quad (4.5)$$

Where $C_{m_{\alpha, fus}}$ is the pitching moment derivative contribution of the fuselage. η_h is the horizontal empennage efficiency, set at 0.9 (typical value [5]). S_w and S_h are the reference surfaces of the wing and horizontal empennage respectively. The aerodynamic center of the wing X_{acw} has been extracted from VLM [19] and lies at 6.88 and 11.64 feet from the nose for BROL-21 and BROL-42 respectively. For the horizontal empennage (X_{ach}) it is estimated at the quarter chord (symmetrical airfoil). The downwash derivative has been estimated at $\frac{d\epsilon}{d\alpha} = 0.43$.

Static margin

The aircraft's center of gravity can be obtained from the CAD drawing (cfr. Section 3.7) and varies depending on the amount of fuel and number of persons on board. The propeller disk produces a vertical force due to the turning of the freestream airflow. To account for this destabilising effect, every mean aerodynamic chord length that the propeller is ahead of the center of gravity the static margin is reduced by 2% [5]. In Fig. 4.6 and 4.7, the most aft and fwd center of gravity positions are plotted for the BROL-21 and BROL-42 aircraft respectively. For the BROL-21, the most fwd position of the center of gravity is obtained when the airplane carries no passengers (pilot included) nor fuel whereas the most aft position is computed using a completely filled fuel tank and the maximum number of persons (2) allowed on board. Concerning the BROL-42, the most fwd center of gravity position corresponds to the aircraft with the two front passengers on board and the maximum amount of fuel.



The most aft position is the case where nobody is on board and the fuel tanks are empty. This defines the range of the static margin for both aircraft.

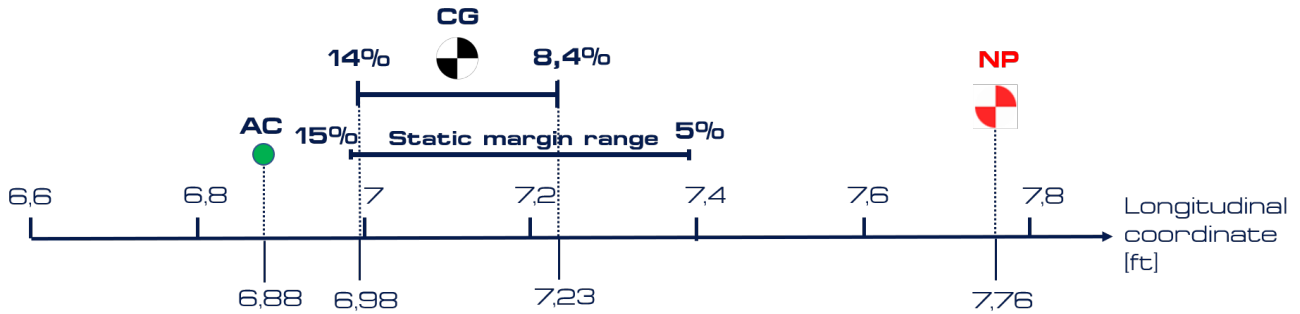


Figure 4.6: Static margin range for BROL-21. In green is the aerodynamic center position

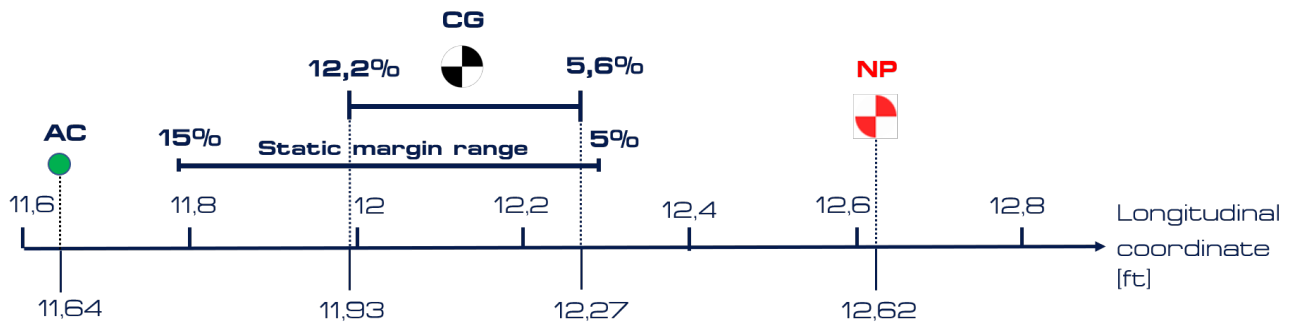


Figure 4.7: Static margin range for BROL-42. In green is the aerodynamic center position

4.2.2 Directional stability

Directional stability is the tendency of the aircraft to return to its original direction in relation to the freestream. This describes the stability in yaw. The requirement for directional static stability can be expressed mathematically as:

$$C_{n_\beta} = \frac{\partial C_n}{\partial \beta} > 0 \quad \text{and} \quad C_n = 0 \quad \text{if} \quad \beta = 0 \quad (4.6)$$

Where C_{n_β} is the yawing moment derivative with respect to the sideslip angle β . The contribution of the wings, fuselage and fin are summed up to obtain the total yaw moment derivative:

$$C_{n_\beta} = C_{n_{\beta,w}} + C_{n_{\beta,fus}} + C_{n_{\beta,vt}} \quad (4.7)$$



These contributions have been computed following the Torenbeek methodology [20]. As the aircraft have low mounted wings, the wing contribution $C_{n_{\beta,w}}$ is set to 0.024. The fuselage causes a destabilising yawing moment ($C_{n_{\beta,fus}}$) of -0.047 and -0.053 for the BROL-21 and BROL-42 respectively. The fin is designed in order to acquire a sufficient stabilising contribution in order to be in the range of $0.03 - 0.1$ which are typical values for general aviation. This gives a total directional stability of $C_{n_{\beta}} = 0.051$ for the BROL-21 and $C_{n_{\beta}} = 0.099$ for the BROL-42.

4.2.3 Lateral stability

Finally, lateral stability can be analysed. Lateral stability requires sideslip or yaw, and not roll itself, to be corrected. This is called the dihedral effect. The requirement for the aircraft to be laterally stable is mathematically expressed as:

$$C_{l_{\beta}} = \frac{\partial C_l}{\partial \beta} < 0 \quad \text{and} \quad C_l = 0 \quad \text{if} \quad \beta = 0 \quad (4.8)$$

The arm Z_v between the general center of gravity and the CG of the fin is approximated as half its span. The total moment derivative in roll is obtained by summing the contribution of the vertical tail and the dihedral effect:

$$C_{l_{\beta}} = -\frac{2}{3\pi} C_{L_{\alpha,w}} \Gamma + C_{l_{\beta,vt}} \quad (4.9)$$

where $C_{l_{\beta,vt}}$ is the fin contribution:

$$C_{l_{\beta,vt}} = -C_{L_{\alpha,vt}} \frac{Z_v S_{vt}}{b_w S_w} \quad (4.10)$$

Considering a dihedral of 3° for both aircraft, we obtain $C_{l_{\beta}} = -0.075$ and $C_{l_{\beta}} = -0.104$ respectively.



4.3 Dynamic stability

This section discusses the aircraft attitude and stability to control inputs by the pilot. The aerodynamic and control stability derivatives are estimated following the lecture notes from the Flight Dynamics and Control course [21]. These values are compared to the results obtained with Aircraft Design Software (ADS) from the Optimal Aircraft Design (OAD) company. The linearised system of equations of motion for longitudinal and lateral stability are solved for both aircraft. As the aircraft geometry is symmetric, longitudinal and lateral stability can be decoupled. The results below are computed at cruise conditions (max payload, half fuel weight).

4.3.1 Stability derivatives

The values of the stability and control derivatives for both aircraft are displayed in Tab. 4.4 and 4.5.

Longitudinal			Lateral		
	Lecture notes	ADS		Lecture notes	ADS
$C_{L\alpha}$	5.66	5.29	$C_{n\beta}$	0.052	0.075
$C_{D\alpha}$	0.188	0.295	$C_{l\beta}$	-0.075	-0.008
$C_{M\alpha}$	-0.772	-0.683	$C_{y\beta}$	-0.223	-0.357
C_{Lu}	0.636	0.012	C_{np}	-0.041	-0.037
C_{Du}	0.061	0.004	C_{lp}	-0.365	-0.446
C_{Mu}	0.0126	0.00	C_{yp}	-0.03	-0.065
C_{Lq}	7.43	5.93	C_{nr}	-0.086	-0.084
C_{Dq}	0	0	C_{lr}	0.113	0.097
C_{Mq}	-14.68	-15.01	C_{yr}	0.10	0.20
$C_{L\dot{\alpha}}$	2.06	1.88	$C_{n\xi}$	-0.013	-0.008
$C_{D\dot{\alpha}}$	0	0	$C_{l\xi}$	0.317	0.185
$C_{M\dot{\alpha}}$	-5.63	-5.34	$C_{y\xi}$	0.000	0.000
$C_{L\eta}$	0.1084	0.42	$C_{n\zeta}$	0.044	-0.053
$C_{D\eta}$	0.000	0.015	$C_{l\zeta}$	-0.007	0.006
$C_{M\eta}$	-0.298	-1.2	$C_{y\zeta}$	-0.108	-0.053

Table 4.4: Dynamic stability and control derivatives for the BROL-21



The results from the lecture notes methodology are quite close to what is given by ADS, except for some derivatives such as the longitudinal speed derivatives. This is because ADS is based entirely on Roskam's presentation of the USAF DATCOM methodology [22], which ignores the effect of the trimmed lift and drag values on the longitudinal speed derivatives. On the contrary, the lecture notes methodology [21] includes these terms. An additional explanation for the differences is that ADS does not output the exact same aircraft parameters. For example, the wing and empennage are at a slightly different position.

Longitudinal			Lateral		
	DATCOM	ADS		DATCOM	ADS
$C_{L\alpha}$	5.90	5.46	$C_{n\beta}$	0.114	0.17
$C_{D\alpha}$	0.194	0.299	$C_{l\beta}$	-0.104	-0.10
$C_{M\alpha}$	-0.55	-0.59	$C_{y\beta}$	-0.36	-0.58
C_{Lu}	0.672	0.023	C_{np}	-0.058	-0.039
C_{Du}	0.07	0.004	C_{lp}	-0.382	-0.448
C_{Mu}	0.013	0.00	C_{yp}	-0.078	-0.164
C_{Lq}	7.63	6.23	C_{nr}	-0.152	-0.159
C_{Dq}	0	0	C_{lr}	0.133	0.101
C_{Mq}	-17.4	-17.7	C_{yr}	0.184	0.38
$C_{L\dot{\alpha}}$	2.37	2.18	$C_{n\xi}$	-0.012	-0.006
$C_{D\dot{\alpha}}$	0	0	$C_{l\xi}$	0.323	0.146
$C_{M\dot{\alpha}}$	-6.77	-6.48	$C_{y\xi}$	0.000	0.000
$C_{L\eta}$	0.123	0.49	$C_{n\zeta}$	0.042	-0.094
$C_{D\eta}$	0.000	0.018	$C_{l\zeta}$	-0.009	0.013
$C_{M\eta}$	-0.349	-1.44	$C_{y\zeta}$	-0.109	0.214

Table 4.5: Dynamic stability and control derivatives for the BROL-42

The stability derivatives are used to construct the linearised equations of motion of the aircraft in matrix form:

$$\dot{\mathbf{x}} = \mathbf{A}\mathbf{x} + \mathbf{B}\mathbf{u} \quad (4.11)$$

where \mathbf{A} is the system state matrix and \mathbf{B} is the input matrix. For longitudinal stability, the vector \mathbf{x} and control input \mathbf{u} are defined as $\mathbf{x} = [u \ w \ q \ \theta]^\top$ and $\mathbf{u} = [\eta \ \tau]^\top$ where η and τ are the elevator deflection and thrust perturbation respectively. For the lateral stability they are defined as $\mathbf{x} = [v \ p \ r \ \varphi \ \psi]^\top$ and $\mathbf{u} = [\xi \ \zeta]^\top$ where ξ and ζ are the aileron and rudder deflections respectively. The poles of



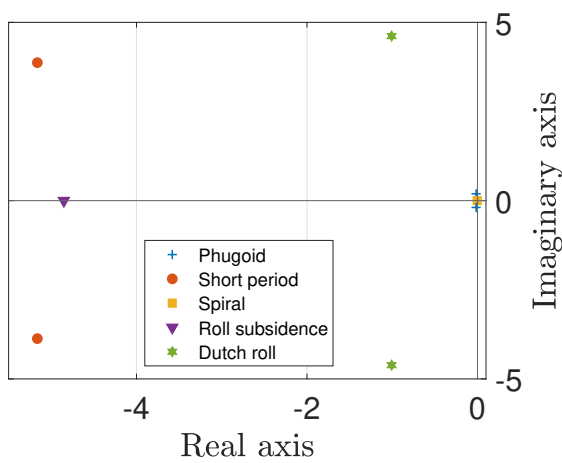
the two aircraft are displayed in Tab. 4.6 and 4.7 and are plotted in Fig 4.8.

Longitudinal	Lateral
$-0.0158 + 0.191 i$	$0.0000 + 0.000 i$
$-0.0158 - 0.191 i$	$-0.0036 + 0.000 i$
$-5.163 + 3.870 i$	$-4.852 + 0.000 i$
$-5.163 - 3.870 i$	$-1.007 \pm 4.615 i$

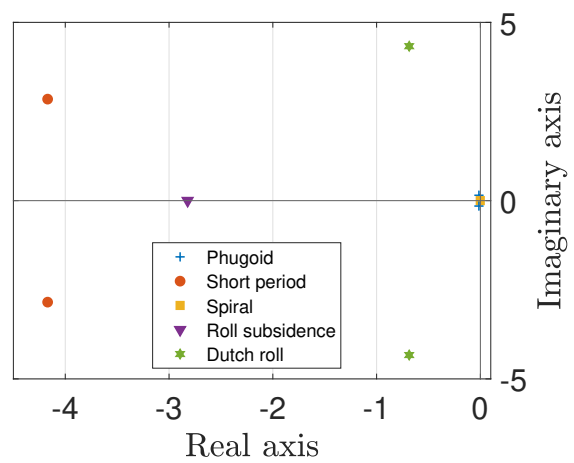
Table 4.6: Eigenvalues of A for BROL-21

Longitudinal	Lateral
$-0.014 + 0.151 i$	$0.0000 + 0.000 i$
$-0.014 - 0.151 i$	$-0.0012 + 0.000 i$
$-4.17 + 2.847 i$	$-2.821 + 0.000 i$
$-4.17 - 2.847 i$	$-0.686 \pm 4.331 i$

Table 4.7: Eigenvalues of A for BROL-42



(a) BROL-21



(b) BROL-42

Figure 4.8: Eigenvalues of A and their corresponding mode

4.3.2 Longitudinal modes

From the poles of the longitudinal equations, two modes can be deduced. The Phugoid mode is a very large period oscillation with low damping. On the contrary, the short period oscillation mode is a highly damped motion of the aircraft. The frequencies and damping ratio's corresponding to each of the two modes and for both aircraft are displayed in Tab. 4.8 and 4.9.

	ω_n	ζ
Phugoid	0.192	0.082
Short-period	6.45	0.80

Table 4.8: BROL-21

	ω_n	ζ
Phugoid	0.151	0.092
Short-period	5.05	0.826

Table 4.9: BROL-42



4.3.3 Lateral modes

The different lateral modes can be extracted from the non-zero eigenvalues of A . First, the non oscillatory roll subsidence mode is a high damping mode and corresponds to the most negative real eigenvalue. Next, the spiral mode is a low damping mode. This corresponds to the real eigenvalue with a lower amplitude. Finally, the complex conjugate eigenvalues correspond to the dutch roll. The frequencies and/or damping ratios of each mode are displayed in Tab. 4.10 and 4.11.

	ω_n	ζ
Roll subsidence	/	1.0
Spiral mode	/	1.0
Dutch roll	4.72	0.213

Table 4.10: BROL-21

	ω_n	ζ
Roll subsidence	/	1.0
Spiral mode	/	1.0
Dutch roll	4.38	0.156

Table 4.11: BROL-42

4.4 Structure

The following structural analysis aims to select appropriate fuselage and wing structural elements. For this purpose, aerodynamic loads are computed while considering critical flight conditions presented through flight envelopes. On the other hand, the shear forces, bending moments and torques generated by aircraft components distribution are estimated with the help of CAD models provided by the Siemens NX software.

In the scope of this analysis, the considered material for structural elements is 2024 T3 age-hardening aluminum alloy. The properties of 2024 T3 alloys are illustrated in Tab. 3.13. Maximum pitching moment $\ddot{\theta}$ and maximum yaw angle ψ being highly complex to estimate at this level of aircraft design, their values are respectively fixed to $60 \text{ }^\circ/\text{s}^2$ and 20 ° .



4.4.1 Flight envelopes

The various flight configurations encountered by the aircraft are represented through flight envelopes. Fig. 4.9 presents the BROL-21 trainer flight envelope. The maneuver envelope (drawn in dark blue) shows the extreme load factors that can be reached while maneuvering the airplane as a function of the equivalent speed. The considered aircraft altitude is 8,000 ft, which is the cruise height. On the other hand, the gust envelope (drawn in dark orange) informs about the loads experienced when the aircraft encounters a strong gust. It can be observed that loads related to gust can exceed worst maneuver loads in some cases.

The flight envelope represented in Fig. 4.9 indicates critical velocities attainable: the positive stall speed (V_{S1}), the design maneuvering speed (V_A), the design speed for maximum gust intensity (V_B), the design cruise speed (V_C) and the design dive speed (V_D). Furthermore, critical load factors are specified (n_{limit} and $n_{ultimate}$) as well as critical flight conditions (point A to F). Numerical values related to velocities, load factors and critical flight conditions are presented in Tab. 4.12 and 4.13.

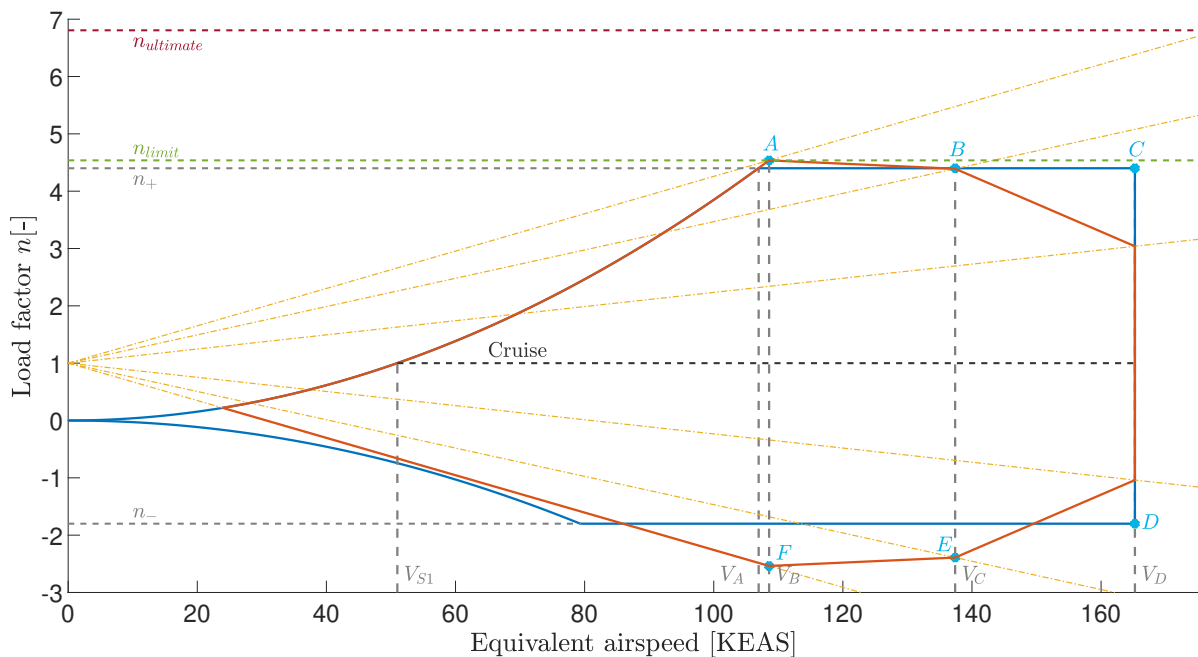


Figure 4.9: BROL-21 aircraft maneuver envelope (dark blue), gust envelope (dark orange) and critical flight conditions (light blue) at 8,000 ft

The maneuver limit load factors (n_+ and n_-) are set respectively to 4.4 and -1.8 (see Tab. 4.12). This selection is justified by the BROL-21 aircraft *utility* category.

V_{s1}	51.0
V_A	107.0
V_B	108.6
V_C	137.4
V_D	165.2
n_+	4.4
n_-	-1.8
n_{limit}	4.54
$n_{ultimate}$	6.81

	V_{eq} [KEAS]	n
A	108.6	4.5
B	137.4	4.4
C	165.2	4.4
D	165.2	-1.8
E	137.4	-2.3
F	108.6	-2.5

Table 4.12: BROL-21 Flight envelope numerical values (airspeed in KEAS)

Table 4.13: BROL-21 Critical flight conditions

The BROL-42 flight envelope presented in Fig. 4.10 has been outlined similarly than for the BROL-21 case. The numerical values for critical velocities, limit factors and critical flight conditions are indicated in Tab. 4.14 and 4.15. It can be noted that the considered altitude is 12,000 ft, which is the BROL-42 cruise height.

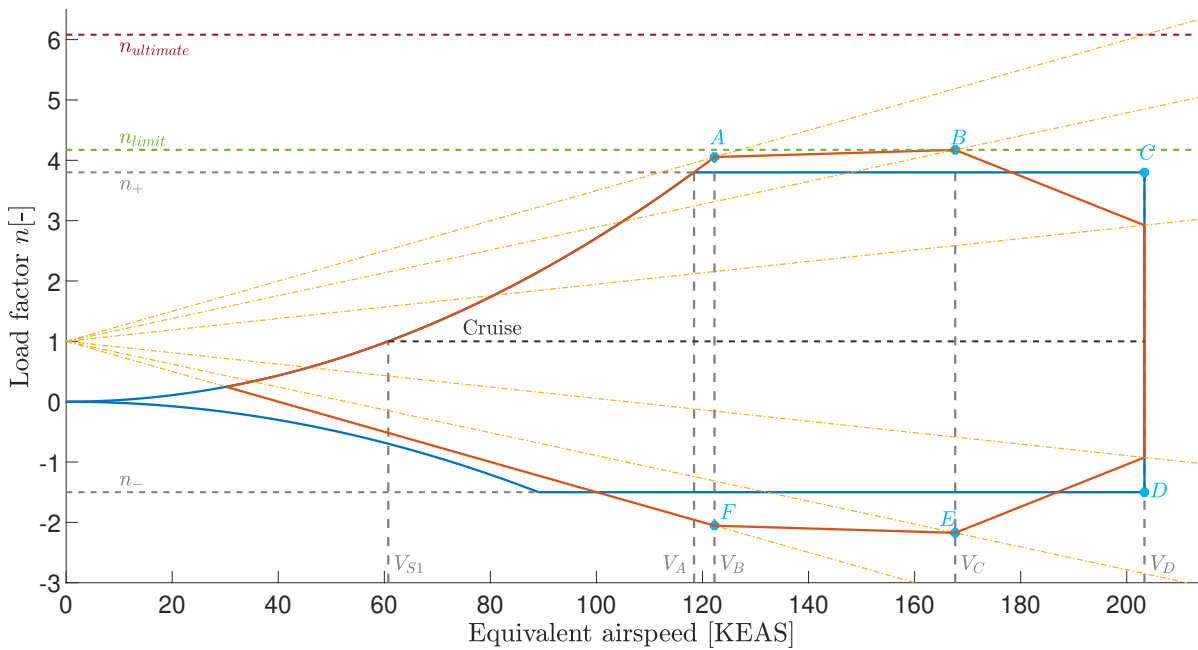


Figure 4.10: BROL-42 aircraft maneuver envelope (dark blue), gust envelope (dark orange) and critical flight conditions (light blue) at 12,000 ft



The maneuver limit load factors (n_+ and n_-) are set respectively to 3.8 and -1.5 (see Tab. 4.14). This selection is justified by the BROL-42 aircraft *normal* category.

V_{s1}	60.7
V_A	118.4
V_B	122.3
V_C	167.7
V_D	203.3
n_+	3.8
n_-	-1.5
n_{limit}	4.17
$n_{ultimate}$	6.26

Table 4.14: BROL-42 Flight envelope numerical values (airspeed in KEAS)

	V_{eq} [KEAS]	n
A	122.3	4.1
B	167.7	4.2
C	203.3	3.8
D	203.3	-1.5
E	167.7	-2
F	122.3	-2

Table 4.15: BROL-42 Critical flight conditions

4.4.2 Aircraft loading

Every aircraft loads and respective positions are summarized in Fig. 4.11. This diagram is a simplified representation of the aircraft loading which indicates wing lift (L), tail lift (P), engine thrust (T), body drag (D_b), wing drag (D_w), pitching moment induced by the wing (M_w) and angle of attack (α). The variable nW represents the aircraft maximum takeoff weight multiplied by the considered flight condition load factor (selected from Fig. 4.9 and 4.10).

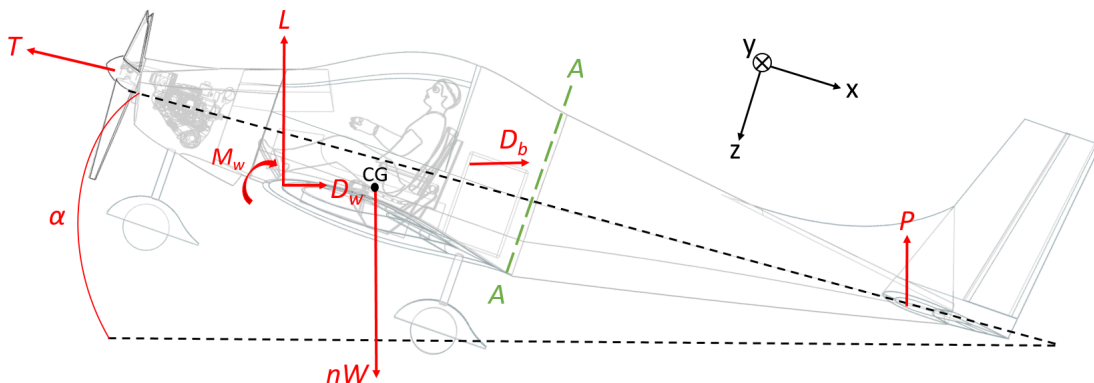


Figure 4.11: Aerodynamic loads acting on BROL-21 aircraft

In order to define loads related to aerodynamics, the following equilibrium equations are considered:



$$\begin{cases} L + P + T \cdot \sin(\alpha - \alpha_0) = nW \\ l_L \cdot L + l_{D_w} \cdot D_w + l_{D_b} \cdot D_b + l_P \cdot P + l_T \cdot T + M_w = I_\theta \cdot \ddot{\theta} \end{cases}$$

where the lengths l_i correspond to the distance from the load application point to the aircraft center of gravity, I_θ is the moment of inertia of fully loaded aircraft about the center of gravity. The various coefficients l_i as well as the moment of inertia I_θ are directly given by aircraft CAD models. Moreover, angles of attack α related to every flight configurations are found by iteration using Matlab software.

Tab. 4.16 and 4.17 present the numerical values of loading and angles of attack for the critical configurations presented in flight envelopes (see Section. 4.4.1). The force F_{fin} represents the fin loading generated when the aircraft encounters the maximum yaw angle ψ . M_{fus} relates the sum of torques created by the tailplane during asymmetric slipstream and fin loading due to yaw applied to aircraft rear fuselages.

Case	α [°]	L [lbf]	P [lbf]	nW [lbf]	D_B [lbf]	D_w [lbf]	M_w [lbf.ft]	F_{fin} [lbf]	M_{fus} [lbf.ft]
A	12.2	7 882	612	8 554	113	148	-1 846	384	1 813
B	6.8	7 775	480	8 484	178	242	-2 893	602	2 330
C	3.15	7 656	245	8 484	269	382	-4 372	910	3 062
D	-5.3	-2 579	-874	-3 470	269	448	-4 372	910	3 062
E	-7.6	-3 546	-779	-4 356	178	311	-2 893	602	2 330
F	-10.9	-3 961	-683	-4 697	113	214	-1 846	384	1 813

Table 4.16: BROL-21 aircraft critical angles of attack and loading (8, 000 ft)

Case	α [°]	L [lbf]	P [lbf]	nW [lbf]	D_B [lbf]	D_w [lbf]	M_w [lbf.ft]	F_{fin} [lbf]	M_{fus} [lbf.ft]
A	12.8	13 380	801	14 249	140	231	-3 116	1 035	5 512
B	6.2	14 103	277	14 406	251	438	-5 589	1 856	8 449
C	2.6	13 310	-546	13 259	385	705	-8 558	2 842	11 197
D	-4.4	-2 785	-2 424	-5 233	385	799	-8 558	2 842	11 197
E	-6.8	-5 391	-2 008	-7 427	251	548	-5 589	1 856	8 449
F	-10.0	-5 772	-1 445	-7 270	140	329	-3 116	1 035	5 512

Table 4.17: BROL-42 aircraft critical angles of attack and loading (12, 000 ft)



4.4.3 Fuselage loading

The fuselage loading is studied while considering the reference frame presented in Fig. 4.11. It is focused on the AA -section (see Fig. 4.11), which is the limit of aircraft rear fuselage. The effect of the various loads presented in Tab. 4.16 and 4.17 is studied at AA -section due to the high direct stress encountered in this area. It can be noted that T_x is zero for all the flight configurations.

Case	T_y [lbf]	T_z [lbf]	M_x [lbfft]	M_y [lbfft]	M_z [lbfft]
A	-384	-94	-1 813	-3 513	4 050
B	-602	31	-2 330	-2 137	6 348
C	-910	266	-3 062	311	9 594
D	-910	658	-3 062	7 920	9 594
E	-602	509	-2 330	6 639	6 348
F	-384	389	-1 813	5 544	4 050

Table 4.18: BROL-21 aircraft rear fuselage loading

Case	T_y [lbf]	T_z [lbf]	M_x [lbfft]	M_y [lbfft]	M_z [lbfft]
A	-1 035	-53	-5 512	-4 490	10 377
B	-1 856	477	-8 449	764	18 612
C	-2 842	1 242	-11 975	8 614	28 497
D	-2 842	2 145	-11 975	22 742	28 497
E	-1 856	1 599	-8 449	18 009	18 612
F	-1 035	1 038	-5 512	12 505	10 377

Table 4.19: BROL-42 aircraft rear fuselage loading

4.4.4 Wing loading

In order to estimate its loading, the wing is considered as a beam upon which forces are applied. The loads primary considered for this analysis are the wing self-weight, the tank weight as well as the engine weight (for BROL-42 only). Wing lift, drag, pitching moment and engine thrust are afterwards taken into account. The latter is once again considered for BROL-42 only. The wing weight is placed on its center of mass while the aerodynamic loads (wing lift, drag and pitching moment) are placed at wing aerodynamic center. The BROL-42 thrust force is placed at the propeller location. It is to be noted that the tank is considered as empty, which leads to higher loads.



The considered reference frame is composed of a x -axis pointing in the chord direction (towards trailing edge) and a y -axis pointing towards the wing tip. The z -axis is perpendicular to both other axes. The loads at the wing root are presented in Tab. 4.20 and 4.21.

Case	T_x [lbf]	T_z [lbf]	M_x [lbf.ft]	M_y [lbf.ft]	M_z [lbf.ft]
A	-567	-2 735	-23 452	-1 846	2 727
B	-265	-2 839	-24 209	-2 893	-121
C	-3	-2 695	-23 256	-4 372	-2 436
D	162	837	7 699	-4 372	366
E	18	1 198	10 658	-2 893	1 880
F	-126	1 348	11 855	-1 846	3 268

Table 4.20: BROL-21 aircraft wing root loading

Case	T_x [lbf]	T_z [lbf]	M_x [lbf.ft]	M_y [lbf.ft]	M_z [lbf.ft]
A	-978	-3 856	-38 618	-3 116	-923
B	-435	-4 267	-42 174	-5 590	-8 157
C	-1	-4 112	-40 345	-8 558	-12 065
D	281	406	6 143	-8 558	3 298
E	29	1 285	14 396	-5 590	8 132
F	-222	1 492	15 947	-3 116	10 516

Table 4.21: BROL-42 aircraft wing root loading

4.4.5 Analytical analysis

The sizing of structural elements is performed by using an idealization of the aircraft structure. As a matter of fact, the stringers are supposed to carry no shear stress while carrying the entire direct loading. On the other hand, the skin panels carry the entire shear stress. Since the distances between stringers are small, the shear flow is considered as constant on each skin panel. This assumption allows to compute analytically the required size for structural elements. Its veracity is studied by the finite element analysis performed in Section 4.4.6.

For designing the structural elements, the *elastic design approach* is considered. This method uses *allowable* stress obtained from 0.1 percent proof test, with a factor of safety (1.5 is considered). These stress are combined with actual loads (illustrated in Tab. 4.18 and 4.19 for the fuselage and Tab. 4.20



and 4.21 for the wing) to define structural elements size and positioning.

The allowable direct and shear stress are respectively defined as:

$$\sigma_{max} = \frac{\sigma_{0.1\%}}{s} = \frac{33600}{1.5} = 22400 \text{ psi} \quad \text{and} \quad \tau_{max} = \frac{\tau_{strength}}{s} = \frac{21030}{1.5} = 14020 \text{ psi}$$

Analytical sizing of fuselage structural elements

The rear fuselage structure is composed of stringers oriented towards the fuselage axis. They are connected to one another by the fuselage skin. To prevent buckling, the fuselage is also composed of frames. It is to be noted that the fuselage being unpressurized, the loading occurring over the frames presents a relatively low magnitude. The stringers minimal area (B_{min}) is computed by considering worst-case loading presented in Tab. 4.18 and 4.19. It is given by:

$$B_{min} = \left(\frac{M_y}{\sum_{i=1}^{N_{stringers}} z_i^2} z - \frac{M_z}{\sum_{i=1}^{N_{stringers}} y_i^2} y \right) \frac{1}{\sigma_{max}}$$

where the index i indicates the considered stringer, M_y and M_z are bending moments and y and z are the stringers positioning with respect to fuselage center. By using 20 equally spaced and sized stringers for BROL-21 aircraft, the selected area for stringers is 0.031 in^2 . BROL-42 fuselage is itself composed of 24 stringers of 0.056 in^2 area.

In order to determine the required skin thickness, the shear flow (q) is computed by:

$$q^{i+1} - q^i = -\frac{T_z}{I_{yy}} B_i z_i - \frac{T_y}{I_{zz}} B_i y_i$$

where the index i indicates the considered skin panel and y and z are the panel positioning with respect to fuselage center. I_{yy} and I_{zz} are respectively the moment of inertia with respect to y and z -axis. The skin thickness is computed by considering worst-case loading presented in Tab. 4.18 and 4.19. Its value is 0.039 in for both aircraft.



Analytical sizing of wing structural elements

The wing is composed of stringers oriented towards the span. They are linked together by the wing skin. Ribs and spars allow the maintain of wing shape. The orientation of ribs and spars is respectively chordwise and spanwise. Fig. 4.12 presents the positioning of spanwise structural elements. The location of presented elements is valid for both aircraft wings.

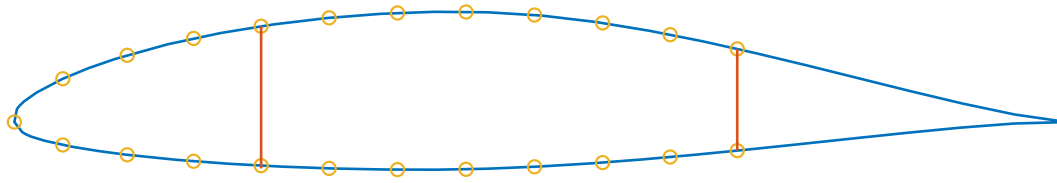


Figure 4.12: Wing stringers and flanges positioning (yellow circles). The spars (red lines) are placed near aerodynamic center (left spar) and upfront control panels (right spar)

The stringers minimal area is determined while considering worst-case loading from Tab. 4.20 and 4.21. The bending direct stress is computed by:

$$\sigma_{yy,i} = \frac{(I_{zz}M_x + I_{xz}M_z)z_i - (I_{xz}M_x + I_{xx}M_z)x_i}{I_{xx}I_{zz} - I_{xz}^2}$$

where the index i indicates the considered stringer. The bending stress ($\sigma_{yy,i}$) has to stay below the allowable direct stress (σ_{max}). By using 23 equally sized stringers for the BROL-21 wing, the selected area for stringers is 0.132 in^2 . The BROL-42 wing is itself composed of 23 stringers of 0.233 in^2 area.

The wing skin thickness is computed by determining the shear flow (q) in the two-cell wing section. Due to the asymmetrical profile of the wing, q is computed by means of the "open section shear flow" (q_b), where the skin is artificially cut between in the top skin panels. It is determined by:

$$q_b = -\frac{I_{zz}T_z - I_{xz}T_x}{I_{xx}I_{zz} - I_{xz}^2} A \sum_i z_i - \frac{I_{xx}T_x - I_{xz}T_z}{I_{xx}I_{zz} - I_{xz}^2} A \sum_i x_i$$

where the index i indicates the considered skin panel. The twist rate compability allows to correct the open section shear flow. The wing shear center is then computed and the moment M_y contribution is

added to obtain maximum wing shear flow q by considering the highest loading from Tab. 4.20 and 4.21. After computation, the skin and spar thickness is fixed to 0.039 in for both aircraft. Even though selecting the same thickness for such a large amount of elements can be considered as oversizing, it allows to reduce significantly the production costs.

4.4.6 Finite element analysis

Fuselage and wing CAD layouts are respectively presented in Fig. 4.13 and 4.14. The structure specifications are based on the analytical study (see Section 4.4.5). While the BROL-21 structure characteristics are detailed in Section 4.4.5, a finite element analysis is performed for the BROL-42 structural components. This choice is motivated by the higher constraints occurring over the BROL-42 trainer rear fuselage and wings. The backbone of the BROL-21 trainer can be then approximated using scale-lowering process. This latter is safer and guarantee the solidity of both aircraft structure. This finite element element analysis is performed thanks to Siemens NX software.

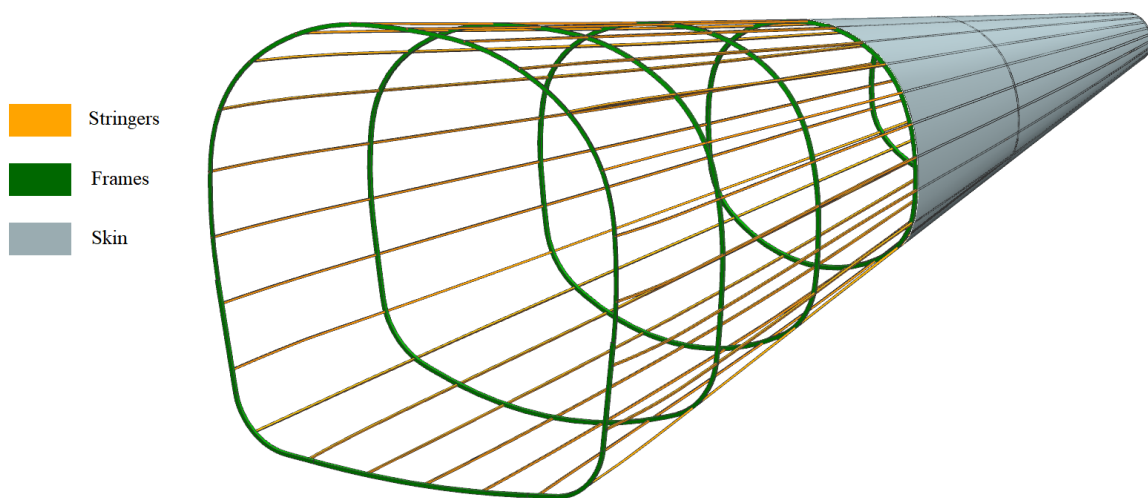


Figure 4.13: Internal structure of the BROL-42 fuselage

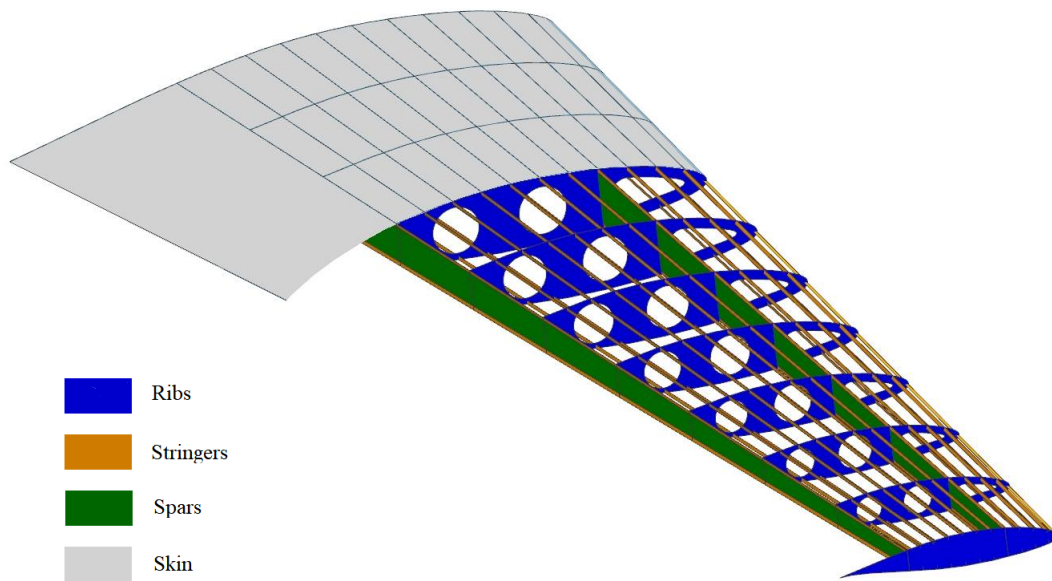


Figure 4.14: Internal structure of the BROL-42 wing

Fuselage simulation

A summary of the BROL-42 fuselage structural elements is presented in Tab. 4.22. These elements are used to perform the various finite element simulations of the aircraft rear fuselage. While stringers appears as cylinders in Fig. 4.13, their shape is actually the one presented in Fig. 4.15.

	Area/Thickness	Quantity
Stringers	0.056 in ²	24
Frames	0.1674 in ²	6
Skin	0.039 in	/

Table 4.22: Summary of BROL-42 fuselage structural elements

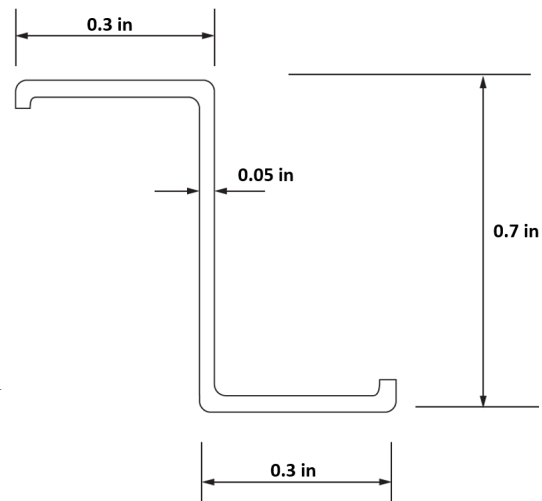


Figure 4.15: Fuselage stringers geometry

In order to perform the simulation of the rear fuselage in a worst-case scenario, highest stress related to fin loading F_{fin} and tail lift P are taken into account (see Tab. 4.17). For applying those forces on the physical points of application, rigid links are set between the rear fuselage tail and the points of interest (i.e. fin pressure center for the fin loading and tail aerodynamic center for the tail lift). The point D of the BROL-42 flight envelope (see Fig. 4.10) is considered as worst-case flight condition. The fuselage and tail self-weight are as well taken into account, their values are given by the CAD models of the BROL-42 aircraft. Fig. 4.16 presents the finite element model selected for the BROL-42 rear fuselage.

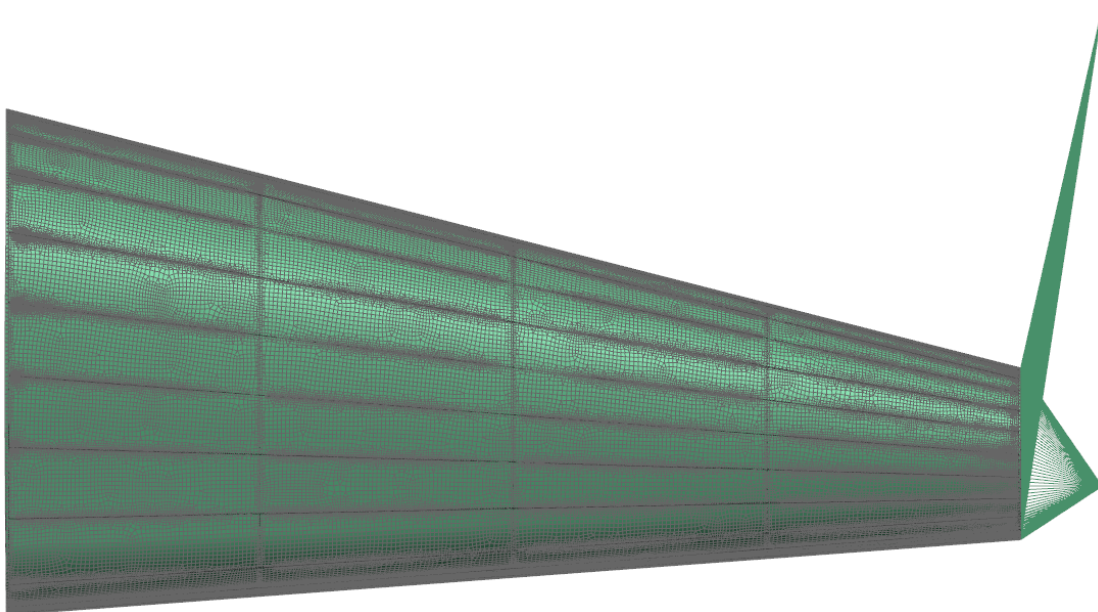


Figure 4.16: Finite element model of the BROL-42 rear fuselage (with rigid link on the right)

Fig. 4.17 shows the rear fuselage stress field of BROL-42. It can be observed that an important stress concentration, probably due to the rigid links, is encountered at the fuselage tail. However, the values of stress are in accordance with the analytical results (see Tab. 4.23). As expected analytically, a small increase of the stress at nodes close to the rear fuselage base can be observed.

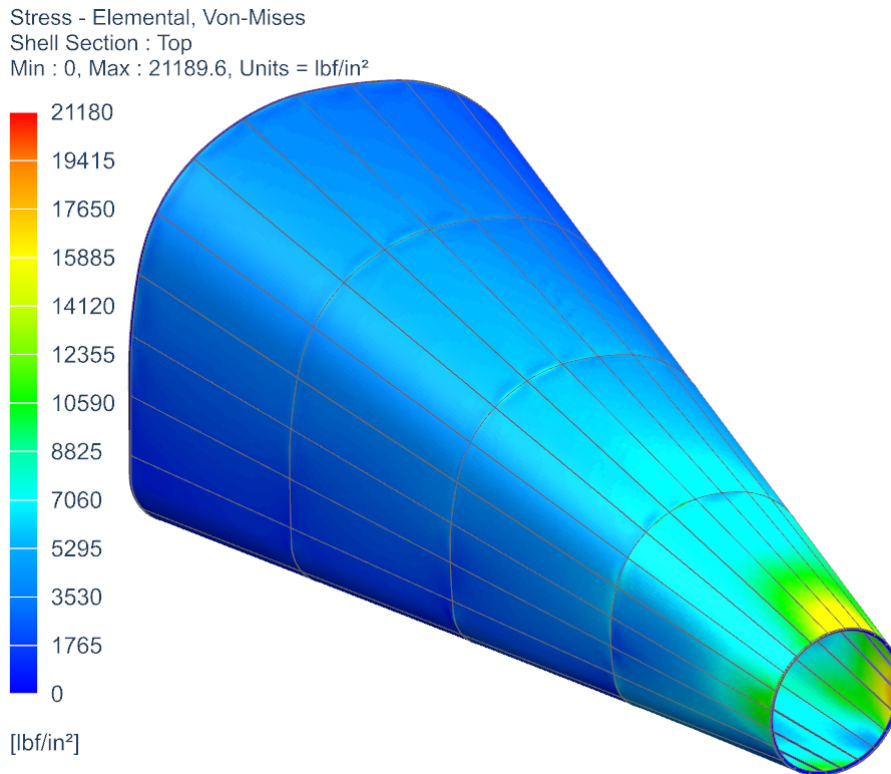


Figure 4.17: Von-Mises critical stress field on the BROL-42 rear fuselage

	Analytical	FEM
Max. shear stress [lbf/in²]	9700	11300
Max. direct stress [lbf/in²]	22400	21000

Table 4.23: Comparison of the maximum stress between analytical and numerical analysis for the BROL-42 fuselage

By consulting Tab. 4.23, it can be observed that the maximal shear and direct stress produced by finite element analysis presents respectively higher and lower values compared to analytical results. This can be explained by the analytical study assumptions. The direct stress are considered to be fully sustained by stringers while the skin panels carry the entire shear stress. The finite element analysis does not consider this approximation and it results into a balancing between shear and direct stress.

It is to be noted that the maximal fuselage displacement is 0.153 in. This displacement is acceptable and is located at the rear fuselage tail (further away from fixed rear fuselage base). In order to stay concise, the fuselage displacement is not presented in the scope of this analysis.

Wing simulation

A summary of the BROL-42 wing structural elements is presented in Tab. 4.24. These elements are used to perform the various finite element simulations on the aircraft wing. While stringers appears as cylinders in Fig. 4.14, their shape is actually the one presented in Fig. 4.18.

	Area/Thickness	Quantity
Stringers	0.233 in ²	23
Skin	0.039 in	/
Spars	0.039 in	2
Ribs	0.118 in	11

Table 4.24: Summary of BROL-42 wing structural elements

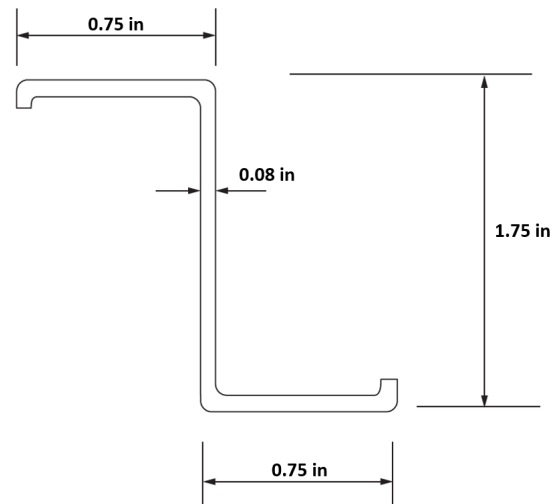


Figure 4.18: Wing stringers geometry

To perform the finite element analysis, the half of the wing is considered, which allows faster computation and is possible due to the wing symmetry (with respect to the fuselage). The point C of the BROL-42 flight envelope (see Fig. 4.10) is considered as worst-case flight condition. The pressure distribution (given by the Vortex Lattice Method), which will be encountered at this flight condition, is considered. An overview of this pressure distribution is presented in Fig. 4.19. The self-weight of the wing (given by CAD model) is also taken into account. Finally, the weight of the engine as well as the thrust force and moment are considered. The fuel tank is considered as empty, which leads to higher loads. The wing is fixed at its root chord and the control surfaces are not implemented as loads carrier and do not contribute to the wing stiffness.

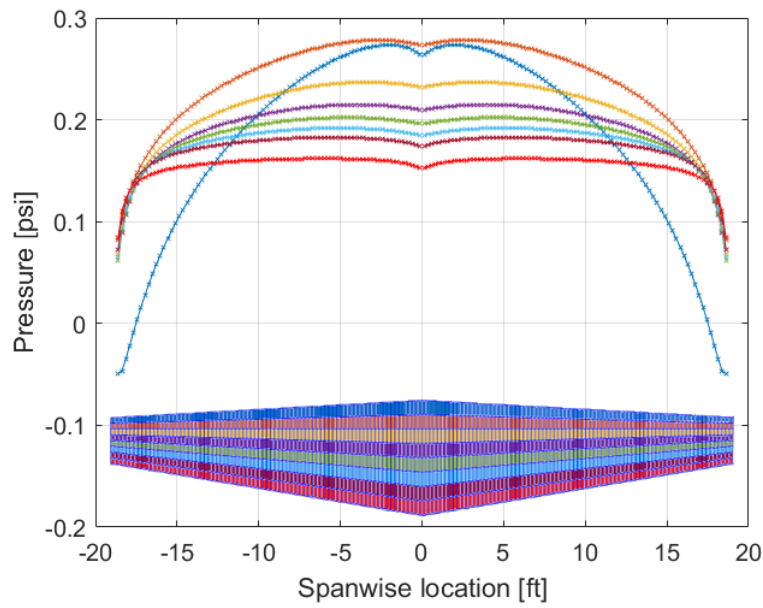


Figure 4.19: Spanwise pressure distribution for various chordwise positions

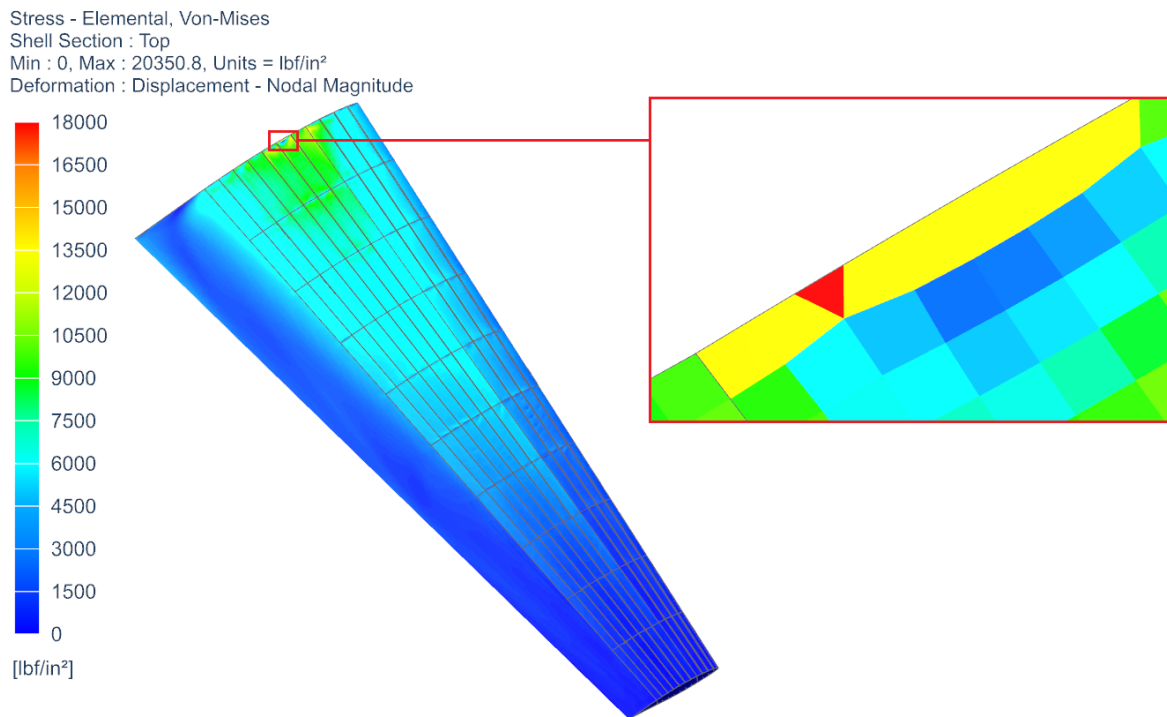


Figure 4.20: Von-Mises critical stress field for the BROL-42 half wing

As expected analytically, the stress distribution (shown in Fig. 4.20) decreases along the spanwise direction, and is minimum at the wing tip. As the result in terms of Von-Mises stress seems plausible, a more advanced analysis can be performed, by separating the direct and shear stress.

The results are displayed in Fig. 4.21. The direct stress field is represented within the internal structure and the shear stress field on the skin. It is to be noted that the maximum value indicated by Fig. 4.21(a) is due to a stress singularity.

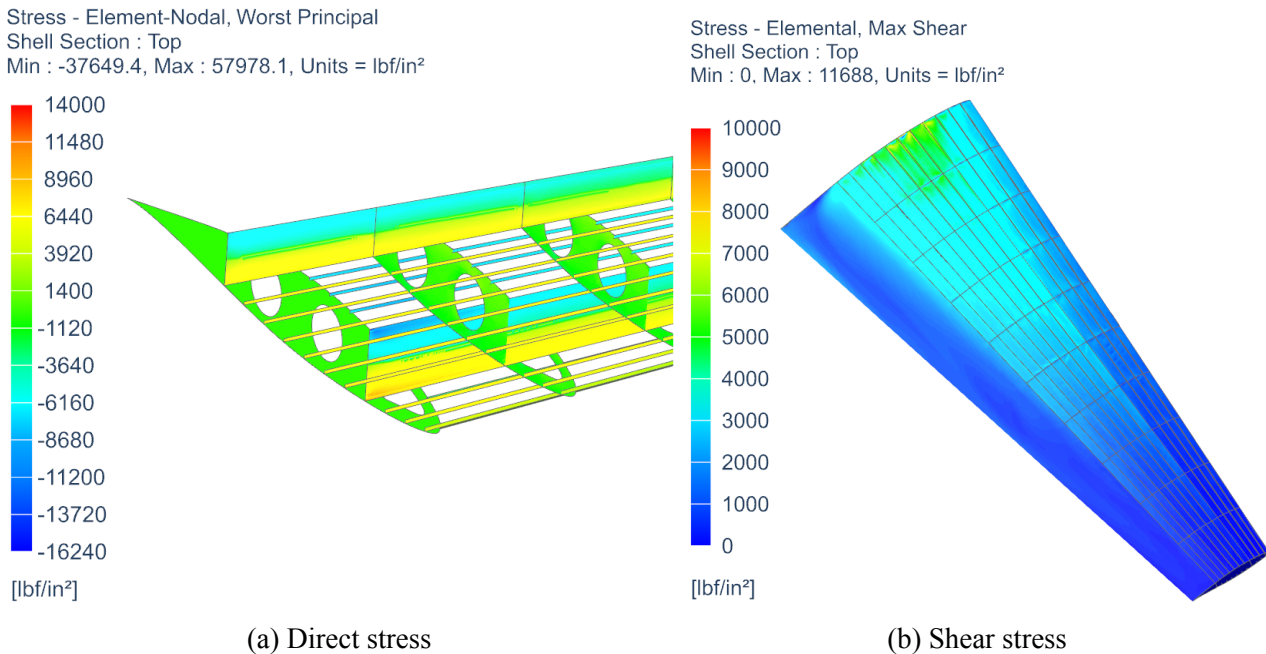


Figure 4.21: Maximal stress on the BROL-42 half-wing

As predicted by the analytical analysis, the significant magnitude of the direct stress is observed within the stringers. The spars and skin sustain the majority of the shear stress. The maximum direct stress is lower than the value given by the analytical solution while the maximum shear stress is higher than the one computed with the analytical method. As for the fuselage analysis, it can be explained by the balancing of stress due to analytical assumptions. Unlike what is assumed analytically, the stringers sustain a fraction of the shear stress and the skin and frames sustain a fraction of the direct stress. It can explain the reduction of the maximal direct stress and the rise of maximal shear stress while performing the wing finite element analysis.

	Analytical	FEM
Max. shear stress [lbf/in²]	6300	10100
Max. direct stress [lbf/in²]	18560	16240

Table 4.25: Comparison of the maximum stress between analytical and numerical analysis for the BROL-42 half-wing



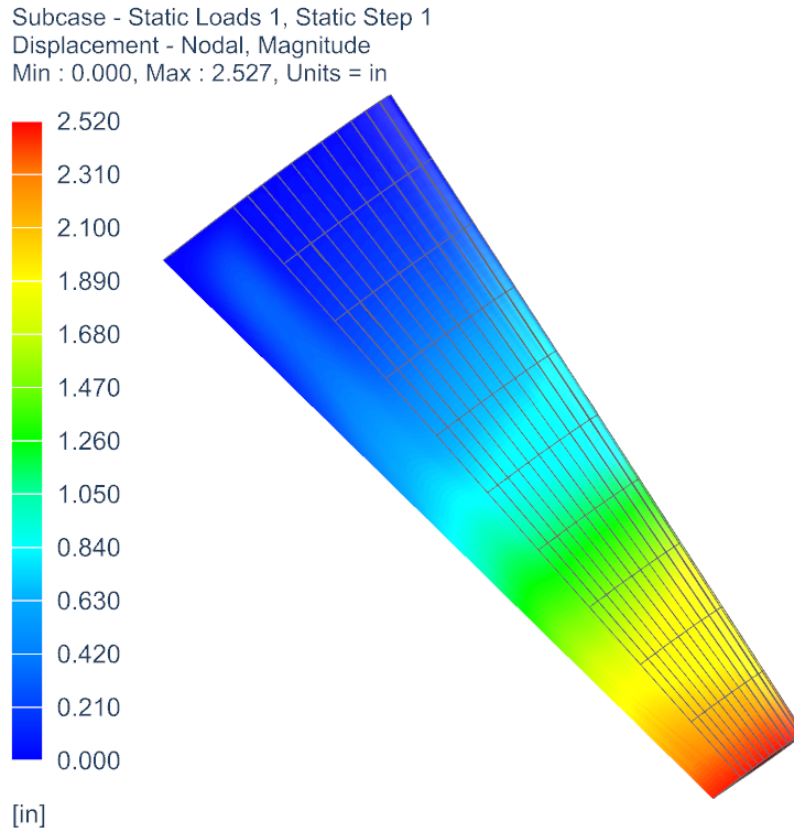


Figure 4.22: BROL-42 half-wing critical displacement

The wing displacement induced by the critical loading is presented in Fig. 4.22. The profile is parabolic, with a maximal displacement at the wing tip. The amplitude is relatively low, but it can be explained by the over-sizing of the structural elements due to large security factor implemented in the analytical study. For further development, the wing can be designed less stiff (with a scale-lowering process of structural elements). This can lead to weight saves and therefore a reduction of flying costs (lower fuel consumption) as well as production costs (lower material quantity need to build the aircraft).

4.5 Performance

4.5.1 Payload-range diagram

The payload range diagrams for both aircraft at best-range speed (corresponding to the best lift to drag speed) are presented in Fig. 4.23 and 4.24. Since the payload of both aircraft is composed only

of the number of persons on board, these diagrams show how the maximum range evolves when the number of passengers varies. It is computed by subtracting each time the weight of one person from the total weight. It hence gives ferry ranges (range at no payload) of 1624 nmi for the single-engine aircraft and 1929 nmi for the twin-engine aircraft with a reserve of fuel. At MTOW, a range of 1266 nmi and 1531 nmi have been computed for the single and twin engine aircraft respectively, meeting the RFP requirements. The reserve fuel is the amount needed to fly 45 minutes at max continuous power [6].

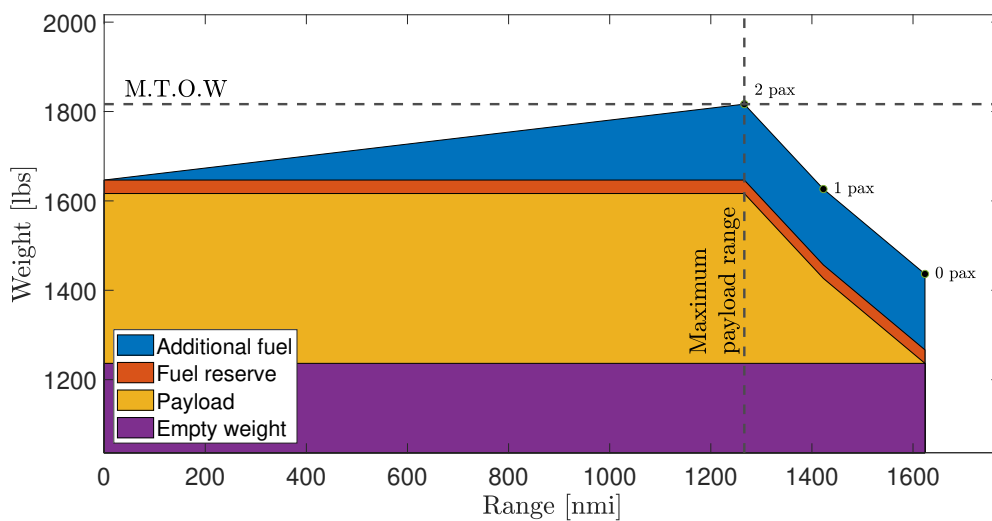


Figure 4.23: Payload range diagram at best range speed for BROL-21

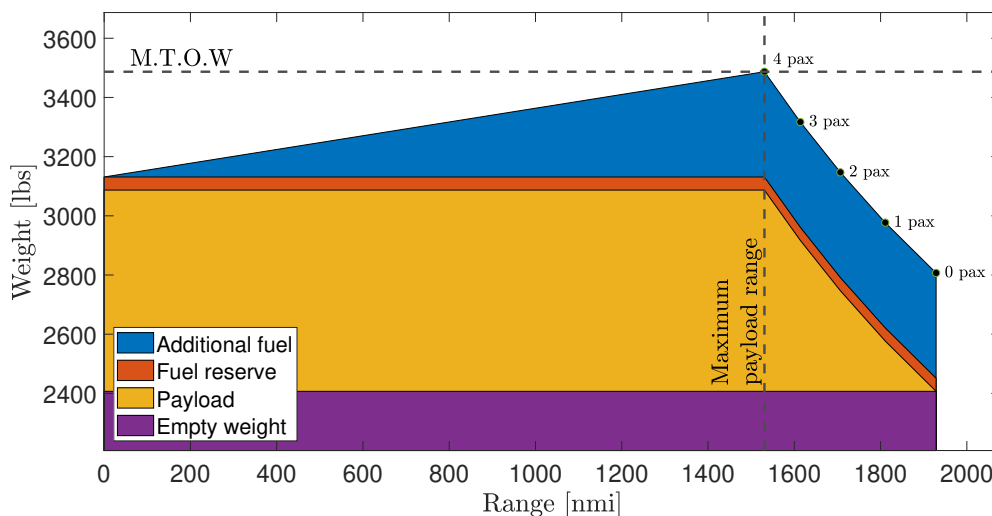


Figure 4.24: Payload range diagram at best range speed for BROL-42



4.5.2 Placard diagram

The Placard diagram (Fig. 4.25) shows the influence of the variation of the density and the temperature with respect to the altitude on the velocities. The blue curve represents the evolution of the design cruise speed with respect to the altitude. Above the cruise altitude, aircraft will fly at a constant design cruise Mach number ($M_c = 0.242$ for BROL-21 and $M_c = 0.318$ for BROL-42). Under the design cruise altitude, they will then flight at a constant cruise speed. The red curve shows the evolution of the dive speed with respect to the altitude.

The service ceiling altitude of BROL-21 and BROL-42 are respectively 30600 ft and 23000 ft. At 12500 ft., oxygen for the crew members is mandatory. As the BROL-21 does not have oxygen bottle, it can not fly above 12500 ft.: this is its maximum operating altitude. In order to reach the service ceiling altitude requirement, BROL-42 must have oxygen bottle and masks for all.

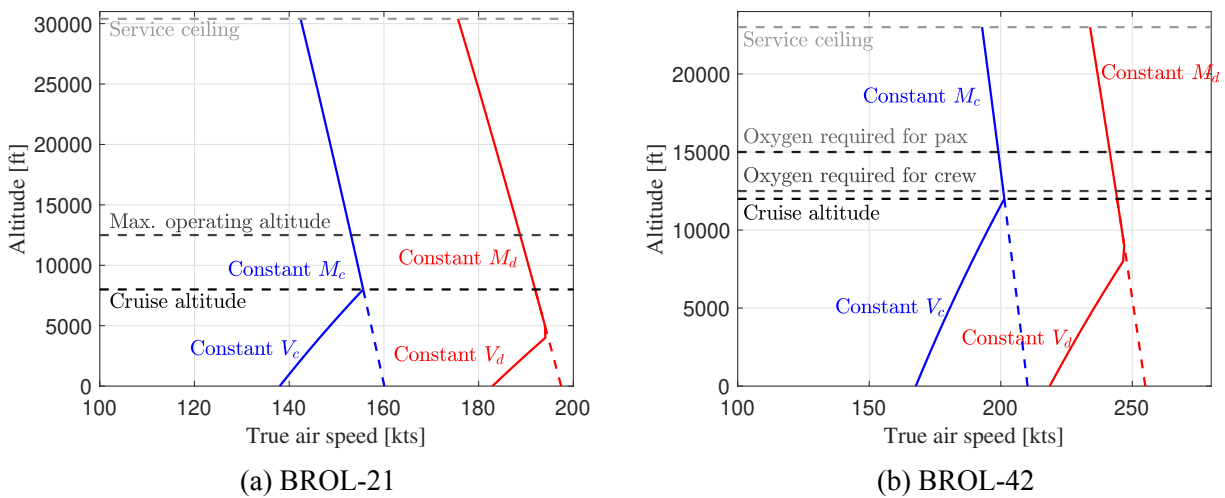


Figure 4.25: Placard diagram of the two aircraft

4.5.3 Takeoff

The takeoff distance has been computed following the Snorri Gudmundsson methodology [4]. The different takeoff segment are shown in Fig. 4.26 and are identified as:

- Acceleration from brake to lift off speed considering 1 second between rotation and lift-off.



- Transition from lift-off to climb
- Climb to an obstacle of 50ft as required by the FAR [6]

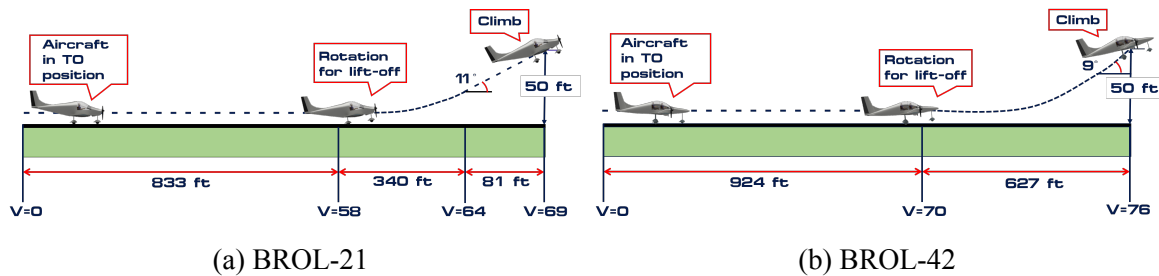


Figure 4.26: Distances and speeds for the different takeoff segments. Speeds are in knots.

BROL-42 reaches the height of the imaginary 50 feet obstacle during the transition phase reaching a total takeoff distance of 1551 feet. For BROL-21, the total takeoff distance is 1256 feet satisfying the requirements.

Balanced field length & Decision speed

The Balanced Field Length (BFL) refers to the One Engine Inoperative (OEI) condition for takeoff. It is determined by the decision speed V_1 , defined as the speed at which the accelerate-stop distance is equal to the 50ft obstacle clearance. If an engine failure occurs at $V > V_1$ the aircraft has to pursue the takeoff. The following methodology has been used to determine the different segments of the OEI takeoff for the BROL-42:

- A: Two engine operative acceleration from brake to engine failure speed
- B: One engine inoperative acceleration from engine failure speed to lift-off speed
- C: 50ft obstacle clearance with one engine inoperative
- D: Reaction time of the pilot (2s) + brake system activation (2s)
- E: Braking distance with the engines shutdown

The condition is thus $A + B + C = A + D + E$. All distances are measured at MTOW. A friction coefficient $\mu = 0.05$ corresponding to dry asphalt had been considered for the ground roll and $\mu = 0.4$ when brakes are activated (mid value for dry asphalt [4]). In segments B, C and D, additional drag due to rudder deflection has been evaluated using the VLM software. The rudder deflection is chosen such that the lateral force on the fin is enough to counteract the yaw induced by the thrust of the remaining engine and reaches a maximum value of 21° .

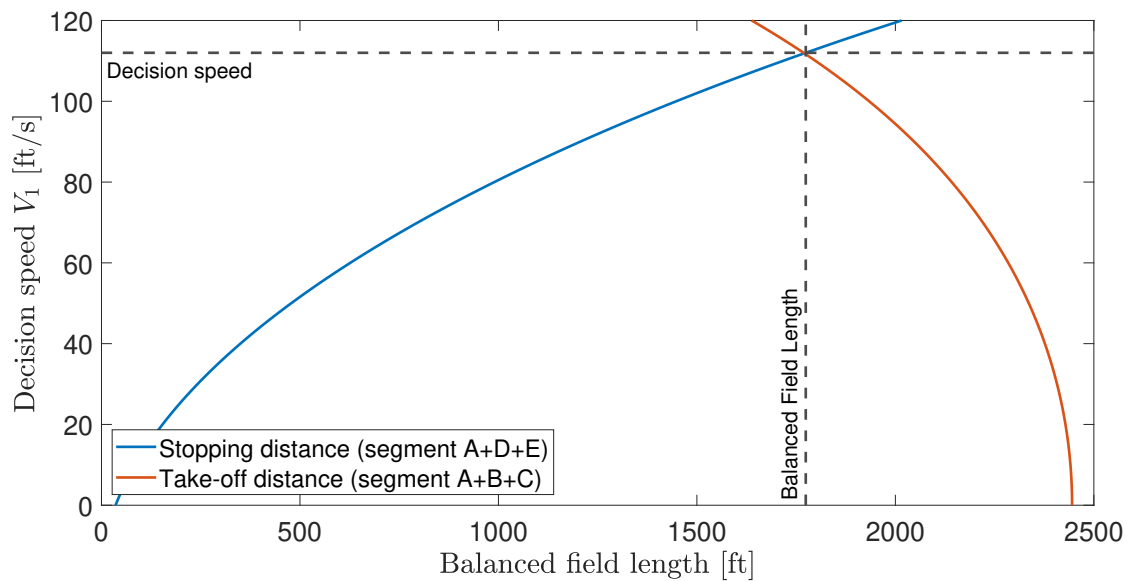


Figure 4.27: Balanced field length and decision speed for BROL-42

The results for the OEI takeoff are shown in Fig. 4.27. The decision speed $V_1 = 66$ KEAS and corresponds to a BFL of 1774 feet, which matches the RFP's request. The condition $V_1 < V_{LOF}$ is also met.

4.5.4 Climb

This section intends to evaluate the performance in climb for both BROL-21/42. For this study, the method developed by S. Gudmundsson was used [4]. Denoting the climb angle by θ , it represents the force balance of the aircraft during climb as:

$$\left. \begin{aligned} L &= W \sin \theta \\ T &= D + W \cos \theta \end{aligned} \right\} \Rightarrow \theta = \arcsin \left(\frac{T - D}{W} \right) \quad (4.12)$$

where the total drag force is evaluated under the assumption of a quadratic drag model. The Rate-Of-Climb (ROC) is then simply computed by using Eq. 4.13,

$$ROC = V_z = V \sin \theta = V \left(\frac{T - D}{W} \right) \quad (4.13)$$

To summarise the climb performance of both BROL-21/42, a map of the ROC as a function of the altitude and the aircraft velocity is presented in Fig. 4.28. The variation along the altitude of the level flight stall velocity (i.e. with load factor $n = 1$) of both aircraft is also available in this map.

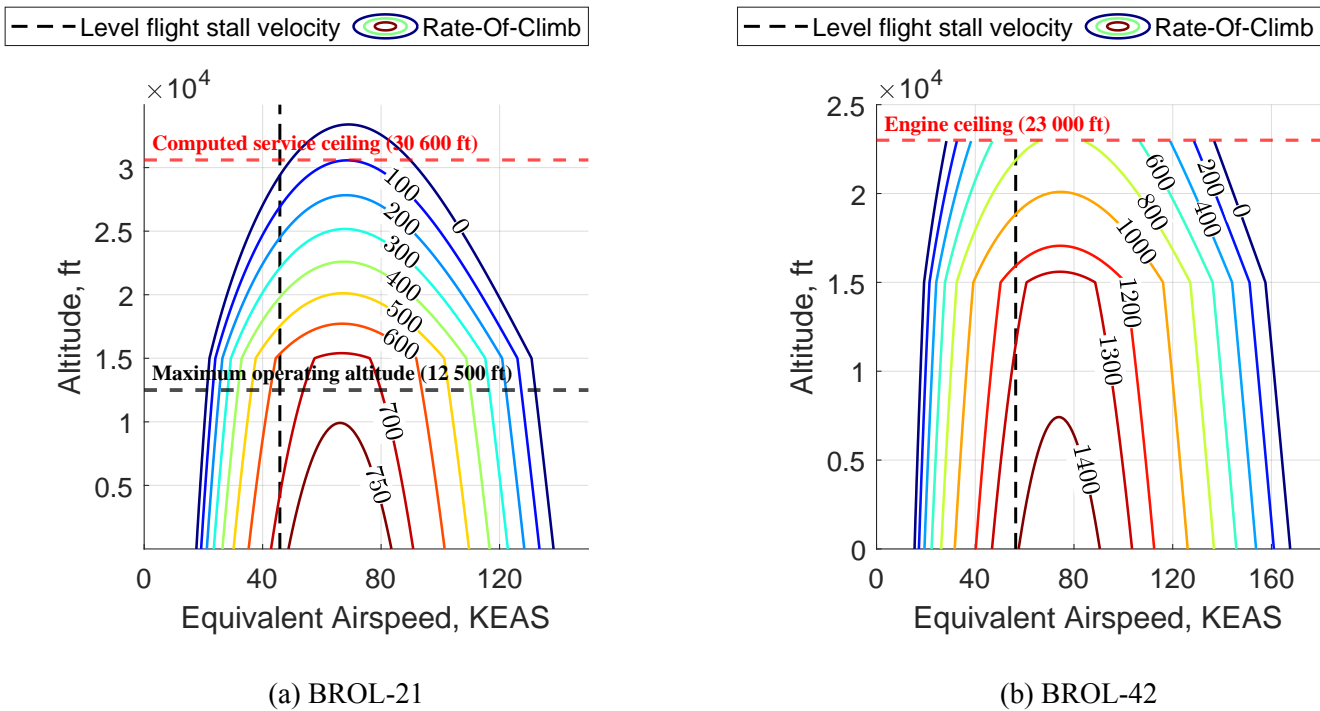


Figure 4.28: Map of the Rate-Of-Climb (ROC) as a function of the altitude and the aircraft velocity.

In addition, key climb characteristics such as the climb velocity V_{climb} , the maximum climb angle θ_{max} with its corresponding velocity V_X and the best rate of climb ROC_{max} , with its corresponding climb angle θ_{best} and velocity V_Y , are listed in Tab. 4.26 for an altitude of 50 ft. This altitude corresponds to the end of the takeoff phase.



	BROL-21	BROL-42
V_{climb} [kts]	69.16	76.43
θ_{max} [°]	17.8	34.3
V_X [kts]	34.32	30.74
ROC_{max} [ft/min]	782.8	1450.8
V_Y [kts]	60.45	73.35
θ_{best} [°]	7.3	11.3

Table 4.26: Key climb performance parameters at an altitude of 50 feet.

However, it is important to notice that all the results presented here are rather optimistic. It should be kept in mind that they come from many approximations such as point mass force equilibrium approximation, approximate thrust loss correction along the altitude, approximate drag polars, etc. At the end, only in flight measurements may assess the reliability of such climb performance.

Service ceiling

The service ceiling is the altitude at which the aircraft achieves a $\text{ROC}_{\text{max}} = 100$ ft/min. It can be seen from Fig. 4.28a that the computed service ceiling of the BROL-21 is 30 600 ft. However, its maximum operating altitude will be limited to 12 500 ft. It is due to the fact that, according to the regulation, above this altitude wearing oxygen masks is mandatory and the BROL-21 is not equipped with such equipment. On the other hand, although the BROL-42 has such equipment (for the crew and passengers), its service ceiling is 23 000 ft which corresponds to the engine service ceiling.

One engine inoperative

For the BROL-42, additional studies has been carried out in order to fulfil the 14 CFR §23.67 for climb performance under one engine inoperative. According to the regulation, since the aircraft have a $V_{\text{SO}} > 61$ kts, it must be able to maintain a steady climb gradient $> 1.5\%$ at a pressure altitude of 5000 ft with climb speed not less than $1.2 V_{\text{S1}}$. For this purpose the best ROC and its corresponding climb gradient have been computed under the case of one engine inoperative. Values are presented in Tab. 4.27. It can be seen that the BROL-42 fulfils the OEI climb requirements since $V_{\text{YSE}} > 1.2 V_{\text{S1}} = 76.44$ kts and the climb gradient found is bigger than 1.5%.



	BROL-42
Climb gradient [%]	6.15
ROC _{max} [ft/min]	490.6
V _{YSE} [kts]	78.95

Table 4.27: Climb performance parameters of BROL-42 at a pressure altitude of 5000 feet with one engine inoperative.

4.5.5 Cruise

The characteristics of the steady cruise for both aircraft are listed on Tab. 4.28. These have been calculated following the methodology of the Gudmundsson [4]. The minimum level airspeed is the lower of the two airspeeds at which the power required and power available are equal. The maximum speed corresponds to the maximum velocity attainable by the aircraft at cruise conditions. The thrust needed for waiting is the minimum thrust needed so that the aircraft can loiter for a prolonged period of time in a specific geographic location. This thrust is used to determine the airspeed that requires the least amount of thrust, which is also the maximum endurance airspeed for a propeller-powered aircraft. The best glide speed is the speed of the aircraft when engines are inoperative and corresponds to the best range airspeed. The Carson's speed can be considered as the "fastest efficient airspeed" to fly and is computed to be about 32% higher than the best glide airspeed. The maximum Lift to Drag coefficient is independent of the altitude and is one of the most important performance parameters since it indicates how far an airplane can glide from a given altitude. The percentage of thrust for best endurance is the ratio between the thrust needed for waiting and the engine maximum power.



	Units	BROL-21	BROL-42
Minimum speed	[KEAS]	33.90	40.33
Maximum speed	[KEAS]	137.4	167.7
Thrust needed for waiting	[N]	90.38	170.13
Maximum endurance speed	[KEAS]	58.5	68.3
Best glide speed	[KEAS]	69.5	81.4
Carson speed	[KEAS]	91.8	107.4
Design cruise speed	[KEAS]	122.3	150.7
L/D_{max}	[/]	20.22	19.33
Percentage of thrust for best glide speed	[%]	42.63	40.5

Table 4.28: Steady cruise flight characteristics for the single-engine and the twin-engine

Glide

In case of an engine shutdown during cruise, the gliding performance has to be analysed. Using the data from Tab. 4.28, the obtained results for the gliding distance and glide angle for both aircraft are displayed in Fig. 4.29. The corresponding descent rates are 5.6 and 7.4 kts for the BROL-21 and BROL-42 respectively.

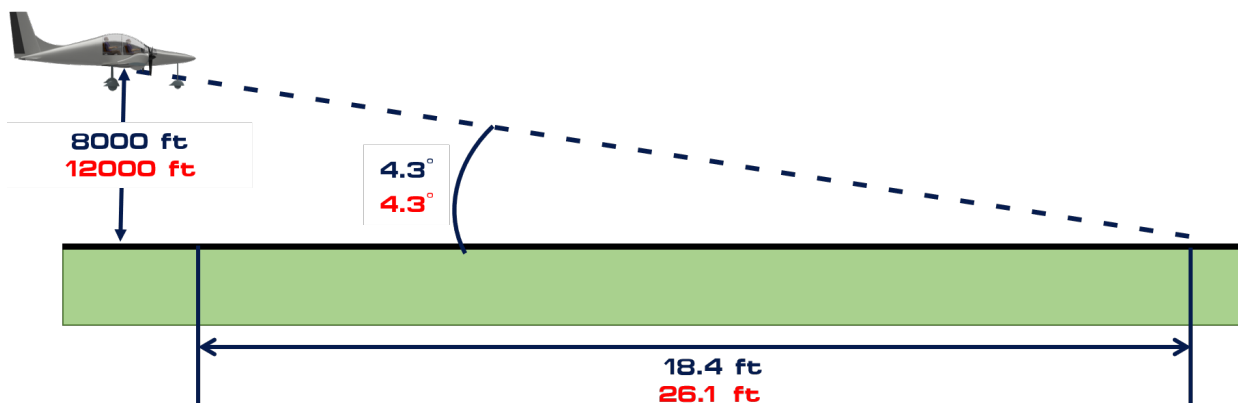


Figure 4.29: Glide distance and angle from cruise altitude. In blue are the results for the BROL-21 and in red for the BROL-42

4.5.6 Turning rate and banking angle

This section intends to evaluate turning maneuvers at constant speed and cruise altitude. The Fig. 4.30 and Fig. 4.31 illustrate how rapidly an aircraft can maneuver at specific airspeeds for the

BROL-21 and BROL-42 respectively. The turn rate value depends onto the flight speed and the radius of gyration of the aircraft, causing it to undergo an increasing load factor with the turn rate.

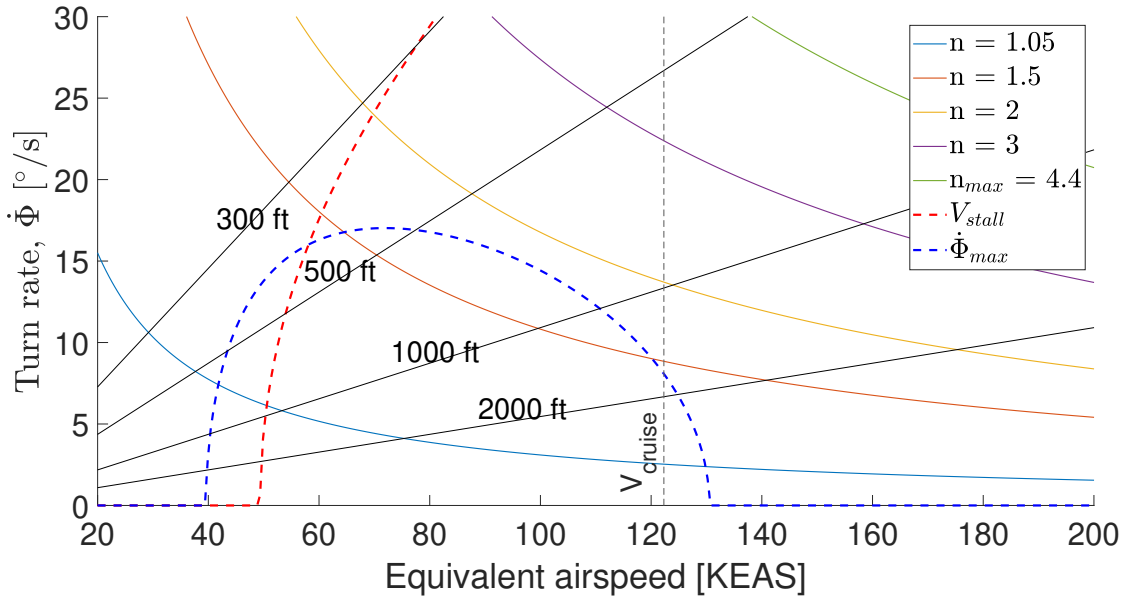


Figure 4.30: BROL-21 turn performance map at cruise altitude (8000 ft). The black straight lines represent constant turning radius in feet.

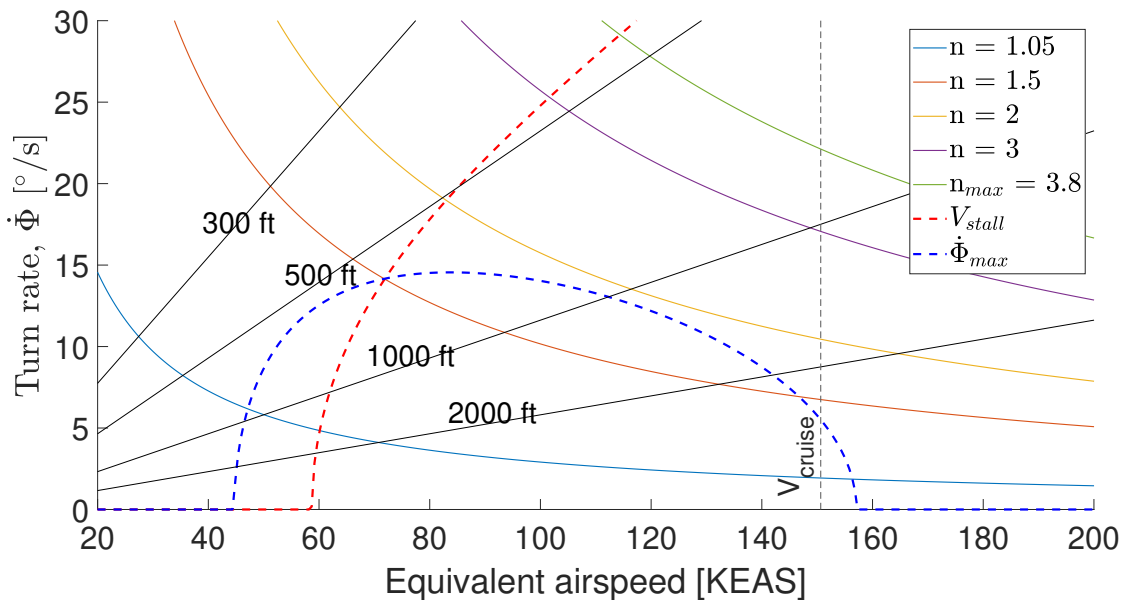


Figure 4.31: BROL-42 turn performance map at cruise altitude (12000 ft). The black straight lines represent constant turning radius in feet.

For both aircraft, the maximum affordable load factor before structural break is 4.4 and 3.8 times the Earth gravitational attraction for the BROL-21 and BROL-42 respectively. However, the turn



performance map shows that both aircraft turning capabilities are limited by the stall velocity (red dotted line) and the maximum turn rate in function of the velocity (blue dotted line). This evolution of the stall and maximum turn rate is characterised by the fact that an increase in the turning rate, at constant velocity, is followed by an increase in the load factor. The latter involves an increase in drag causing the range of admissible velocities to shorten as the aircraft goes to higher turn rate and load factors. The range of admissible velocities is therefore not limited by the aircraft structural capacities but by turning capabilities while maintaining a constant altitude. As a matter of fact, if the pilot tries to turn 20 degrees per second at cruise speed, since it isn't in the range of admissible values for a constant level and velocity turn, the aircraft will start to lose altitude during the turn.

Some of the turning characteristics are presented on Tab. 4.29.

	BROL-21	BROL-42
Maximum turn rate [$^{\circ}/s$]	17	14.6
Minimum turning radius [ft]	394	589
Maximum load factor [l]	1.8	1.9
Maximum bank angle [$^{\circ}$]	56.2	58.2

Table 4.29: Cruise turn performance

The different stall speeds in function of the banking angle for different flight configurations are shown on Tab. 4.30 and Tab. 4.31 in KEAS units for the BROL-21 and BROL-42 respectively. The up configuration of the flaps is related to the cruise and the stall speeds have therefore been computed at cruise conditions. The 35° deflection is, on the other hand, related to the landing of the aircraft and thus the corresponding stall speeds have been calculated at ground level.

Flap deflection	Banking angle				
	0°	15°	30°	45°	60°
0° (Cruise)	49.53	50.40	53.23	58.90	70.05
35° (Landing)	47.30	48.13	50.83	56.25	66.90

Table 4.30: BROL-21 stall speeds in KEAS units as function of banking angle and flaps configuration

Flap deflection	Banking angle				
	0°	15°	30°	45°	60°
0° (Cruise)	58.93	59.96	63.33	70.08	83.34
35° (Landing)	56.96	57.96	61.21	67.74	80.55

Table 4.31: BROL-42 stall speeds in KEAS units as function of banking angle and flaps configuration



4.5.7 Landing

As shown in Fig. 4.33, the landing phase is split into multiple segments:

- Approach distance at an angle of 3° starting from a 50ft obstacle to the flare height.
- Flare distance from flare height to touchdown, considering a 1 second roll time.
- Braking distance from touchdown speed to a complete stop. Braking-friction coefficient $\mu_B = 0.4$ (dry asphalt mid value) and a 35° flap deflection.

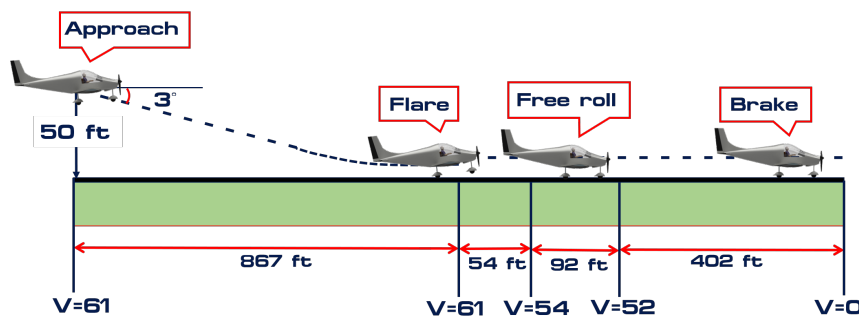


Figure 4.32: BROL-21 distances and speeds for the different landing segments (speeds in knots)

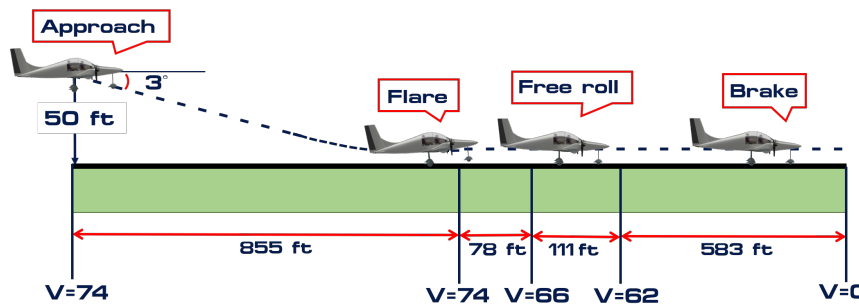


Figure 4.33: BROL-42 distances and speeds for the different landing segments (speeds in knots)

The total landing distance for the BROL-21 and BROL-42 aircraft are respectively 1415 and 1628 feet, which satisfy the RFP requirements.

5 TRADE-OFF STUDY

The aim of this section is to measure the variation of the aircraft flight characteristics according to some geometrical modifications. These new performance are then compared in order to define which configuration is more suitable. The parameters typically studied are the wing surface, the fuselage length and the cruise altitude. All these different parameters underwent a variation of 10% around their initial value. The results are displayed in Table 5.1 and 5.2 for BROL-21 and BROL-42.

Wing surface variation: For both aircraft, the reduction of the wing surface causes a reduction of the lift force. This reduction implies to increase the power plant in order to balance the aircraft weight. Automatically follows an augmentation of weight and fuel consumption, leading to reduced performances such as takeoff, landing distance or even range. Moreover, a trainer aircraft is supposed to fly intensively, making the fuel consumption one of the most important parameters to monitor in order to minimize the fly costs. Besides, with this reduction, the BROL-21 landing distance becomes larger than the one required. A similar conclusion arises with a wing area increment. An enlargement leads to higher lift but induces heavier mass and higher drag, which requires higher engine power to fulfil the requirements. Final consequences are again mass and fuel consumption increase. The takeoff and landing performances are enhanced but at the expense of the range and fuel consumption, where the latter is, as mentioned earlier, one of the key parameters.

Fuselage length variation: Changing the length of the fuselage does not affect heavily any of the two aircraft. Still, a decrease can lead to small decrease of the maximum weight and the fuel consumption. Nonetheless, a fuselage length reduction has to be done carefully since it has to ensure room for every components as well as aircraft good stability.

Cruise altitude variation: Modifications of the cruise altitude by 10% is not impacting both aircraft significantly enough for conclusion to be made on whether or not one altitude is preferable.

Since none of the different variations led to a significant improvement of the capabilities, one can conclude that the initial configuration adopted is a judicious choice that can greatly fulfil the requirements given in Tab. 1.1.

Evaluation criteria	Wing surface [ft ²]			Fuselage length [ft]			Cruise altitude [ft]		
	-10%	0%	+10%	-10%	0%	+10%	-10%	0%	+10%
Variation	-10%	0%	+10%	-10%	0%	+10%	-10%	0%	+10%
Value	127.8	142	156.2	19.8	22	24.2	7 200	8 000	8 800
Takeoff distance [ft]	+5.22%	1255.3	-17.59%	+0.06%	1255.3	-0.05%	~ 0%	1255.3	~ 0%
Landing distance [ft]	+5.99%	1415.3	-3.08%	-0.01%	1415.3	+0.01%	~ 0%	1415.3	~ 0%
Range [ft]	-16.1%	1344.2	-3.64%	-0.79%	1344.2	+0.60%	+0.09%	1344.2	-0.10%
Maximum speed [KEAS]	+6.70%	137.4	-0.65%	~ 0%	137.4	~ 0%	-0.88%	137.4	+0.89%
Cruise speed [KEAS]	+6.92%	122.3	~ 0%	~ 0%	122.3	~ 0%	-0.82%	122.3	+0.83%
Takeoff weight [lb]	+0.05%	1825.2	+2.52%	-0.93%	1825.2	+0.97%	+0.06%	1825.2	-0.06%
Fuel for cruise [lb]	-3.83%	150.15	-4.26%	+0.08%	150.15	-0.08%	-0.07%	150.15	+0.07%

Table 5.1: BROL-21 aircraft trade-off study

Evaluation criteria	Wing surface [ft ²]			Fuselage length [ft]			Cruise altitude [ft]		
	-10%	0%	+10%	-10%	0%	+10%	-10%	0%	+10%
Variation	-10%	0%	+10%	-10%	0%	+10%	-10%	0%	+10%
Value	162	180	198	26.1	29	31.9	10 800	12 000	13 200
Takeoff distance [ft]	+5.69%	1551.3	-14.28%	+0.02%	1551.3	-0.01%	~ 0%	1551.3	~ 0%
Landing distance [ft]	+4.67%	1627.8	-3.59%	-0.01%	1627.8	+0.01%	~ 0%	1627.8	~ 0%
Range [ft]	-9.66%	1629.5	-1.55%	-0.51%	1629.5	+0.33%	+0.17%	1629.5	-0.24%
Maximum speed [KEAS]	~ 0%	167.7	~ 0%	~ 0%	167.7	~ 0%	-0.71%	167.7	~ 0%
Cruise speed [KEAS]	+6.32%	150.7	~ 0%	~ 0%	150.7	~ 0%	-1.26%	150.7	1.29%
Takeoff weight [lb]	+0.80%	3650.5	+4.00%	-1.19%	3650.5	+1.20%	+0.08%	3650.5	-0.08%
Fuel for cruise [lb]	-1.85%	315.02	-2.46%	+0.04%	315.02	-0.10%	-0.13%	315.02	+0.07%

Table 5.2: BROL-42 aircraft trade-off study



6 COSTS ANALYSIS

Besides designing components and establishing aircraft performance, a very important study to drive is about the cost. From the manufacturing cost to the selling price through the price of each component, it is of paramount importance to conduct an economic analysis beforehand.

For that, a modified version of the DAPCA-IV (Development and Procurement Costs of Aircraft) model is used. Based on technical data such as the empty weight and the maximum airspeed of the aircraft and thanks to the cost estimating relationships (CERs) it is possible to predict aircraft costs.

Several costs will be detailed such as the non-recurring and recurring costs, the selling price and the operating cost. A production of 600 aircraft over a period of 5 years will be taken into account to compute the prices. It is important to note that equations used must be adapted to take into account the cost of living. Indeed, the calculation model is based on the cost of living in 2012. All costs will be updated to year 2020 with the Consumer Price Index (CPI) equals to 1.12 [23].

6.1 Non-recurring costs

The non-recurring development and production costs can be divided into two parts. On the one hand there are the fixed costs which take into account the development and flight tests. On the other hand, there are the tooling and engineering costs which depend on the number of units produced.

The total cost of development includes logistics, human resources, administration, etc. The flight tests operations covers the development and the certification. Those costs can be estimated with the following equations [4]:

$$C_{dev} = 0.06458 \cdot W^{0.873} \cdot V^{1.89} \cdot N_p^{0.346} \cdot CPI \cdot F_{cert} \cdot F_{cf} \cdot F_{comp} \cdot F_{press}$$

$$C_{ft} = 0.009646 \cdot W^{1.16} \cdot V^{1.3718} \cdot N_p^{1.281} \cdot CPI \cdot F_{cert}$$

With W the empty weight, V the maximum airspeed, N_p the number of prototypes; set to 5 in this case. Since the aircraft are 14 CFR Part 23 certified, are not pressurized, that simple flaps are used



and that there is no composite part in it, all variables (F_{cert} , F_{cf} , F_{comp} , F_{press}) are equal to 1.

The total engineering and tooling costs cover the design of the aircraft, the system engineering, the build of tools/molds as well as research, development, test, and evaluation (RDT&E). They are calculated as follows:

$$C_{eng} = 2.0969 \cdot H_{eng} \cdot R_{eng} \cdot CPI$$

$$C_{tool} = 2.0969 \cdot H_{tool} \cdot R_{tool} \cdot CPI$$

Where H_{eng} and H_{tool} are the number of engineering and tooling man-hours required to complete the above mentioned tasks. R_{eng} and R_{tool} are calculated based on 2019 salaries, they are \$102 per hour and \$68 per hour respectively.

All non-recurring costs are summarized in the following table:

	BROL-21	BROL-42
Development	430	981
Flight test	124	318
Tooling	6 080	10 676
Engineering	9 268	18 774
Non-recurring costs	15 904	30 750

Table 6.1: Details of fixed costs for 600 units, in thousand USD

6.2 Production method

The production process has a huge impact on costs. A way to improve is to maximise the number of same components between both aircraft. Using simple element design will help too. Here below the major items improving the process.

- Same cockpit and systems
- One aluminum sheet for the fuselage and lifting surfaces
- The same material for inner structures and for airframe

- Two different type of tires needed for the landing gears of both aircraft
- Same airfoil (therefore only one mold to manufacture)
- A simple airfoil (NACA0012) for the empennage

The choice of this method and the reuse of various components will simplify manufacturing and maintenance. It will also reduce the production costs and, at the same time, the selling price.

6.3 Recurring costs

The recurring or variable costs of the aircraft include the quality control, manufacturing, materials, avionics, landing gears, engines and propeller costs. These costs increase in direct relation to the production volume and are calculated based on a model from [4].

	BROL-21	BROL-42
Quality control	7 177	11 806
Manufacturing	55 210	90 818
Materials	8 284	13 139
Avionics	9 627	9 627
Landing gears	- 2 563	- 2 563
Engines	11 436	27 358
Propellers	2 429	4 858
Total variables costs	91 601	155 040

Table 6.2: Details of variable costs for 600 units, in thousand USD

Regarding the costs of avionics, landing gears, engines and propellers they have been multiplied by the Quantity Discount Factor (QDF). This factor reduces prices by taking into account the production process improvement and knowledge that technicians develop over time. It is determined assuming an experience effectiveness of 95%. The price of the landing gears is negative because the DAPCA method automatically includes retractable landing gears in its calculations. Therefore, 2 563K\$ must be subtracted as fixed landing gears are used.



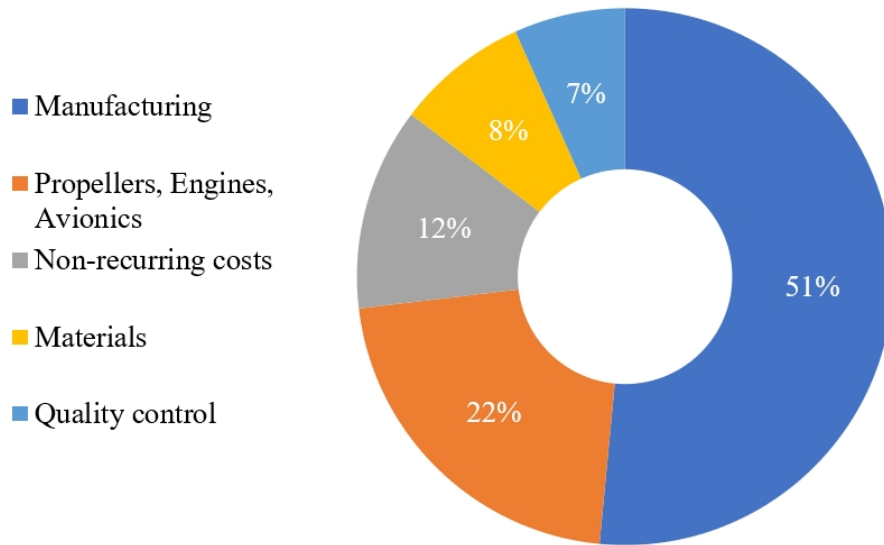


Figure 6.1: Proportion of recurring and non-recurring costs for BROL-21

The fly away cost is the production fee for an additional unit. This includes the costs of manufacturing, tooling, quality control and materials, as well as avionics, engines and propeller.

For each member of the family:

- Single: \$100 880
- Twin: \$165 500

6.4 Selling price

This section will describe the way to find the optimal selling price for both aircraft. The costs calculated in section 6.1 and 6.3 are added, then divided by the number of units produced. In addition, a liability insurance of 12% is inserted. Finally, a 15% profit is applied as requested in the AAIA requirements.

Details of the unit costs can be found in Table 6.3.

	BROL-21	BROL-42
Fixed	26 507	51 250
Variable	152 670	258 400
Total cost	200 680	346 810
Selling price	230 780	398 840

Table 6.3: Costs for one unit, in USD

Note that these costs can be reduced by purchasing components in bulk. Indeed, the prices presented are a bit overestimated since elements including engines, propellers or avionics are considered as bought individually.

6.5 Cost-volume-profit analysis

Most of the time chief financial officer (CFO) is interested to know two parameters that helps him to define the profitability of a new product.

- Break-even point which is the minimum of aircraft to produce before getting benefit
- The pay back period is the number of days before an investment become profitable

The following expression is used to determine the number of aircraft the BROL firm should sell to cover its costs:

$$BE = \frac{\text{Total fixed cost}}{\text{Unit sales price} - \text{Unit variable cost}}$$

Cost-volume-profit (CVP) analysis makes few assumptions, such as considering non-recurring costs as fixed and taking the unit selling price and variable costs on the basis of a production of 600 aircraft.

Number of units to break-even is 203 for BROL-21 and 218 for BROL-42, when they are sold at the minimum selling price. By increasing this price the break-even is reached faster, however, a price that is too high will not attract any customer. In this case, the pay back period is 1 year and 9 months. So, CFO can expect return on investment after that period. Fig. 6.2 shows when the break-even appears for three different prices.



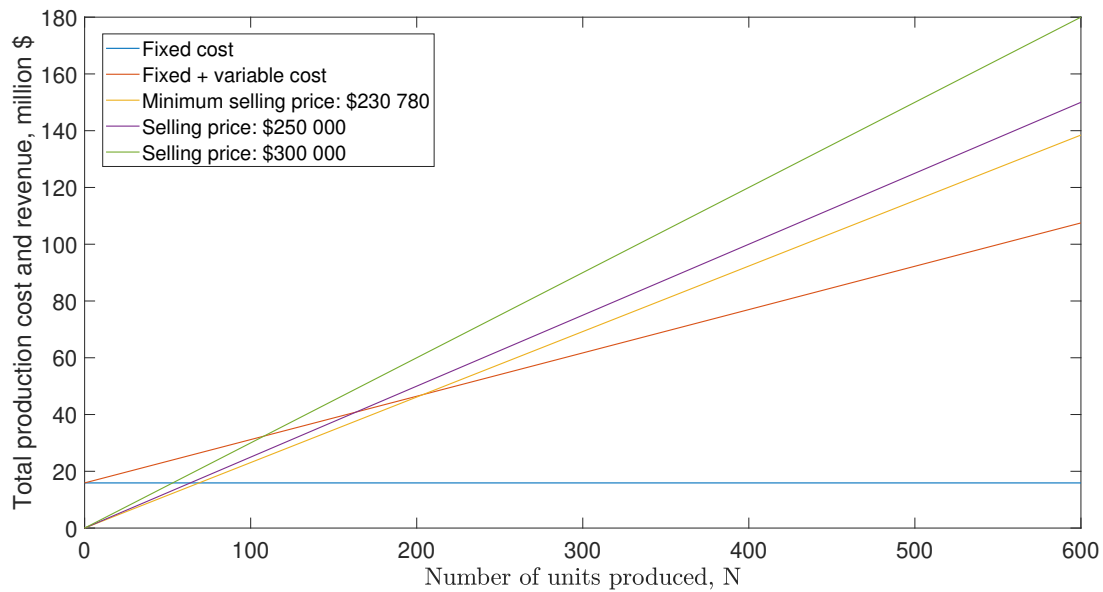


Figure 6.2: Break-even for BROL-21

6.6 Operational costs and features

Once the selling price is determined, other operating costs are added. They represent the fuel and oil costs as well as the maintenance expenses. Including changing elements when necessary. Other factors contributing to these annual costs are the payment of the loan, the amount of insurance and storage. Based on this, the hourly cost of both aircraft is calculated.

	BROL-21	BROL-42
Maintenance	44 710	50 400
Fuel	48 520	51 780
Total yearly	144 220	189 650
Hour	\$80 /hr	\$104 /hr

Table 6.4: Operating costs, in USD/year

Maintenance is to be done approximately every 100 hours of flight time. There are therefore 18 maintenance planned a year. The maintenance cost takes into account the eventual replacement of the engine. In addition, tires and brakes must be replaced at least once a year. Assuming that tires are changed every 600 hours and that new brake pads must be replaced every 800 hours of flight, it means adding the cost of 3 sets of tires and 8 brake pads per year. The discs should be replaced once



a year. The addition of oil for the engine and systems is included in the maintenance too. Its price is calculated on the basis of engine consumption, the volume of oil tank and the actual price of *AeroShell Oil Sport Plus* (\$37/gallon).

As per the standard package a couple of features are included such as:

Constant-pitch propeller	Rotax [®] engine
VFR/IFR instruments	Aluminum airframe
Hydraulic brakes	Anti-icing system
Leather seats	Oxygen Cylinders (BROL-42)
First-aid kit	

Table 6.5: Standard features

To satisfy a larger number of buyers, optional features can be purchased.

Aircraft protective cover	\$430
Pilot Headset - David Clark H10-30	\$370
Touchscreen Flight Displays - G500 TXi	\$12 000
Sun Shields	\$400
Additional Landing/Taxi Lights	\$255 /each
Stand for smartphone	\$60

Table 6.6: Optional features prices



7 CONCLUSION

The American Institute of Aeronautics and Astronautics, willing to tackle the overall decrease of popularity for small range air services, has issued a Request for Proposal concerning a general aviation trainer aircraft family. Answering to this challenge, the BROL Aerospace team from Liège worked hard and proudly presents the BROL-21 and BROL-42.

Such aircraft family has the potential, and the capability, to bring solutions to the small air services that are in need for a new generation of trainer aircrafts.

The BROL aircraft family has been designed with the aim of a controllable, stable and robust aircraft, as the main target customer are beginning pilots in the frame of flight schools. The design has been oriented towards a docile aircraft, able to withstand unusual flight parameters dictated by the pilot. But the BROL-21 and BROL-42 are also robust and affordable, allowing to reach a larger number of customers throughout small and large flight schools. Choices have been made such that the initial price is particularly attractive, and that the aircraft promises a long life. Finally, thanks to wise thinking, both aircraft show a great versatility, allowing any pilot school to tackle more easily usual problems, such as puncture, wearing out, etc. As a matter of fact, several components have been designed to be close alike for both aircraft. This allows to reduce the manufacturing costs, lowering the price, as well as it allows to have spare parts able to be used in both aircraft!

All in all, the BROL aircraft family is a family of versatile, inexpensive and efficient aircraft composed by the BROL-21 and the BROL-42. With a capacity of two and four passengers, these airplanes are perfect trainers for flight schools according to their great performances, low price and robustness.

Following the conceptual design presented in this report, the next steps would be to pursue deeper analysis while keeping the development ongoing on the side. Powerful tools, such as numerical analysis (CFD) and global finite element analysis would be used to enhance the design. After a few years, prototypes shall be produced to validate the work done. A certification phase would then allow to launch production, with a reconsideration of the market of the moment.



APPENDICES

A ACRONYMS

ADS Aircraft Design Software. 48, 49

aft aftetail. 29, 45, 46

AoA Angle of Attack. 20

AR Aspect Ratio. 10

AvGas Aviation Gasoline. 21

BEMT Blade Element Momentum Theory. 20

BFL Balanced Field Length. 70, 71

BSFC Brake Specific Fuel Consumption. 19

CFR Code of Federal Regulations. 17, 22, 73

CG Center of Gravity. 26, 29, 30, 36

CHT Cylinder-Head-Temperature. 23

FAA Federal Aviation Administration. 17, 21

fwd forward. 45

LL Low-leaded fuel. 21

MAC Mean Aerodynamic Chord. 14, 44, 45

MoGas Automotive Gasoline. 19, 21, 22

MON Moteur Octane Number. 21

MTOW Maximum Take-Off Weight. 2, 35–37,
68, 71

OAD Optimal Aircraft Design. 48

OEI One Engine Inoperative. 70, 71, 73

RFP Request For Proposal. 17

ROC Rate-Of-Climb. 72, 73

TBO Time Between Overhaul. 19

UL Unleaded fuel. 21

VLM Vortex Lattice Method. 38, 39, 43

ZFW Zero-Fuel-Weight. 2



BIBLIOGRAPHY

- [1] **Mordor Intelligence.** *AVIATION MARKET - GROWTH, TRENDS, AND FORECAST (2019 - 2024)*. 2019 (cit. on p. 2).
- [2] **Alyssa J. Miller.** *Boeing details 20-year pilot*. July 2015 (cit. on pp. 2, 3).
- [3] **Markets and Markets.** *Ultralight and Light Aircraft Market Aircraft Type*. Feb. 2019 (cit. on p. 2).
- [4] **Gudmundsson, Snorri.** *General Aviation Aircraft Design: Applied Methods and Procedures*. Butterworth-Heinemann, 2013 (cit. on pp. 10, 14, 20, 22, 23, 38, 41, 42, 69, 71, 74, 81, 83).
- [5] **Raymer, Daniel P.** *Aircraft Design: A conceptual approach*. AIAA Education Series, 2012 (cit. on pp. 11, 14–16, 18, 22, 30, 31, 35, 38, 40, 41, 44, 45).
- [6] **Federal Aviation Administration.** *Federal Aviation Regulation Part 23 - Airworthiness standards: Normal, utility, acrobatic, and commuter category airplanes*. Dec. 30, 2016 (cit. on pp. 17, 32, 33, 35, 45, 68, 70).
- [7] **Rotax^l Aircraft Engine.** *Operators Manual for Rotax^l engine type 914 Series*. ref. no.: OM-914, Aug. 01, 2019 (cit. on p. 19).
- [8] **Rotax^l Aircraft Engine.** *Operators Manual for Rotax^l engine type 915 i A Series*. ref. no.: OM-915 i A, Jun. 01, 2019 (cit. on p. 19).
- [9] **Leishman, Gordon J.** *Principles of helicopter aerodynamics*. Cambridge university press, 2006 (cit. on p. 20).
- [10] **McCormick, Barnes W.** *Aerodynamics Aeronautics and Flight Mechanics*. John Wiley & Sons, Ltd, 1995 (cit. on pp. 20, 23).
- [11] **Hartman, Edwin P. and Biermann, David.** *Aerodynamic characteristics of full-scale propeller having 2, 3, and 4 blades of CLARK-Y and R.A.F. 6 airfoil sections*. Tech. rep. 1938 (cit. on p. 20).

- [12] **Ismail, Kamal AR and Rosolen, Célia VAG.** *A Simplified Model For The Aerodynamic Analysis Of A Small Propeller*. 24th ABCM International Congress of Mechanical Engineering, 2017 (cit. on p. 20).
- [13] **Lambert, Thomas.** *Blade Element Momentum Theory Matlab implementation*. Version 2020 (cit. on p. 20).
- [14] **Federal Aviation Administration.** *Unleaded AVGAS Transition Aviation Rulemaking Committee (UAT ARC) Final Report*. Feb. 17, 2012 (cit. on p. 21).
- [15] **Price, Henry J.** *Fact Sheet – Leaded Aviation Fuel and the Environment*. Federal Aviation Administration, Nov. 20, 2019 (cit. on p. 21).
- [16] **Breidenthal, Robert.** *Environmental concerns in general aviation*. Routledge, 2018 (cit. on p. 21).
- [17] **Granta Design.** *CES EduPack 2018*. Version 2018 (cit. on pp. 25, 29).
- [18] **Joseph Katz & Allen Plotkin.** *Low-Speed Aerodynamics*. Cambridge University Press, 2001 (cit. on p. 38).
- [19] **Sanchez, Mariano M.** *Vortex Lattice Method software*. Version 2020 (cit. on pp. 38, 45).
- [20] **Torenbeek, Egbert.** *Advanced Aircraft Design*. John Wiley & Sons, Ltd, June 2013. doi: 10.1002/9781118568101. <https://doi.org/10.1002/9781118568101> (cit. on p. 47).
- [21] **Dimitriadis, D.** *Flight Dynamics and Control*. <http://www.ltas-aea.ulg.ac.be/cms/index.php?page=flight-dynamics-course> (cit. on pp. 48, 49).
- [22] **Roskam, J.** *Methods for Estimating Stability and Control Derivatives of Conventional Subsonic Airplanes*. 1983 (cit. on p. 49).
- [23] **Bureau of Labor Statistics.** *Consumer Price Index*. <http://www.bls.gov>. (accessed: 03.2020) (cit. on p. 81).
- [24] **Kidane, Bereket.** “Design and Analysis of Light GA Aircraft for Agricultural Purpose”. MA thesis. UNIVERSITY OF TURKISH AERONAUTICAL ASSOCIATION, June 2016.
- [25] **David Lednicer.** *Airfoils of US and Canadian Aircraft*.



- [26] **Hoak, D.E. and McDonnell Douglas Corporation. Douglas Aircraft Division.** *USAF Stability and Control Datcom*. USAF Stability and Control Datcom v. 3. Flight Control Division, Air Force Flight Dynamics Laboratory, Wright-Patterson Air Force Base, 1975.
- [27] **U. Military.** *Military specification : Flying qualities of piloted airplanes*. 1969.
- [28] **Bourdouxhe, Maxime.** *Liège sunset*. <https://youpic.com/image/16022583/liege-sunset-by-maxime-bourdouxhe>.
- [29] **Iain Box.** *Aerospace Design Work*. <https://www.behance.net/gallery/6468137/Aerospace-Design-Work>.
- [30] *Brol Aerospace logo*. <https://www.istockphoto.com/fr/vectoriel/vectoriel-logo-aviation-gm1033087658-276677848>.

